Analysis of Disturbances in Large Interconnected Power Systems

By

Mr. Richard Andrew Wiltshire
Bachelor of Engineering
(Electrical and Computer Engineering)
1st Class Honours

A thesis submitted in partial fulfillment of the requirements for the degree of

Doctor of Philosophy

Centre of Energy and Resource Management
School of Engineering Systems
Faculty of Built, Environment and Engineering
Queensland University of Technology
Brisbane, Australia.

2007

Analysis of Disturbances in Large Interconnected Power Systems

by Mr. Richard Andrew Wiltshire

Principal Supervisor: Associate Professor Peter O'Shea
School of Engineering Systems
Faculty of Built, Environment and Engineering
Queensland University of Technology

Associate Supervisor: Professor Gerard Ledwich
School of Engineering Systems
Faculty of Built, Environment and Engineering
Queensland University of Technology

Associate Supervisor: Dr Edward Palmer
School of Engineering Systems
Faculty of Built, Environment and Engineering
Queensland University of Technology

Abstract

World economies increasingly demand reliable and economical power supply and distribution. To achieve this aim the majority of power systems are becoming interconnected, with several power utilities supplying the one large network. One problem that occurs in a large interconnected power system is the regular occurrence of system disturbances which can result in the creation of intra-area oscillating modes. These modes can be regarded as the transient responses of the power system to excitation, which are generally characterised as decaying sinusoids. For a power system operating ideally these transient responses would ideally would have a "*ring-down*" time of 10-15 seconds. Sometimes equipment failures disturb the ideal operation of power systems and oscillating modes with ring-down times greater than 15 seconds arise. The larger settling times associated with such "poorly damped" modes cause substantial power flows between generation nodes, resulting in significant physical stresses on the power distribution system.

If these modes are not just poorly damped but "negatively damped", catastrophic failures of the system can occur.

To ensure system stability and security of large power systems, the potentially dangerous oscillating modes generated from disturbances (such as equipment failure) must be quickly identified. The power utility must then apply appropriate damping control strategies.

In power system monitoring there exist two facets of critical interest. The first is the *estimation* of modal parameters for a power system in normal, stable, operation. The second is the rapid *detection* of any substantial changes to this normal, stable operation (because of equipment breakdown for example). Most work to date has concentrated on the first of these two facets, i.e. on modal parameter estimation. Numerous modal parameter estimation techniques have been proposed and implemented, but all have limitations [1-13]. One of the key limitations of all existing parameter estimation methods is the fact that they require very long data records to provide accurate parameter estimates. This is a particularly significant problem after a sudden detrimental change in damping. One simply cannot afford to wait long enough to collect the large amounts of data required for existing parameter estimators. Motivated by this gap in the current body of knowledge and practice, the research reported in this thesis focuses heavily on rapid detection of changes (i.e. on the second facet mentioned above).

This thesis reports on a number of new algorithms which can rapidly flag whether or not there has been a detrimental change to a stable operating system. It will be seen that the new algorithms enable sudden modal changes to be detected within quite short time frames (typically about 1 minute), using data from power systems in normal operation.

The new methods reported in this thesis are summarised below.

The Energy Based Detector (EBD): The rationale for this method is that the modal disturbance energy is greater for lightly damped modes than it is for heavily damped modes (because the latter decay more rapidly). Sudden changes in modal energy, then, imply sudden changes in modal damping. Because the method relies on data from power systems in normal operation, the modal disturbances are random. Accordingly, the disturbance energy is modelled as a random process (with the parameters of the model being determined from the power system under consideration). A threshold is then set based on the statistical model. The energy method is very simple to implement and is computationally efficient. It is, however, only able to determine whether or not a sudden modal deterioration has occurred; it cannot identify which mode has deteriorated. For this reason the method is particularly well suited to smaller interconnected power systems that involve only a single mode.

Optimal Individual Mode Detector (OIMD): As discussed in the previous paragraph, the energy detector can only determine whether or not a change has occurred; it cannot flag which mode is responsible for the deterioration. The OIMD seeks to address this shortcoming. It uses optimal detection theory to test for sudden changes in individual modes. In practice, one can have an OIMD operating for all modes within a system, so that changes in any of the modes can be detected. Like the energy detector, the OIMD is based on a statistical model and a subsequently derived threshold test.

The Kalman Innovation Detector (KID): This detector is an alternative to the OIMD. Unlike the OIMD, however, it does not explicitly monitor individual modes. Rather it relies on a key property of a Kalman filter, namely that the Kalman innovation (the difference between the estimated and observed outputs) is white as long as the Kalman filter model is valid. A Kalman filter model is set to represent a particular power system. If some event in the power system (such as equipment failure) causes a

sudden change to the power system, the Kalman model will no longer be valid and the innovation will no longer be white. Furthermore, if there is a detrimental system change, the innovation spectrum will display strong peaks in the spectrum at frequency locations associated with changes. Hence the innovation spectrum can be monitored to both set-off an "alarm" when a change occurs and to identify which modal frequency has given rise to the change. The threshold for alarming is based on the simple Chi-Squared PDF for a normalised white noise spectrum [14, 15]. While the method can identify the mode which has deteriorated, it does not necessarily indicate whether there has been a frequency or damping change. The PPM discussed next can monitor frequency changes and so can provide some discrimination in this regard.

The Polynomial Phase Method (PPM): In [16] the cubic phase (CP) function was introduced as a tool for revealing frequency related spectral changes. This thesis extends the cubic phase function to a generalised class of polynomial phase functions which can reveal frequency related spectral changes in power systems. A statistical analysis of the technique is performed. When applied to power system analysis, the PPM can provide knowledge of sudden shifts in frequency through both the new frequency estimate and the polynomial phase coefficient information. This knowledge can be then cross-referenced with other detection methods to provide improved detection benchmarks.

Keywords

Power System Monitoring, Interconnected Power Systems, Power System Disturbances, Power System Stability, Signal Processing, Optimal Detection Theory, Stochastic System Analysis, Kalman Filtering, Poly-Phase Signal Analysis.

Declaration

I hereby certify that the work embodied in this thesis is the result of original research and has not been submitted for a higher degree at any other University or Institution.

Richard Andrew Wiltshire
10 July 2007

Table of Contents

Table of Figures

List of Tables

Acknowledgements

The author wishes to thank the following for their support during the period of this research. Firstly I'd like to extend a sincere thank you to Associate Professor Peter O'Shea, for his guidance, encouragement, input and patience during the period of this research. Dr O'Shea has all the qualities any candidate could ever ask for from a supervisor, both in his technical expertise and his persona, thanks Peter.

I would also like to extend a warm thank you to Professor Gerard Ledwich (QUT) for his comments, guidance, input and insightful understanding of the research topic.

Other people I'd like to mention and thank are Dr Ed Palmer (QUT) for his contributions, support and friendship over many years and Dr Chaun-Li Zhang (QUT) for his endless supply of data when I needed it. I would also like to thank Maree Farquharson (QUT) who, as fellow candidates, supported and encouraged each other over our respective research periods.

In addition I would like to extend a grateful thank you to David Bones (NEMMCO) and David Vowles (University of Adelaide) for giving me permission to use the MudpackScripts as an important validation tool within this thesis, very much appreciated.

Finally, I would like to thank the following for the much welcome financial support over the course of the research; Queensland University of Technology for the APAI and QUTPRA scholarships, the QUT Chancellery for providing the Vice-Chancellor's Award, the QUT Faculty of Built Environment and Engineering for the BEE financial top-up and finally my current employer, CEA Technologies Pty. Ltd, for providing me the study leave I required in the final stages of completing this body of work.

Dedication

There are a number of very special people I would like to dedicate this work to; firstly my mother, Virginia Ann Bryan, who with her guidance, support and never ending devotion has helped me mature into the man I am today. I would also like to dedicate this work to my father, Roger Wiltshire, for providing me the qualities that formulate a good engineer. Also to my two boys, Peter and Jack, who I am eternally proud of and encouraged by to strive to be a better father and person and finally to three very special and lovely ladies, Catherine Louise Kowalski, Meg Malaika (21/9/1966-19/3/2006) and Leslie Elizabeth Peters who in their own extraordinary way have encouraged, inspired, taught and supported me in my endeavours over the last few years.

Love to you all…

Glossary

AESOPS	Analysis of Essentially Spontaneous Oscillations in Power Systems
AMSE	Asymptotic Mean Squared Error
ARI	Adelaide Research and Innovation
CI	Confidence Interval
COA	Centre of Area
CRLB	Cramér-Rao Lower Bounds
CP	Cubic Phase Function
dB	Decibels
DFT	Discrete Fourier Transform
DTFT	Discrete Time Fourier Transform
EBD	Energy Based Detection
FAR	False Alarm Rate
FFT	Fast Fourier Transform
GMFC	Generalized Multi-linear Function Class
GPS	Global Positioning System
HAF	Higher–Order Ambiguity Function
HP	Higher-Order Phase Function
Hz	Hertz
IF	Instantaneous Frequency
IFR	Instantaneous Frequency Rate
IIR	Infinite Impulse Response
KID	Kalman Innovation Detector
LT	Long Term

LTE	Long Term Estimator
ML	Maximum Likelihood
MSE	Mean Squared Error
NEMMCO	National Electricity Market Management Company Limited
NILS	Non-linear Instantaneous Least Squares
NSW	New South Wales
OIMD	Optimal Individual Mode Detection
PDF	Probability Density Function
PPM	Polynomial Phase Method
PPS	Polynomial Phase Signal
PSD	Power Spectral Density
PWVD	Polynomial Wigner-Ville Distributions
RMS (rms)	Root Mean Squared
RV	Random Variable
QLD	Queensland
QP	Quartic-Phase Function
QR	Quadratic
QUT	Queensland University of Technology, Brisbane, Australia
SA	South Australia
SNR	Signal to Noise Ratio
SVD	Singular Value Decomposition
UA	The University of Adelaide
VIC	Victoria
W	Watts

Chapter 1

1 Introduction

1.1 The Analysis of Large Interconnected Power Systems

The worldwide economic restructuring of the electrical utility industry has formulated large interconnected distribution networks, resulting in a greater emphasis on reliable and secure operations [17]. To ensure secure and reliable operations, the large interconnected power systems require ongoing wide-area observation and control. To meet these requirements many wide-area monitoring methodologies have been proposed and established [18-20]. One of the most well accepted approaches is to monitor the power system at various locations within the distribution network and to employ Global Positioning System (GPS) information to synchronise the information acquired [21, 22]. With this approach, the positioning of the measurement locations in the network is an important issue which is discussed in [23].

Monitoring of power system stability is a critical issue for distributed networks with a significant focus on the inter-area oscillations, whereby this stability is largely dependent on all "inter-area oscillations" being positively damped. The latter are oscillations that correspond to transient power flows between clusters of generators or plants within a specific area in the large interconnected power system [24]. Monitoring and control of these oscillations is vitally important, and has proven far more

difficult than monitoring and control of oscillations associated with a single generator [24].

The inter-area oscillations (or modes) are damped sinusoids, at a given frequency with a relevant damping factor. It is the “ring-down” time associated with the damping factor that is of consequence in the transient ability of the system to stabilise post disturbance. It is critical that the transient time is short (and stable) to minimise power flows between the generation clusters and minimise the associated stresses within the generation/transmission infrastructure. As a consequence there has been much work done in the area of damping factor estimation in large distributed power systems. Previous estimation methods have employed Eigen analysis [25-27] as well as Prony [28] analysis [29, 30]. For accurate damping factor estimation, however, one typically requires large amounts of data [12, 13]. Conventional damping factor estimation techniques are therefore not suitable for rapidly detecting sudden modal damping changes. This thesis addresses this shortcoming by presenting a variety of new monitoring methods which are able to provide indications of detrimental modal parameter change with short data records (typically of the order of minutes).

1.2 The Monitoring of Australia's Large Interconnected Power System.

In Australia, the power system associated with the eastern states is an example of a large interconnected power system. The eastern Australian distribution infrastructure contains a number of generation clusters and there are inter-area modal oscillations which arise from the interaction of these clusters. A generalised map of the cluster location in eastern Australia is shown in Figure 1-1, with the capital cities representing the generation nodes. Also listed in Figure 1-1 are the locations of the GPS

monitoring sites as presented in [22]. Due to the importance of monitoring inter-area oscillations, a number of partners have entered into collaboration to effect the monitoring. These partners include Queensland University of Technology (QUT), and various transmission distributors as listed in [22]. The wide-area GPS synchronised techniques outlined in [22] and [23] have provided the real system data analysed in this thesis.

City	GPS Measurement Location & bus rating	
Brisbane	South Pine	275 kV
Sydney	Sydney West	330 kV
Melbourne	Rowville	220 kV
Adelaide	Para	275 kV

Figure 1-1 States associated with the eastern Australian large interconnected power system (shaded). State capital cities that represent generation nodes and measurement site location and ratings are shown.

(Template image of Australia sourced from http://www.rrb.com.au/Images/Australia)

1.3 The use of Externally Sourced Simulated Data for Algorithm Verification

The ultimate goal of power system monitoring algorithms is to perform reliably in real power system scenarios. Before this can be achieved,

however, the algorithms need to be tested via simulations. The simulation environment allows conditions to be varied and consequent performance to be evaluated in a controlled manner. For the simulation environment to provide useful testing, however, it must incorporate modelling which is representative of real systems. Good modelling strategies help to verify new techniques prior to real data implementation and provide confidence in real data analysis results. The task of creating satisfactory models of large dynamically interconnected systems is a challenging and non-trivial task. Fortunately, for the purposes of this PhD research, the author was given access to externally[1] created simulation models and data, based on the eastern Australian interconnected power system. The modelling of the system was performed by Adelaide Research & Innovation (ARI), a group associated with The University of Adelaide (UA), Australia. The formulation of the power system model and associated data was commissioned and contracted by the National Electricity Market Management Company Limited (NEMMCO) to provide benchmark testing of modal estimation methods from various research centres. The Centre of Energy and Resource Management within the School of Engineering Systems at Queensland University of Technology was one of the research centres that was benchmark tested in 2004 [31]. The simulated data provided in [31] was referred to as the "*MudpackScripts*" by the University of Adelaide authors. It consisted of various non-stationary data sets that were of interest in this thesis. The data set of most interest for this thesis is MudpackScript "Case13" which contains large detrimental step changes of damping. The details of the changes in the MudpackScripts will be presented in Chapter 2 Section 2.7 where it is first used for technique verification prior to real data analysis.

[1] Externally in this context means not associated with Queensland University of Technology, Brisbane Australia.

1.4 Review of Existing Modal Estimation Methods

With power systems becoming increasingly large and interconnected, the resulting advantages in efficiency have been offset somewhat by the disadvantage of greater vulnerability to system instability. This latter problem has made it very important to be able to perform reliable detection of system disturbances from modal oscillation data records. These data records can be associated with either a single isolated disturbance or with continuous random disturbances. The power industry's chief concern is in the detection of exponentially growing disturbance modes potentially present in the power system. If a growing mode is detected then the power utilities must introduce some dampening to counteract the mode. As a result, methods for fast, reliable and accurate estimation of the modal parameters are very important.

1.4.1 Single Isolated Disturbance

The parameter estimation methods in this section of the literature review focus on the power system's response to a single isolated disturbance.

1.4.1.1 Eigenanalysis of Disturbance Modes

There are a number of well established methods that have been used for the analysis of power systems. Many of these methods assume that the intrinsically non-linear power system can be approximated as a linear system for small perturbations from the steady state. Under this assumption Kundur *et. al*. [32] showed that eigenvalue analysis techniques could be quite effective. Conventionally, eigenanalysis of a power system is carried out by explicitly forming the system matrix, then using the standard QR algorithm to compute the eigenvalues of the matrix [32]. Modal oscillation parameters were then obtained from the eigenvalues. This basic method has proven to be generally reliable and has been extensively used by power utilities worldwide. Unfortunately

this method is unsuitable for large interconnected systems [26]. To enable large system mode monitoring the basic Eigen methods above have undergone various adaptations. Byerly *et. al.* [7] developed the best-known algorithm – AESOPS (Analysis of Essentially Spontaneous Oscillations in Power Systems). The advantage of AESOPS is that it does not require the explicit formation of the system state matrix [7]. The shortfall of the AESOPS method is the inadequacy for analysing very large interconnected systems.

Uchida and Nagao [25] made another development in eigenanalysis by proposing the use of the "S matrix method". In this method, it is assumed that the dynamics of power systems can be linearly approximated with a set of differential equations of the form, $\dot{x} = Ax$, where x is the (vector) state of the system and A is the system matrix. The S matrix method transforms the matrix, A, into the matrix, $S = (A + hI)(A - hI)^{-1}$, where I is the unit matrix and h is a positive real number. It can be shown that the dominant eigenvalues of S are the same as the dominant eigenvalues of A, but with an appropriate choice for *h*, can be computed with better numerical precision and speed [25]. The refined Lanczos process is also employed to make high-speed calculation possible [25]. Despite the computational advantage of the "S matrix method" eigenanalysis has limited application for very large interconnected power systems [33].

1.4.1.2 Spectral Analysis using Prony's Method

The spectral analysis of modal parameters for power system disturbance monitoring is another area of research which has received much attention. In this approach power system disturbance data records are spectrally analysed immediately after a fault or disturbance. One popular technique used for the spectral analysis is Prony's method, which originated in an earlier century [28]. Its ability to be practically implemented, though, was

delayed until the advent of the digital computer. Numerical conditioning enhancements developed in 1982 by Kumaresan and Tufts [3] broadened its applicability to modal estimation. C.E Grund *et. al.* [33] compared Prony analysis to eigenanalysis and stated that "*Prony analysis has an important advantage over eigenanalysis techniques in that it does not require the derivation of a medium-scale model*". Additionally, it can also be applied to field measurements for the derivation of control design models [33]. Many papers have been written on the use of Prony analysis for oscillation modal parameter estimation [34], [29] , [35], with each providing its own insights.

It should be noted however that the above applications of Prony's method assume that the signal contains little noise. In practice methods based on the Prony technique are only effective where the noise power is relatively small. Trudnowski *et. al.* [30] alluded to this when they stated for Prony analysis *"...The accuracy of the mode estimates is limited by the noise content always found in field measured signals..."*.

The poor conditioning of Prony's method exists because of an ill-conditioned matrix inversion in the method. To improve the ill conditioning, Kumaresan and Tufts [3] [4] proposed using a "Pseudo-Inverse" matrix, incorporating Singular Value Decomposition (SVD). This technique was further explored by Kumaresan and Tufts in [4] and was an improvement of the backward linear prediction methods proposed by Nuttall [36], which in turn were improvements of Prony's original method.

This process of applying a truncated SVD analysis effectively increases the SNR in the data prior to obtaining the solution vector. In [3], simulations show that this method gives much more accurate estimates of the modal parameters than traditional Prony methods. In [2], Kumaresan also provided further enhancement to Prony's method with the introduction of FIR pre-filtering to reduce the sensitivity of measurement

errors in observed signal samples when determining the parameters of sinusoidal signals.

Gomez Martin and Carrion Perez also introduced some extensions in working with noisy data with the application of Prony's method [6] by using a moving window in both forward and backward directions. This application of forward and backward methodologies were further explored by Kannan and Kundu [37].

A time-varying Prony method for instantaneous frequency estimation from low SNR data was introduced by Beex and Shan [38]. This was pertinent since power systems do have substantially non-stationary components on occasions.

1.4.1.3 The Sliding Window Derivation

Prony's method is a parametric spectral analysis method. Some authors have pursued solutions using classical spectral analysis based on Fourier methods. For example; Poon and Lee [39] developed a technique to determine the modal parameters by employing a Sliding Window Fourier Transform. The frequency components of the modes were first identified in the frequency spectrum. The damping constants could then be obtained by comparing the spectral magnitudes of a given modal component in different time windows. These Fourier techniques proved to be quite robust to noise and worked well as long as the oscillation modes were well separated and could be separately distinguished within the Fourier spectral domain.

Basically the method developed by Poon and Lee uses the rate of decay of the Fourier Transform as a rectangular window slides to determine the damping factor of the mode. The results of this method provided good correlation compared to conventional techniques. However the fundamental limitation of the Poon and Lee method was the tight restrictions on the length of the window that could be used.

It was subsequently shown that this restriction was needed to avoid errors due to the interference from the superposition of the positive and negative frequency components [9]. This interference was formulated by the large side lobes of the spectral *sinc* function introduced by the rectangular windowing. Hence, Poon and Lee specified that the window lengths only have certain discrete values, at which the interference (zeros in the *sinc* function) turned out to be zero. The problem was that the window length was dependent upon the modal frequency, and hence this frequency had to be accurately estimated prior to the windowing implementation. Additionally, a different set of windows was required to process every different mode present. O'Shea [8] extended Poon and Lee's Fourier method and showed that a relaxation of the restriction on window lengths could be achieved by applying a smooth tapering window (Kaiser window) rather than a rectangular one [40], [9].

Although the sliding spectral window methods in [39] and [9] were robust to noise, they only allowed analysis of multiple modes if the modes were sufficiently well separated to be resolved with conventional Fourier techniques. To deal with multiple closely spaced modes Poon and Lee [41] developed a modified technique. For lightly damped closely spaced low frequency oscillation modes exhibiting beat phenomenon they made use of the imaginary part of the Fourier Transform of the swing curves. Their simple dual modal case was modelled by:

$$f(t) = a_1 \cos(2\pi f_1 t) e^{-\sigma_1 t} + a_2 \cos(2\pi f_2 t) e^{-\sigma_2 t} \tag{1.1}$$

and f_1 and f_2 were assumed to be close in frequency and unable to be resolved using Fourier techniques.

Although not specifically stated by Poon and Lee, a major problem with their method was that it was not straightforward to determine either f_1 or f_2. It was therefore not straightforward to determine the damping factors.

O'Shea [42] showed that a simpler and more reliable method of determining modal parameters for closely spaced modes was to extend the earlier Sliding Window method in [9] by calculating the spectrum in more than two windows. Using the results from the multiple spectral windows, a set of simultaneous equations in the desired parameters could be created. These parameters were the complex amplitudes, frequencies and damping factors of the modes. These simultaneous equations could then be solved in a least squares sense [4] to obtain estimates for the modal parameters. The presented simulations indicated good results.

1.4.2 Continuous Random Disturbances

The methods for modal analysis so far discussed all assumed that the data record could be well modelled as a sum of complex exponential modes. This is an acceptable model if the record has been obtained after a single isolated disturbance. However this is not acceptable for a record obtained from continuous random disturbances (which is the scenario for power systems in normal operation [11]). The following sections investigate modal parameter analysis in relation to continuous random disturbances.

1.4.2.1 Autocorrelation Methods

The estimation of modal parameters from data records corresponding to continuous random disturbances was discussed by Ledwich and Palmer in [11]. They reasoned that the continuous random disturbances exciting a power system in normal operation should be fractal in nature, having a $1/f$ shaped spectrum [11], i.e. it should be equivalent to integrated white noise. They also reasoned that a power system could be approximated as an IIR filter. With these assumptions about the excitation and power system, Ledwich and Palmer showed that if one differentiated the output of the power system, the result would be equivalent to the output of an IIR filter driven by white noise. Since the autocorrelation function of a system driven by white noise reveals the impulse response of that system

[43], then the autocorrelation function of the differentiated power system disturbance output should be the impulse response of the power system, i.e. it will have the form of a sum of complex exponentials. The modal parameters can then be determined using Prony analysis [11].

Autocorrelation techniques were further examined by Banejad and Ledwich [12] to determine resonant frequencies and mode shape by modelling disturbances using white noise to represent customer load variations and an impulse to represent a disturbance. The simulation results provided tangible relationships to a known system's eigenvalue, resonant frequencies and mode shape, but did not make any reference to the limitations of mode spacing.

1.4.2.2 Review of Kalman Filter Innovation Strategies

In the 1950s, increased control requirements for advancing avionics led to the formulation of what is now commonly known as the Kalman filter. Although earlier radar tracking work by Swerling had formulated very similar algorithms [44] the more highly recognised publications by Kalman [45], [46] then Kalman and Bucy [47] were generally recognised as the origins of the Kalman filter. Since that time the Kalman filter has been recognised as a very important (and optimal) linear estimator; it has been used extensively in a multitude of areas that encompass stochastic models, state and parameter estimation and control requirements. There have also been a multitude of Kalman filter variations for non-linear systems, such as the extended Kalman filter [48] and unscented Kalman filter [49]. In this thesis, the focus of interest is on the Kalman filter innovation. The innovation is defined as the difference between the measured output and the estimated output [50]. It is well known that the innovation from a Kalman filter is spectrally white as long as the assumed model parameters are valid [50, 51]. However under faulty or changed conditions the innovation sequence will demonstrate large systematic trends as the model will no longer represent the physical system [50].

Various Kalman filter innovation approaches, that target fault detection, diagnosis of dynamic systems and least squares estimation, are presented in [50-55]. In this thesis the Kalman filter model is used to estimate the system output. By monitoring the whiteness of the innovation one can detect if there are any sudden detrimental changes in the model parameters [50], otherwise the innovation sequence is equivalent to the original excitation under normal plant conditions [51].

1.5 Review of Frequency Estimation Methods

Although modal damping estimates are of critical importance, the frequency of the modes also provides an opportunity to determine changes in system behaviour and dynamics. In the case of large interconnected power systems, if a particular major site disconnects from a national grid (example South Australia disconnects from the Australian Eastern network) then the resulting power system will undergo a dynamic shift in an attempt to re-establish an equilibrium state. In doing so it is expected that the frequencies of the remaining modes will also change. Therefore to rapidly detect and estimate the changes in modal frequencies is of critical importance.

The nature of the frequency changes that occur in a power system over time will not be known precisely. To allow for the arbitrary nature of the frequency trajectories, polynomial modelling will be used. Note that if the frequency trajectory is a polynomial as a function of time, then the phase trajectory will also be polynomial. It will be assumed that the component/mode in question is given by:

$$z_r(n) = b_0 e^{j\phi(n)} + z_w(n), \tag{1.2}$$

where b_0 is the amplitude, the polynomial phase coefficients are given by $\{a_0, a_1, \ldots, a_P\}$ and the phase is:

$$\phi(n) = \sum_{p=0}^{P} a_p n^p \tag{1.3}$$

and $z_w(n)$ is complex white Gaussian noise.

1.5.1 Polynomial-Phase Estimation Methods

To determine the frequency/phase trajectory of a component/mode conforming to the model in (1.2) it is necessary to determine the polynomial phase coefficients. An obvious solution to the problem of obtaining estimates of these parameters is to use the direct Maximum Likelihood (ML) method. However as discussed in [56] the implementation of this method is very computationally intensive, requiring a *P*-dimensional search. To overcome the computationally restrictive implementation of the ML method, various authors have introduced alternative strategies [57], [58], [59], [60] and [61]. Fundamentally these strategies employ multi-linear transforms that reduce the search requirements from a *P*-dimensional search to a far more computationally efficient *P*-one-dimensional search.

More recently O'Shea introduced a "time-frequency rate" representation which is defined in equation (1.4) [16]:

$$CP_{z_r}(n,\Omega) = \sum_{m=0}^{(N-1)/2} z_r(n+m) z_r(n-m) e^{-j\Omega m^2}. \tag{1.4}$$

This representation reveals the rate of change of frequency of a signal as a function of time. This has some relevance to the power system scenario where frequency changes are of particular interest. If *n* is set equal to 0 in equation (1.4) the Cubic Phase (CP) function is obtained. This function has been demonstrated to be very effective in the estimation of Polynomial Phase Signals (PPS) up to orders of $P = 3$. The computationally efficient implementation of the CP was procedurally outlined by O'Shea in [62]. This fast algorithm was shown to produce

predictable estimate Mean Squared Errors (MSE) in close proximity to relevant Cramér-Rao Lower Bounds (CRLBs), above a given Signal to Noise Ratio (SNR) threshold. The relevant CRLBs associated with the Polynomial Phase Coefficients for a given order PPS are outlined in [63].

Generalised higher order (HP) phase functions were also introduced by O'Shea in [62]. The HP function formed a multi-linear extension to the CP function, specifically for the purposes of parameter estimation of PPS of order greater than three. The definition of this function is shown below in (1.5),

$$HP_{z_r}^{P}(n,\Omega) = \sum_{m} K_{z_r}^{P}(n,m)\, e^{-j\Omega m^2}, \tag{1.5}$$

where $$K_{z_r}^{P}(n,m) = \Pi_{i=1}^{I}\left[z_r\left(n + c_i m\right)^{k_i}\, z_r\left(n - c_i m\right)^{k_i} \right]^{r_i *}$$

is the kernel and $[.]^{r_i *}$ indicates conjugation of $[.]$ *iff* $r_i = 1$.

The parameters c_i, k_i, r_i, and I are selected to ensure unbiased parameter estimates for a phase polynomial of order P. The choice of these parameters was conducted in a comparable manner to procedures outlined in [61] and [59], to ensure unbiased phase coefficient estimates.

Further work on the HP function was explored by Farquharson *et. al.* in [56]. New HP functions were devised that allowed parameters to be determined in isolation [56]. It was noted in [56] that the new HP functions had some similarities to functions introduced in [60], but they also had some notable differences. In particular the new HP function based estimates in [56] had much lower SNR thresholds and were therefore much more practically applicable.

1.6 Conclusion

Despite the advances of the last decades for modal parameter estimation techniques, there is a common recognition by many authors that no

individual technique accounts for all the various situations that arise in practice. Each tool has its own merits and applications, and provides a different view into dynamic system behaviour. With technological advances constantly changing the face of power systems, the need to continually improve oscillation modal estimation algorithms has been widely accepted as being very important. Reliable detection of sudden detrimental changes in modal oscillations is also extremely important so that catastrophic failures can be avoided. Relatively little work has been done to date on optimal procedures for such detection.

In relation to frequency and frequency rate estimates methods outlined earlier, it is important to keep in mind the desire of the power industry to obtain estimates as quickly as possible with an acceptable level of error. In the situation of angle measurements from sites around a national power system, it is generally recognised that these recorded measurements have a reasonable SNR. These SNRs should be adequate for the PPS modelling approaches considered in this thesis for estimating/detecting changes in post-separation modal frequencies.

Therefore the major focus of this thesis will be the rapid acquisition of system information (both modal damping and modal frequency) under the scenario of sudden detrimental change to a quasi-stationary large interconnected power system.

1.7 Organisation of the remainder of the thesis

The remainder of the thesis is organised as follows. *Chapter 2* introduces a unique energy based method that is primarily focused on the rapid detection of deteriorating modal damping in power systems. In *Chapter 3* the technique in *Chapter 2* is further extended and optimised for monitoring of individual modal damping changes in multi-modal power systems. *Chapter 4* will then introduce another prospect of modal parameter monitoring which is based around the Kalman filter innovation

spectrum. *Chapter 5* will introduce a new class of multi-linear functions for polynomial phase signal analysis and examine implementation opportunities in power system monitoring. *Chapter 6* will be devoted to a general discussion and *Chapter 7* will present conclusions and future directions.

Chapter 2

2 Rapid Detection of Deteriorating Modal Damping

2.1 Introduction

In this chapter a new method is introduced that deals with the problem of detecting sudden changes in the damping of inter-area modes in large interconnected power systems. The motivation for focus on rapid detection, rather than the more traditional modal parameter estimation, is drawn from the verity that standard modal parameter estimation methods require long data records to yield accurate estimates – typically an hour or more of data is needed. This is too long to wait if there is a sudden and seriously problematical change of damping.

While accurate estimation of the modes requires long time scales, detection of sudden deterioration from a known quiescent point can be done in much shorter time scales (typically a minute). The "sudden change" can be detected very easily via a sudden change in the energy of the system modes. However to be able to make an informed decision on whether a change has actually occurred a statistical characterisation of the quiescent system energy must be established. Once the statistical characterisation has been formulated the thresholds for rapid detection of modal deterioration may be set that can provide an alarm benchmark with a defined confidence level.

2.2 The Power System Model in the Quiescent State

To establish an energy characterisation of a power system, first an understanding of system behaviour is required. In [11] the power systems are assumed to be in normal operation and as such, are assumed to be excited by multiple quasi-continuous random disturbances. Such disturbances arise naturally as a result of load changes in the form of connections and disconnections. Once excited, each of the disturbances is then damped according to the modal resonances of the power system. This type of scenario can be modelled well with a single continuous random background noise exciting a filter whose resonances are characteristic of the power system. The model for the excitation is based on the work of Ledwich and Palmer [11]. This model introduced the hypothesis that the disturbance is fractal in nature, possessing a $1/f$ type spectral shape. Therefore the excitation noise can be well modelled as white noise that has passed through an integrator. The power system output is then the output of a "power system filter" driven by the above-mentioned excitation. This model is illustrated in Figure 2-1.

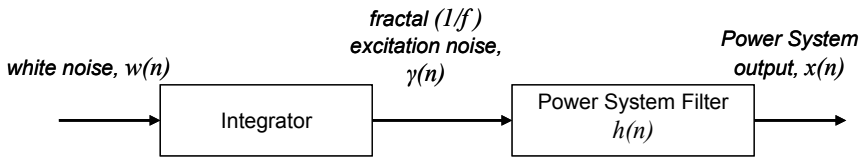

Figure 2-1 Model for quasi-continuous modal disturbances in a power system.

The model in Figure 2-1 can be used to derive the equivalent model shown in Figure 2-2. As indicated in Figure 2-2, if the output of the power system is differentiated, the resulting signal, *y(n),* can be considered to have been obtained from a white noise based excitation of the power system filter, *h(n).* It is recommended that the measured output, *x(n),* be taken as the angle of the generator cluster at the measurement point, with respect to the steady state (i.e. *50Hz/60Hz*) angle component. The measurement point to extract the "angle of the generator cluster" is

ideally obtained according to the procedure in [23]. This procedure maximises the lightly damped inter-area mode information and minimises the effect of the more heavily damped local modes (that are less critical in regards to overall supply stability and control).

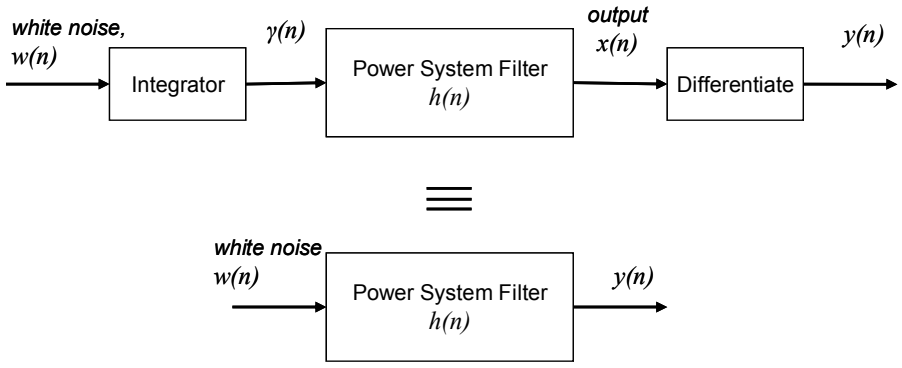

Figure 2-2 Equivalent model for quasi-continuous modal oscillations in a power system.

With the power system model established, a statistical characterisation of the system energy will be formulated in the following section.

2.3 The Power System Statistical Characterisation

The rationale behind the method proposed in this chapter is that the energy of the output, *y(n),* will remain stable unless either the power system filter transfer function or the excitation noise level changes suddenly. If the power system transfer function changes such that there is less damping of the excitation noise, then the result is more energy within the output signal. Alternatively if there is a sudden (and sustained) increase in excitation energy there could be a fault. In either case an alarm should be created so that appropriate investigation/control can be implemented.

This section will apply the knowledge of the power system model established in [11] to generate a statistical system characterisation. A formula is derived for a probability density function (PDF) of the energy

y(n) under quasi-stationary operating conditions. The statistical characterisation of the energy *y(n)* enables a reliable threshold to be set so alarms can be raised if the energy deviates too much from these quasi-stationary operating conditions. These operating conditions can be determined by the types of techniques described in [11]. As the detection condition is for large detrimental change then the False Alarm Rate (FAR) for detection is usually set fairly low (1% or lower). Such a low FAR facilitates the minimisation of unwanted false alarms. Once an alarm has been triggered, further monitoring of the system energy is necessary. Sequential data windows are collected and a statistical analysis with respect to the PDF is undertaken. Repeated alarms due to consistently high energy readings would induce corrective action by the power system utility.

To develop the PDF for the energy in *y(n)* we return to the model in Figure 2-2. It follows from Figure 2-2 that the output signal's discrete Fourier transform is:

$$Y(k) = H(k)W(k), \tag{2.1}$$

where *H(k)* is the discrete Fourier transform (DFT) of *h(n), W(k)* is the DFT of *w(n)* and *Y(k)* is the DFT of *y(n)*. Now, according to Parseval's theorem, the energy of *y(n)* can be determined from the samples in either the time domain or the frequency domain. Because the samples are independent in the frequency domain, though, this domain is most conducive to developing a statistical characterisation. Note also, that for real signals, all the information in the frequency domain is contained in the positive half of the spectrum – the information in the negative half is just a copy of that contained in the positive half. Using Parseval's theorem and the fact that half the energy is contained in the positive half of the spectrum for real signals, total energy of *y(n)* is:

$$E = \frac{2}{N}\sum_{k=1}^{N/2}\{|H(k)|^2|W(k)|^2 + \frac{1}{2}|H(0)|^2|W(0)|^2\} \quad (2.2)$$

Note that $W(k)$ is a complex Random Variable (RV) with real and imaginary parts:

$$|W(k)|^2 = \mathrm{Re}\{W(k)\}^2 + \mathrm{Im}\{W(k)\}^2 \quad (2.3)$$

Now if the variance of *w(n)* is σ^2, then the left hand side of (2.3) is a chi-squared RV with two degrees of freedom and variance, $\frac{\sigma^2}{N}$ [15]. Therefore the PDF at any discrete ensemble frequency k_i is:

$$f\left\{|W(k_i)|^2\right\} = \frac{N}{\sigma^2}e^{\frac{-xN}{\sigma^2}}, \quad (2.4)$$

where *x* is the random variable power.

Using (2.1) and (2.4) the PDF of $Y(k_i)$ can be deduced to be:

$$\begin{aligned} f_y\left(Y_{k_i}\right) &= \left|\frac{1}{|H(k_i)|^2}\right| f_w\left(\frac{x}{|H(k_i)|^2}\right) \\ &= \frac{N}{|H(k_i)|^2\sigma^2}e^{-x\frac{N}{|H(k_i)|^2\sigma^2}}. \end{aligned} \quad (2.5)$$

From (2.2) it is evident that the energy is obtained by summing $N/2+1$ RVs and then scaling by *2/N*. Furthermore these RVs have PDFs given by (2.5). The PDF of the sum is obtained by convolving the PDFs of all the RVs being summed. That is, the PDF of this sum is:

$$f_y(x) = f_{y_{N/2}}(x_{N/2}) * f_{y_{N/2-1}}(x_{N/2-1}) * \cdots * f_{y_0}(x_0) \quad (2.6)$$

$$= \frac{N}{\sigma^2} \begin{bmatrix} \frac{1}{2}\left|H\left(0\right)\right|^{-2} e^{-xN\frac{1}{2}\left|H(0)\right|^{-2}\sigma^{-2}} \\ *\left|H\left(1\right)\right|^{-2} e^{-xN\left|H(1)\right|^{-2}\sigma^{-2}} \\ *\cdots*\left|H\left(N/2\right)\right|^{-2} e^{-xN\left|H(N/2)\right|^{-2}\sigma^{-2}} \end{bmatrix}, \qquad (2.7)$$

where * denotes convolution.

Finally the PDF of the energy is obtained from the sum by scaling by *2/N*. The final energy PDF must therefore have its axes re-scaled accordingly.

From the PDF the threshold for detection of change can be formulated. Establishing say the 1% false alarm rate is obtained via the cumulative summation of the PDF area until the 99% point is determined.

2.4 PDF Verification

To verify the theoretically determined system output PDF, a comparison of a theoretical PDF and simulated histogram was undertaken. Using known modal parameters, simulations created a collection database of outputs that were formulated into a histogram. A theoretical PDF was then formulated and compared directly to the histogram.

The procedure for verification involved 10,000 simulation runs of random noise, $N \sim (0,1)$, feeding a known modal system, depicted in Figure 2-2 and defined below:

$$h(n) = h_1(n) + h_2(n) \quad , \qquad (2.8)$$

where

$$h_i(n) = A_i e^{-\sigma_i n} \sin(\omega_i n + \phi_i) \quad i = 1,2 \qquad (2.9)$$

with modal parameters:

$$\omega_1 = 1.7r/s, \sigma_1 = -0.4s^{-1}, A_1 = 1, \phi_1 = 0^\circ$$

$$\omega_2 = 2.7r/s, \sigma_2 = -0.52s^{-1}, A_2 = 1, \phi_2 = 0^\circ$$

Energy measurements were based on a 20, 40 and 60 second data window with a sampling rate of 5Hz. Statistical characteristics of the simulated histogram and of the theoretical PDF were calculated and compared. The statistical characteristics examined were the first three central moments, mean, variance and skewness [64]. The percentage errors between the theoretical and simulated PDFs are shown in Table 2-1. The errors are all comparatively low, inspiring confidence in the fact that the derived PDF is correct.

TABLE 2-1 RELATIVE ERROR OF MOMENTS

TIME WINDOW		20SEC	40SEC	60SEC
NOISE VARIANCE		1.0	1.0	1.0
% ERROR	MEAN	0.04%	0.43%	1.67%
	VARIANCE	0.82%	1.65%	0.24%
	SKEWNESS[64]	2.59%	5.76%	6.53%

Further validation of the theoretical PDF is provided by a visual comparison with a histogram. The result from a 60sec analysis window is shown in Figure 2-3. There is a close visual alignment.

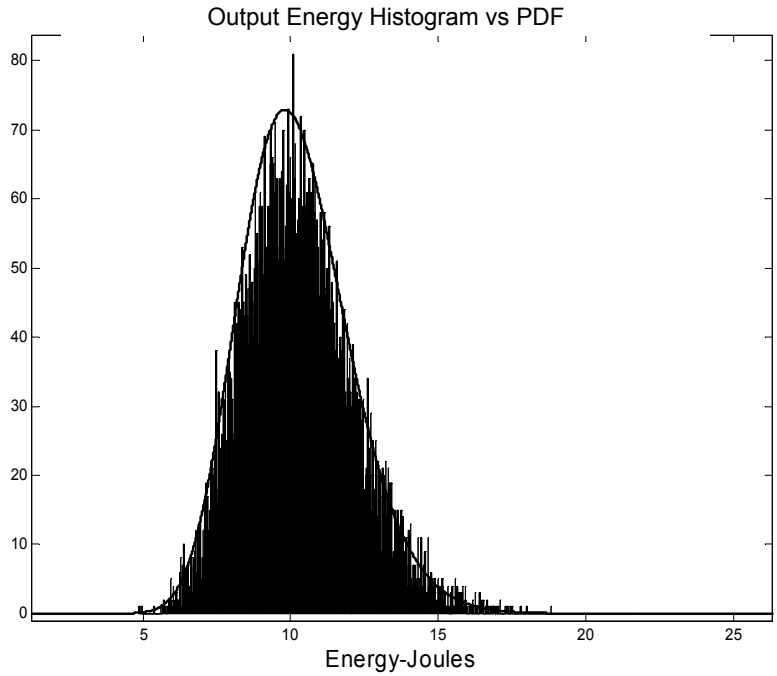

Figure 2-3 Energy PDF and Histogram Comparison (60 second window).

2.5 Setting the Threshold for Alarm

From the PDF the threshold for detection of change can be formulated. Establishing say the 10% false alarm rate is via the cumulative summation of the PDF area until the 90% point is determined.

2.6 Simulated Results

It will be seen in this section that the simulations for detecting change provided good results. The modal values were initially set to:

Mode 1: $e^{-0.4t}\sin(2t) \quad \therefore \sigma_1 = -0.4 \;\&\; \omega_1 = 2.0r/s$

Mode 2: $e^{-0.52t}\sin(2.7t) \quad \therefore \sigma_2 = -0.52 \;\&\; \omega_2 = 2.7r/s$

In the 300 minutes of simulated data, mode 1 underwent two damping changes; a step deterioration to $\sigma_1 = -0.1$ damping at 100 mins and another step change to $\sigma_1 = -0.2$ damping at 200 mins. The variance of

the driving noise, *w(n)*, was set to unity. The output, *y(n)*, was generated as per the model shown in Figure 2-2. Energy measurements for the output were then taken over 1 minute block periods. The first 100 minutes represent the quasi-stationary system prior to the damping changes.

The graphical results and relevant statistics are shown in Figure 2-4 and Table 2-2 respectively. The results are as one would expect – a low alarm rate for the quiescent conditions, a high alarm rate during the major damping change, and a lesser alarm rate during the period when the damping "corrects itself" somewhat.

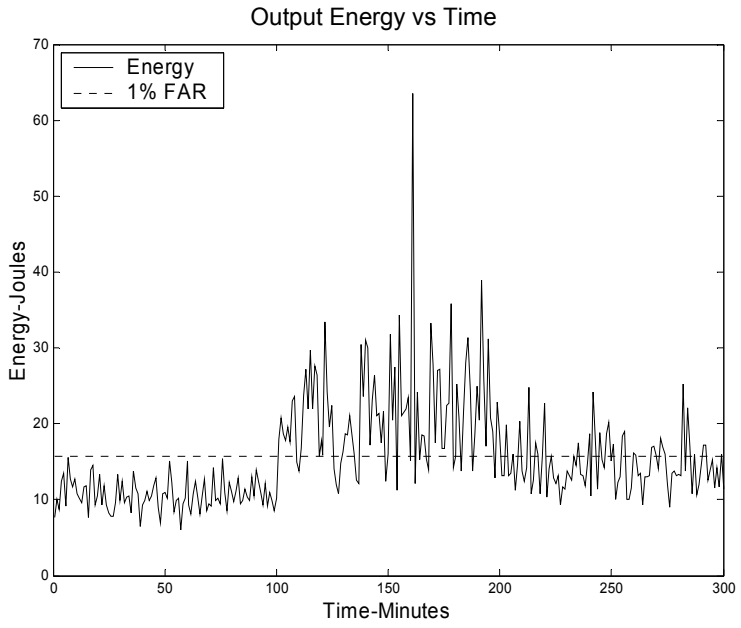

Figure 2-4 60 second Data Window of Energy Measurements with 1% False Alarm Rate Shown.

TABLE 2-2 PERCENTAGE OF ALARMS

	FALSE ALARM RATE SET AT 1%		
	0-100 MIN NO CHANGE $\left(\sigma_1 = -0.4s^{-1}\right)$	100-200 MIN STEP CHANGE $\left(\sigma_1 = -0.1s^{-1}\right)$	200-300 MIN STEP CHANGE $\left(\sigma_1 = -0.2s^{-1}\right)$
% OF TIME ALARM ON	0.0%	80.0%	32.0%

2.7 Validation of Method using MudpackScripts

In this section the energy based method is verified using the Case13 MudpackScript data.

This data set is useful as it contains an initial 2 hour section that may be regarded as representing the power system in a quasi-stationary state with acceptable damping. It is this initial 2 hour section that is analysed by the LTE to generate the required system PDF. From this the desired threshold can be set. This data set used for verification represents the Queensland (QNI) mode of the power system. Within this QNI data, the damping suddenly deteriorates from an acceptable -0.25 to a very undesirable -0.05. The trajectory of the damping factor associated with the Case13 script can be seen in Figure 2-5.

The detection results from the analysis of the first 12 hours of data can be seen in Figure 2-6. The analysis window used is a block window set to 60 seconds at a 5Hz sampling rate. Comparison of Figure 2-5 and Figure 2-6 shows that the energy experiences sudden jumps when the damping experiences sudden jumps, as one would hope. Various different alarm thresholds are shown in Figure 2-6; for the data under analysis it is seen that if one uses a 1% false alarm rate, one only gets alarms when there are genuine damping changes.

In the following section, the energy detection technique will be applied to real multi-site data obtained from wide area monitoring sites.

Figure 2-5 Mode Trajectory of QNI Case13 MudpackScript Data.

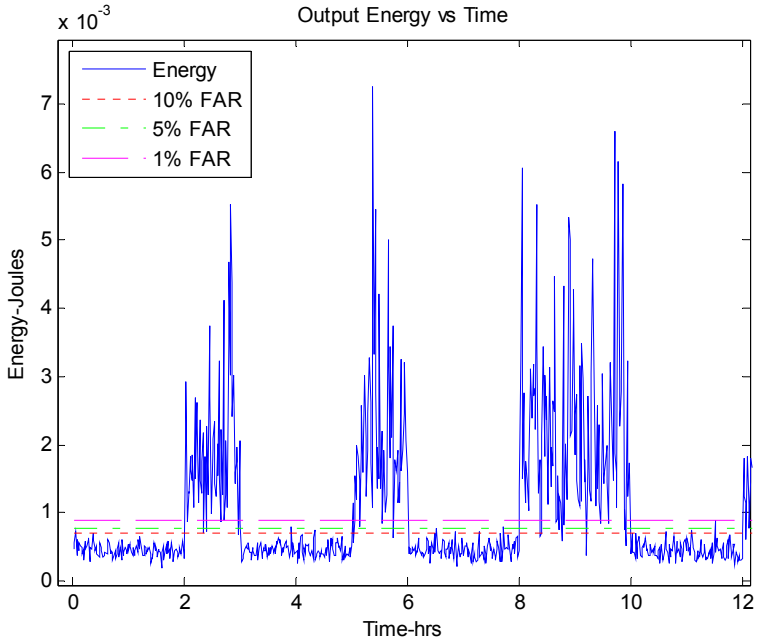

Figure 2-6 Output Energy vs 1, 5, 10% thresholds.

2.8 Application to Real Data

To apply the energy detection method to a real data situation a long term estimator is required to provide an estimation of the quiescent modal values. Initially the long term estimator establishes estimates for the system transfer function. From this an estimated impulse response can be determined. With this knowledge an approximation of the variance of the excitation signal, *w(n)* in Figure 2-1, can be estimated. Once the system transfer function, *h(n)*, and the excitation variance, σ^2, have been estimated then the expected energy PDF can be formulated. It is this formulated PDF that enables a threshold to be set (given a suitable false alarm rate). Note that the long-term estimate is periodically updated, and the threshold is changed, based on the updated estimate.

The process for simultaneously performing the long-term estimation, generating the energy estimate, thresholding and alarming is depicted diagrammatically in Figure 2-7. As shown in Figure 2-7, the first task is to differentiate the power system output signal (as per the model in Figure 2-2). The long term modal estimator used in this thesis is based on work by Zhang and Ledwich [13] and applies a greater than one hour data window to the differentiated output signal, *y(n)*, and generates a system transfer function in the Laplace domain. By applying the traditional inverse Laplace transform method of partial fraction expansion, the individual modes can be determined and an estimated impulse response found.

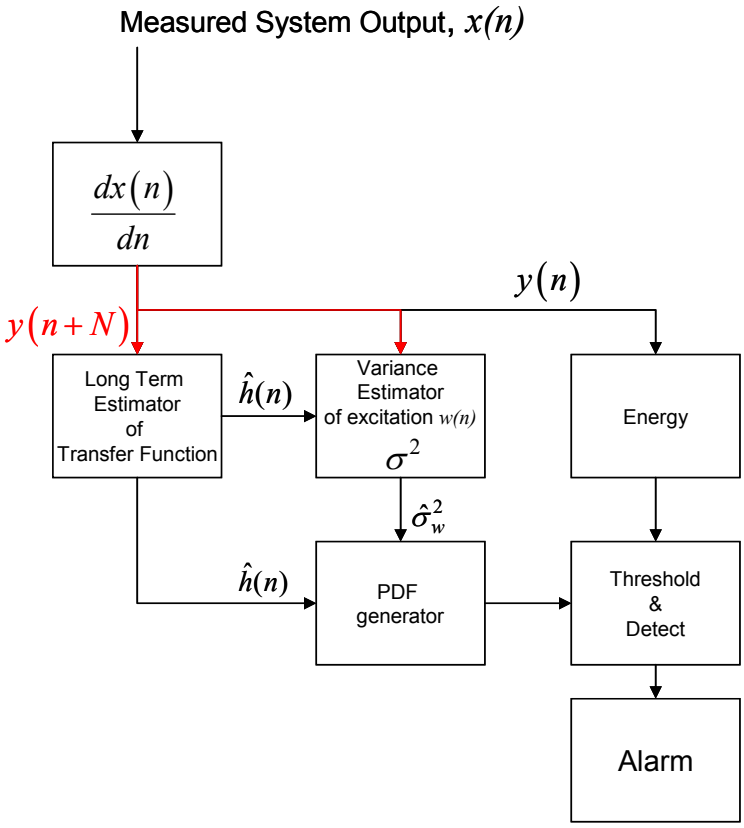

Figure 2-7 Short Term Energy Detection Applied to Real Data, red denotes past data used to formulate long term estimates.

Once an estimate of the transfer function is found then an estimate of the excitation spectrum may be determined according to:

$$\hat{W}(k) = \frac{Y(k)}{\hat{H}(k)}, \tag{2.10}$$

where $Y(k)$ and $\hat{H}(k)$ denote the DFTs of $y(n)$ and $\hat{h}(n)$ respectfully, evaluated at bin, *k*.

Then the estimate of the excitation variance (noise power) is estimated as:

$$\hat{\sigma}_w^2 = \frac{1}{N}\sum_{k=0}^{N-1}\left|\hat{W}(k)\right|^2. \tag{2.11}$$

At this point the two system characteristics, $\hat{\sigma}^2$ and $\hat{H}(k)$, are established and can then be employed to generate the required system PDF. Once the system PDF is established a suitable threshold for alarm can be set with respect to a desired FAR.

2.8.1 Results of Real Data Analysis

In this section, real multi-site data obtained from the Australian power system is analysed using the energy based method. The recorded data was collected on 02/10/2004 over a 24 hour period and is shown in Figure 2-8. In this section the first 6 hours only will be examined. The measurement sites that represent the intra-area generation clusters are referred to as Queensland, NSW, Victoria or South Australia, as previously discussed in Chapter 1. In the analysis performed, the LTE used the first three hours of data to determine the site transfer functions and impulse responses. The plots in Figure 2-9 to Figure 2-12 show the site impulse responses as estimated by the long term estimator. Subsequently, the expected energy PDF for a short-term window of 60 seconds is shown in Figure 2-13 to Figure 2-16. These figures of site PDFs also contain verification histograms that would result from a pure white noise, of power $\hat{\sigma}^2$, feeding into the respective site transfer functions. Finally in Figure 2-17 to Figure 2-20 the resulting site energy measurements are shown with respect to three false alarm rate thresholds, 1%, 5% and 10% respectively. The 60 second analysis windows do not overlap and are simple sequential block windows. In the real data, a deteriorating damping event was apparent in three of the four states at around 04:30 hours. Prior to this event, the false alarm rates were as one would expect for quasi-stationary operation. See for example, Table 2-3, which provides statistics of the actual false alarms in the first 3 hours of data. After the event at around 04:30 hours, the false alarm rates increase markedly.

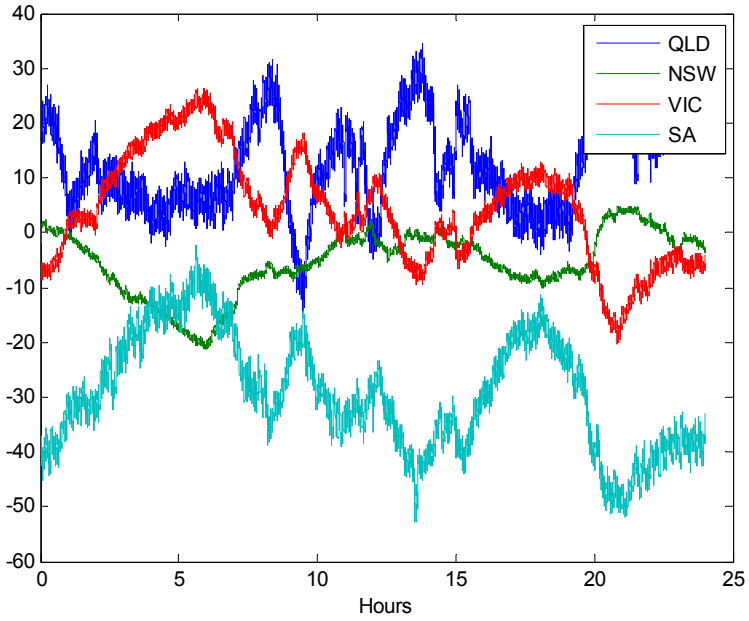

Figure 2-8 24 hours of recorded angle measurements (2nd October 2004), sites as indicated.

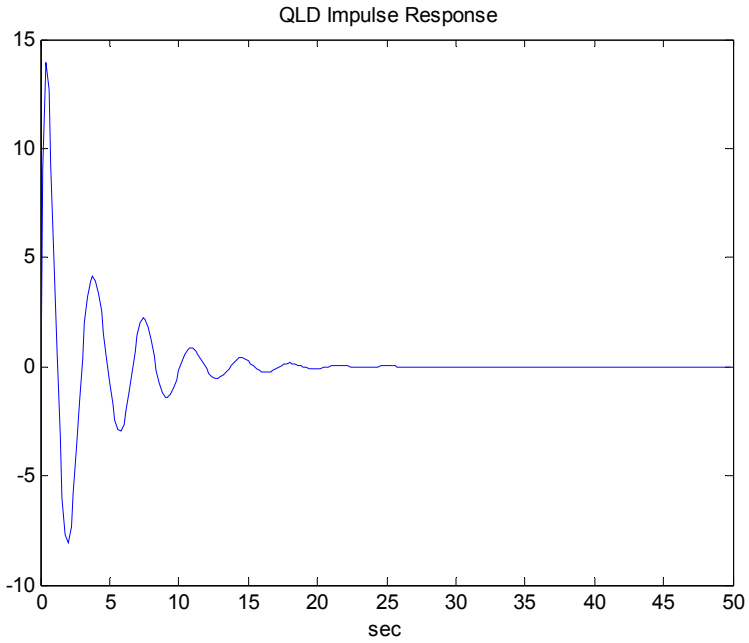

Figure 2-9 Queensland Estimated Impulse Response.

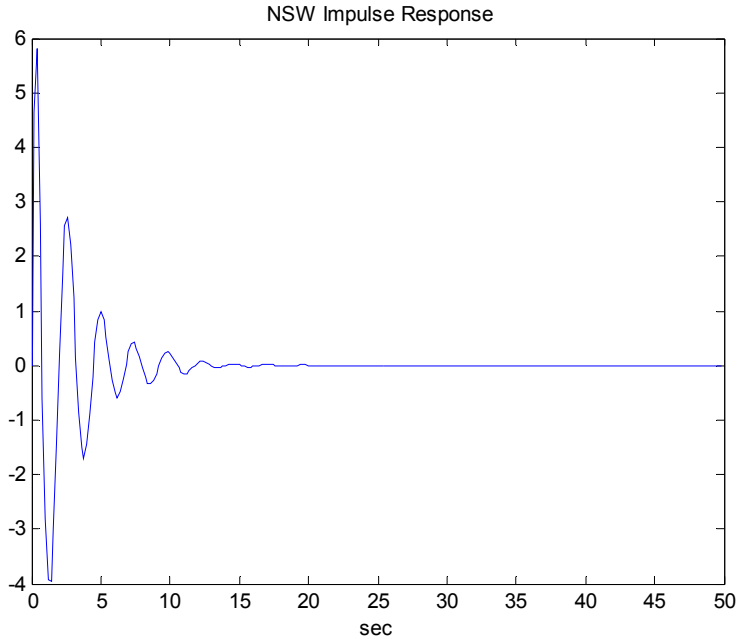

Figure 2-10 New South Wales Estimated Impulse Response.

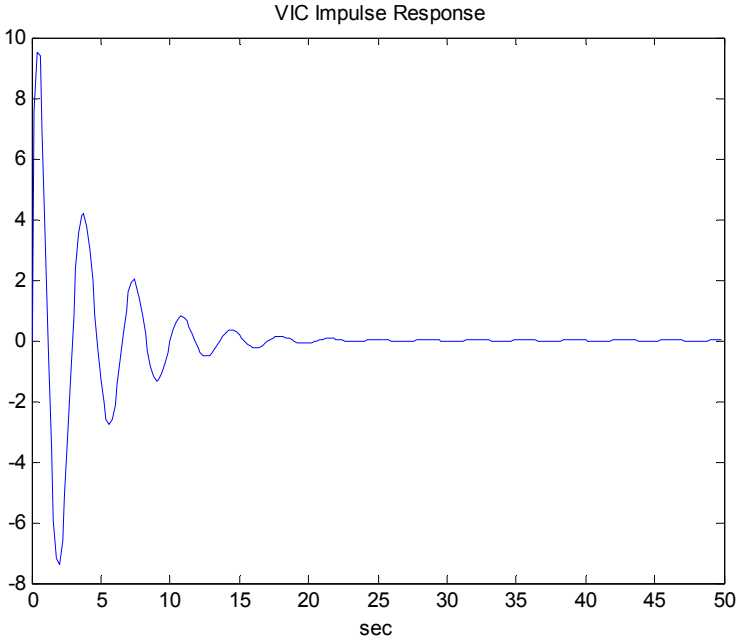

Figure 2-11 Victorian Estimated Impulse Response.

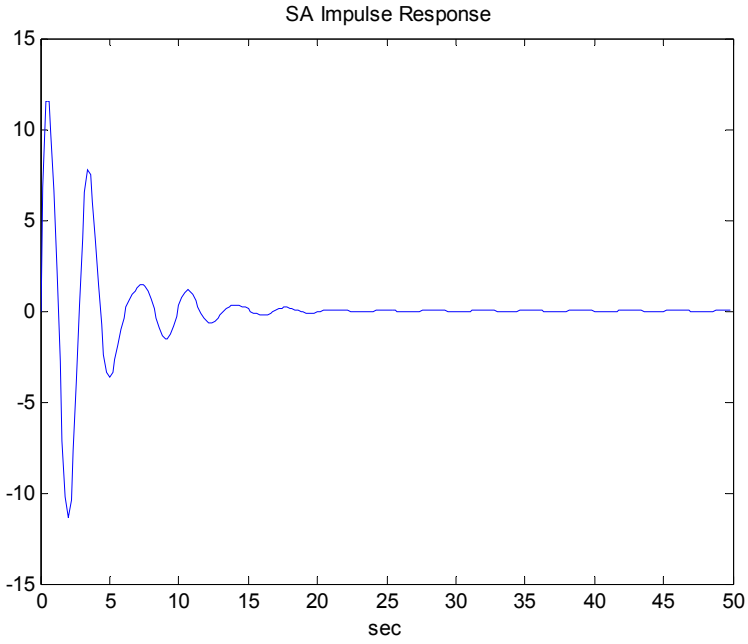

Figure 2-12 South Australian Estimated Impulse Response.

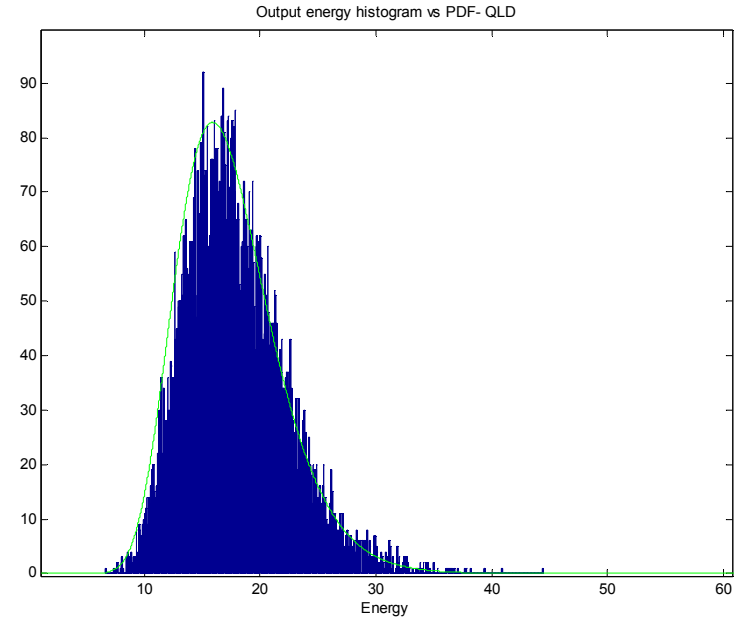

Figure 2-13 Queensland PDF Estimate with white noise verification histogram.

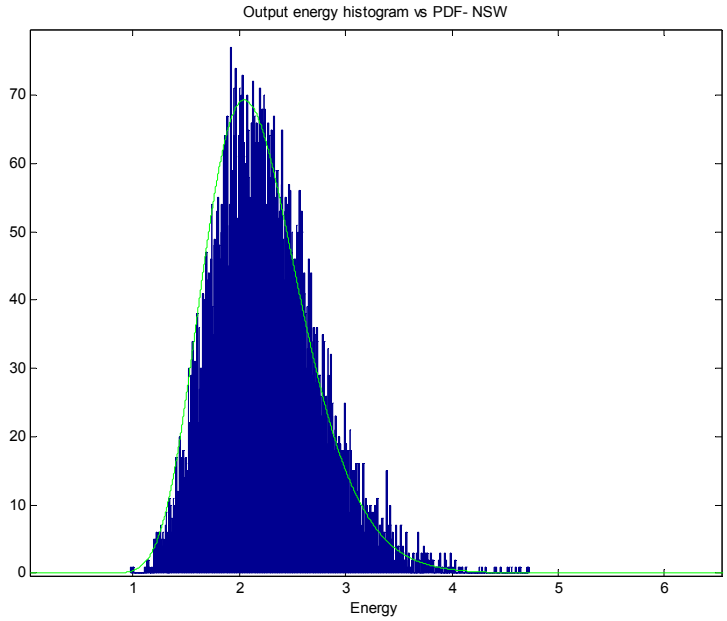

Figure 2-14 New South Wales PDF Estimate with white noise verification histogram.

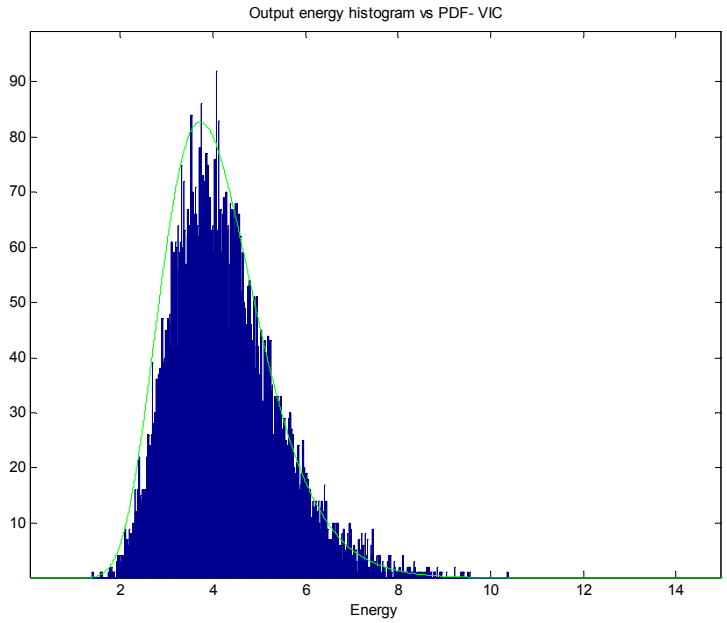

Figure 2-15 Victorian PDF Estimate with white noise verification histogram.

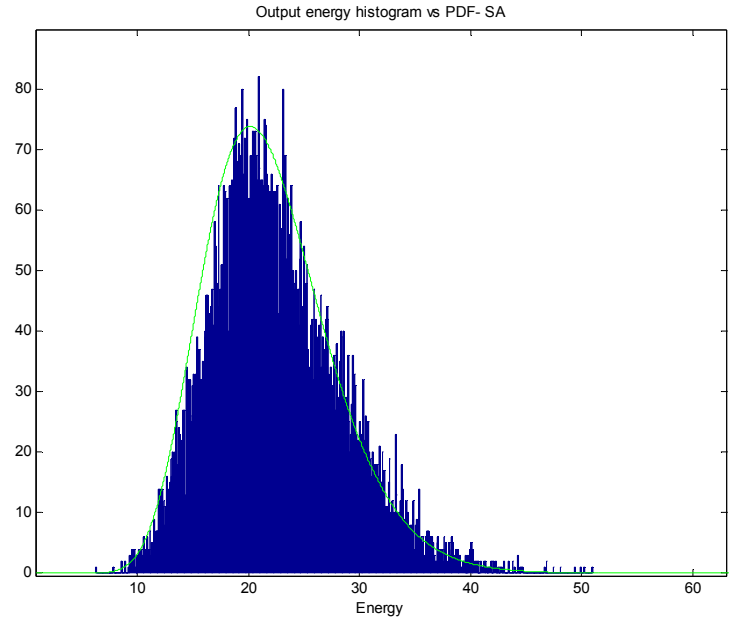

Figure 2-16 South Australian PDF Estimate with white noise verification histogram.

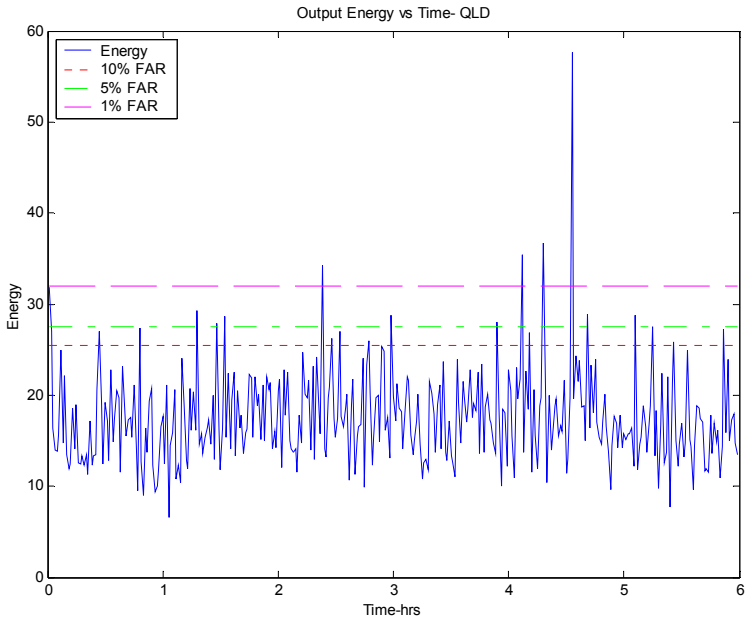

Figure 2-17 Queensland 60 second energy measurements vs various FARs shown.

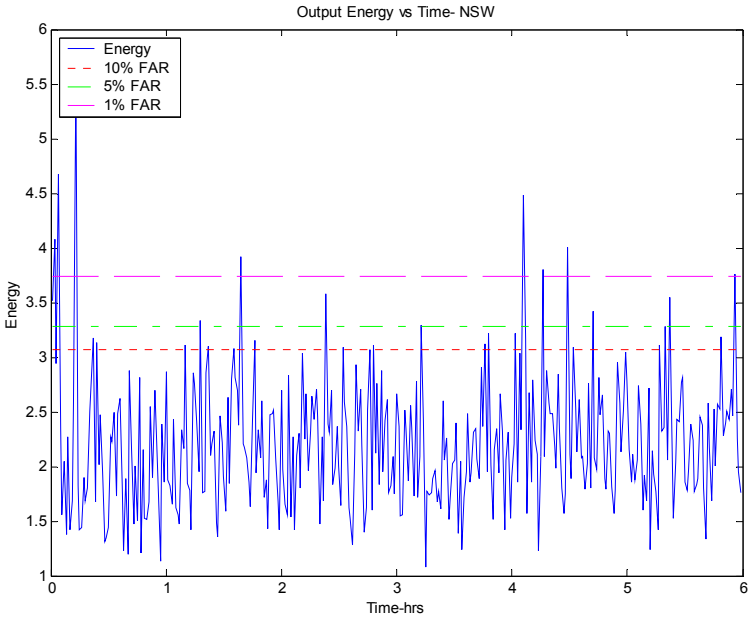

Figure 2-18 New South Wales 60 second energy measurements vs various FARs shown.

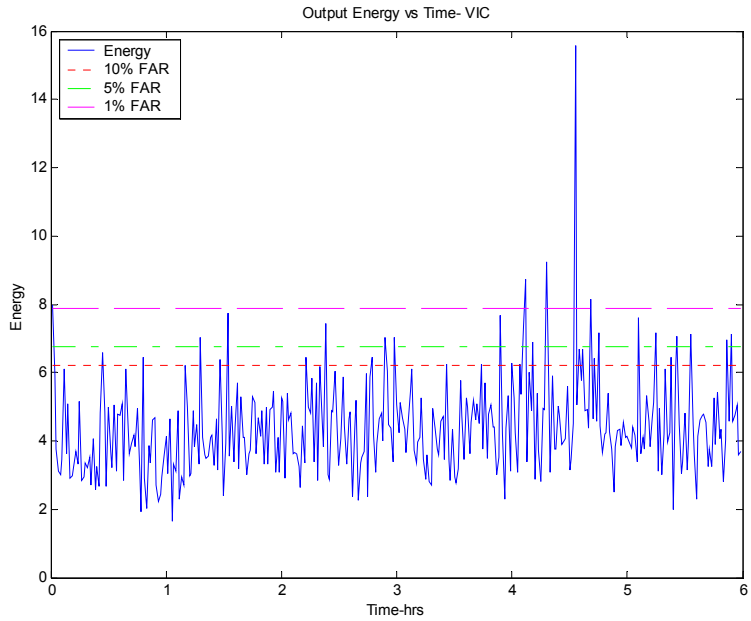

Figure 2-19 Victorian 60 second energy measurements vs various FARs shown.

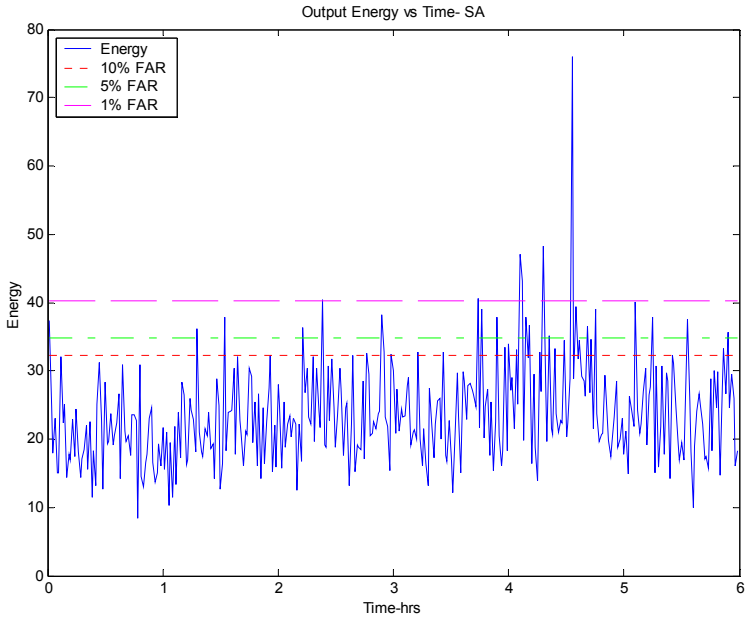

Figure 2-20 South Australian 60 second energy measurements vs various FARs shown.

TABLE 2-3 PERCENTAGE OF FALSE ALARMS OVER INITIAL 3 HOURS OF DATA

60 SECOND ANALYSIS WINDOW

SITE	FALSE ALARM RATES		
	FALSE ALARM RATE 10%	FALSE ALARM RATE 5%	FALSE ALARM RATE 1%
QLD (SOUTH PINE)	6.13%	3.34 %	1.11%
NSW (SYDNEY WEST)	8.35%	3.90%	2.23%
VIC (ROWVILLE)	9.47%	5.57%	1.39%
SA (PARA)	10.31%	6.40%	1.67%

2.9 Discussion

In the simulations shown in Figure 2-6 it was seen that the energy detector method responded in a timely manner to each deteriorating shift in damping factor. In the subsequent real data analysis the modal disturbance just after 04:30 hours can be clearly seen in Figure 2-17, Figure 2-19 and Figure 2-20. However the NSW response in Figure 2-18 does not indicate the disturbance. This is due to the weak response the particular disturbance mode has at the NSW measurement site. The justification of this statement will become more evident in Chapter 3 where the individual modal contribution for each site is estimated and shown spectrally.

In the real data case shown, it can be seen that the poor damping is only temporary as the subsequent post-disturbance energy measurements do not continue alarming. Consequently in practical real data analysis once an alarm has been "raised" it is necessary to further monitor the energy. A series of sequential data windows are collected and statistical comparisons are made with the energy PDF. Consistently high energy readings will trigger corrective action.

2.10 Conclusion

It can be seen from the simulated results that the energy detector method can provide short term alarming of modal deterioration of power systems. It does so with a predetermined level of confidence that sets the alarm at a desired false alarm rate.

Longer time windows reveal changes more clearly and can be used in conjunction with the shorter time windows to confirm or disaffirm a need for remedial action.

When there is no change in the system, the false alarms occur at close to the theoretical rates, both in simulation and in real data analysis.

An important point to note is that this Chapter examines the energy of the systems signal as a whole. It provides a very simplistic method to identify rapid modal deterioration within a system. If the system is a single mode system then any subsequent detected deterioration naturally represents the mode deterioration. If the system was a multi-mode system then this method would provide information that there had been a damping deterioration but would not identify which mode. Identification of exactly which mode is changing in a multi-mode system is an important issue as well but is not addressed in this Chapter. It will be addressed in *Chapter 3*.

Chapter 3

3 Rapid Detection of Changes to Individual Modes in Multimodal Power Systems

3.1 Introduction

The previous chapter introduced a method of rapid detection of modal deterioration by setting a threshold for energy measured from the entire system. This threshold was based on a statistical characterisation of the expected energy under quiescent conditions. Once this threshold was established, the energy of the differentiated system output signal was determined using a short time window and compared to the established threshold. The energy-based method used in the previous chapter would provide adequate information in a single mode power system if it was experiencing sudden deteriorating damping; however in multi-modal power systems it would be far more desirable to highlight which particular mode/s may be experiencing detrimental damping conditions. This would provide the power utilities a heightened ability to administer timely corrective action in the appropriate manner. Motivated by the desire to have more specific modal identification, this chapter introduces a new method for rapidly detecting individual modal deterioration in large interconnected multi-modal power systems. Any "sudden detrimental change" of an individual mode is detected using strategies derived from optimal detection theory. A statistical characterisation of a mode's test statistic is used to establish reliable thresholds for detection of

individual mode changes. To enable the individual monitoring of modal damping conditions the power system is again assumed to be excited by on-going random disturbances, corresponding to such things as load changes [11]. The next section will re-visit the stochastic power system model. Subsequent sections, 3.3 to 3.5, will then go on to apply optimal detection theory to the problem of individual modal monitoring. Section 3.6 will then present and examine simulated data results. Sections 3.7 to 3.9 will outline the integration of the technique into a real power system monitoring application and present a verification/validation stage using the MudpackScript data followed by real data analysis examples.

3.2 The Stochastic Power System Model Revisited

In Chapter 2, the stochastic power system model experimentally hypothesised by Ledwich and Palmer was presented [11]. This simplified model is again shown here in Figure 3-1.

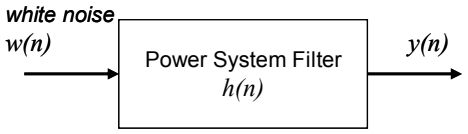

Figure 3-1 Previously introduced stochastic power system model.

One can measure the disturbance output from a power system by extracting the "angle of the generator cluster" at the measurement point with respect to the steady state (i.e. *50Hz/60Hz*) angle component. The measurements are recorded at particular points within the large interconnected power system according to the procedure in [23]. Implementing this procedure maximises the lightly damped inter-area mode information and minimises the effect of the more heavily damped local modes. Differentiating the measurement will then provide the signal, $y(n)$, in Figure 3-1. Once *y(n)* is obtained through differentiation of the measured output then the filter impulse response, *h(n)*, can be

estimated using long term estimators. From the system impulse response estimate the power of the white noise excitation, *w(n)*, may also be estimated.

It is assumed for the purposes of this section that the power system has been in a quasi-stationary operating environment for a long period of time. Then a long term parametric estimator (such as Prony's method [28]) may be used to determine the filter impulse response, $h(n)$ and its transfer function $H(z)$. Subsequently the individual modal contributions that combine to formulate $H(z)$ may be found using partial fraction analysis. Hence for any given mode *i* the transfer function $H_i(z)$ can be found, as can the impulse response $h_i(n)$.

While the work in Chapter 2 addressed the issue of rapidly detecting any changes in damping to the system, this chapter focuses on monitoring all modes to see where the critical detrimental change is occurring. To achieve this, the technique does not follow the traditional approach that has concentrated on estimating modal parameters. The rationale for this is that major changes can be detected with short data records whereas precise estimation of parameters requires long data records. The justification for this is that current algorithms in parameter estimation all require a large amount of data to ensure accurate estimates. Obtaining large data records conspires against the aim of this work, which is to *rapidly* detect and identify a sudden and significant detrimental change in modal damping within a power system. It is important to note that the approach used in this chapter supports the work outlined in [65].

3.3 Application of the Optimal Detection Strategy

To enable the detection of adverse changes to individual modes this chapter employs the theory of optimal detection of random signals [66].

The implementation of the optimal detector is as follows: let the system impulse response, $h(n)$, be considered to be the sum of $h_1(n)$ and $h_2(n)$, with $h_1(n)$ corresponding to the mode of interest, and $h_2(n)$ corresponding to the sum of all the other modal components of $h(n)$. Therefore the output, $y(n)$ is considered to have two components, $y_1(n)$ and $y_2(n)$, with $y_1(n)$ being the output due to the mode of interest and $y_2(n)$ being the output due to the other modes. Defining the "observed signal" as $y(n)$, and the "reference signal" as $y_1(n)$, then the procedure for the generation of the optimal detection statistic is depicted in Figure 3-2 [66]. It involves the whitening of both the power spectral density (PSD) of the "reference signal", $|Y_1(k)|^2$, and the PSD of the "observed signal", $|Y(k)|^2$, followed by cross-correlating. The whitening filter transfer function is the inverse of the discrete Fourier transform of $h_2(n)$. It is assumed that there are *N* samples in the observation.

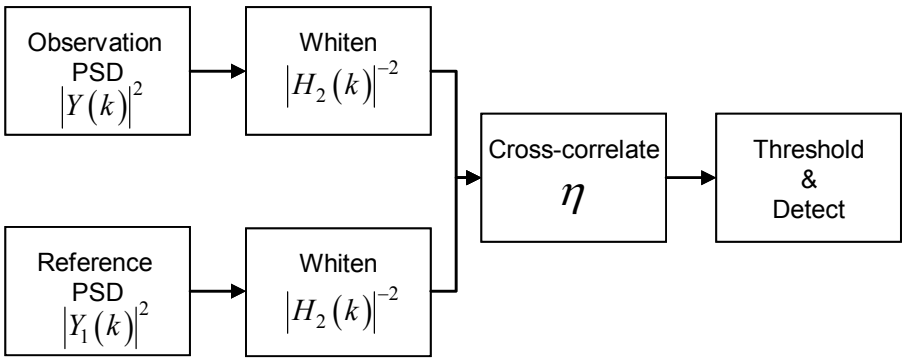

Figure 3-2 Generation of the optimal detection statistic.

It is necessary to determine how to set the threshold for appropriate detection. To do this the Probability Density Function (PDF) of the cross-correlated output must be determined. The availability of the PDF enables reliable thresholds to be set so that one can create alarms if the modal response deviates too much from the normal operating conditions. As the

main focus of this chapter is the rapid detection of large detrimental modal change (as opposed to monitoring small changes) thresholds are typically set to yield False Alarm Rates (FARs) of 1% or less.

In practice, the monitoring process would ideally involve the application of the detection algorithm to all the modes individually and at the same time. In other words, an *n-mode* power system would require *n* parallel detectors to monitor each mode. Because the detection algorithm can be implemented fairly rapidly, the computational overhead does not provide a significant barrier to monitoring all of the individual modes.

Once an alarm has been "raised" it is necessary to further monitor the modes. A series of sequential data windows are collected and statistical comparisons are made with the stationary condition PDFs. Consistently high readings will trigger corrective action on the deteriorating mode.

3.4 Individual Mode Detection Statistic Details

To specify the optimal detector for an individual mode the following quantities are defined:

$$y(n) \overset{\Im}{\Rightarrow} Y(k) = W(k)H(k) \tag{3.1}$$

$$h_1(n) \overset{\Im}{\Rightarrow} H_1(k) \tag{3.2}$$

$$h_2(n) \overset{\Im}{\Rightarrow} H_2(k) \tag{3.3}$$

$$y_1(n) \overset{\Im}{\Rightarrow} Y_1(k) = W(k)H_1(k) \tag{3.4}$$

$$y_2(n) \overset{\Im}{\Rightarrow} Y_2(k) = W(k)H_2(k) \tag{3.5}$$

where $\Im$ indicates discrete Fourier transformation.

Now to detect a change in Mode 1 (the mode of interest); choose $Y_1(k)$ as the (frequency domain) reference signal. The remainder of the frequency

domain observation, $Y_2(k)$, becomes the "interference signal". According to standard optimal detection theory, a whitening filter is created to whiten the interference:

$$H_{wh}(k) = H_2^{-1}(k). \tag{3.6}$$

Also, according to standard optimal detection theory, the whitening filter is applied to both the reference and observation signals. The corresponding PSDs are then determined:

$$\begin{aligned} PSD_{obs}(k) &= |X(k)|^2 |H_{wh}(k)|^2 \\ &= |W(k)|^2 |H_{obs}(k)|^2 |H_{wh}(k)|^2 \end{aligned} \tag{3.7}$$

$$PSD_{ref}(k) = |H_1(k)|^2 |H_{wh}(k)|^2 \; E\{|W(k)|^2\} \tag{3.8}$$

where $E\{\ \}$ denotes the expected value.

Now cross-correlate (3.7) and (3.8) to obtain the detection statistic η shown in Figure 3-2:

$$\eta = \sum_{k=-N/2}^{N/2} PSD_{ref}(k) PSD_{obs}(k). \tag{3.9}$$

To practically apply the detection statistic (3.9) in the detection process a threshold level must be determined. To intelligently set the threshold a probability density function (PDF) of the detection statistic is required. A threshold can then be set based on the PDF at a desired level of confidence.

3.5 Statistical Characterisation of the Detection Statistic η

The formulation of the Mode 1 detection statistic PDF is as follows.

To derive the detection statistic PDF, (3.9) can be expanded using (3.7) and (3.8) to give:

$$\eta = \sum_{k=-N/2}^{N/2} E\{|W(k)|^2\} \, |H_1(k)|^2 |H(k)|^2 |H_{wh}(k)|^4 |W(k)|^2 \quad (3.10)$$

which can then be re-written as

$$\eta = \sum_{k=-N/2}^{N/2} |Z(k)|^2 |W(k)|^2 \quad (3.11)$$

where $Z(k)$ is defined as:

$$Z(k) = |H_1(k)||H(k)||H_{wh}(k)|^2 \sqrt{E\{|W(k)|^2\}}. \quad (3.12)$$

Now the expression in (3.11) contains $W(k)$ which is a complex Random Variable (RV) with real and imaginary parts. Furthermore, the squared magnitude of $|W(k)|^2$ is:

$$|W(k)|^2 = \text{Real}\{W(k)\}^2 + \text{Imag}\{W(k)\}^2 \quad (3.13)$$

where Real$\{\ \}$ and Imag$\{\ \}$ denote the real and imaginary parts respectively. It is assumed that the variance of $w(n)$ is σ^2. Then *W(k)* is a complex Gaussian RV with variance, σ^2/N [67]. Then the left hand side of (3.13) is a chi-squared RV with two degrees of freedom and variance, $\frac{\sigma^2}{N}$ [67]. That is, the PDF of any discrete "bin" in the $W(k)$ power spectrum is:

$$f\{x\} = \frac{N}{\sigma^2} e^{\frac{-xN}{\sigma^2}}, \quad (3.14)$$

where *x* is the random variable, power.

Using (3.11) and (3.14) the PDF of $|Z(k)|^2 |W(k)|^2$ at discrete ensemble frequency k can be deduced to be:

$$f_{ZW_k}(x) = \left|\frac{1}{|Z(k)|^2}\right| f_w\left(\frac{x}{|Z(k)|^2}\right) = \frac{N}{|Z(k)|^2 \sigma^2} e^{\frac{-xN}{|Z(k)|^2 \sigma^2}}. \quad (3.15)$$

From (3.11) it is apparent that the detection statistic (3.9) is obtained by summing N random variables (RVs). Only half of these RVs, however, are independent, because the "negative frequency" half of the spectrum contains the same information as the "positive frequency" half [68]. Since one side of the spectrum contains all the information necessary then the PDF of the detection statistic is formulated from just one half of the spectrum. Therefore the detection statistic in (3.9) is reformulated and redefined to become (3.16):

$$\eta = \sum_{k=1}^{N/2} PSD_{ref}(k) PSD_{obs}(k) + \frac{1}{2} PSD_{ref}(0) PSD_{obs}(0). \quad (3.16)$$

Because (3.16) indicates that the threshold is the sum of $N/2+1$ independent RVs, its PDF can be computed by convolving the PDFs the $N/2+1$ individual RVs. Consequently the PDF of the detection statistic for Mode 1 is given by:

$$f_\eta(zw) = f_{ZW_{N/2}}(zw_{N/2}) * f_{ZW_{N/2-1}}(zw_{N/2-1}) * \cdots \tfrac{1}{2} f_{ZW_0}(zw_0). \quad (3.17)$$

Expanding the above gives the PDF of the test statistic for Mode 1 as:

$$f_\eta(zw) = \frac{N}{\sigma^2} \begin{bmatrix} \frac{1}{2}\left|Z(0)\right|^{-2} e^{-x\frac{N}{2}\left|Z(0)\right|^{-2}\sigma^{-2}} \\ *\left|Z(1)\right|^{-2} e^{-xN\left|Z(1)\right|^{-2}\sigma^{-2}} \\ *\left|Z(2)\right|^{-2} e^{-xN\left|Z(2)\right|^{-2}\sigma^{-2}} \\ \vdots \\ *\left|Z(N/2)\right|^{-2} e^{-xN\left|Z(N/2)\right|^{-2}\sigma^{-2}} \end{bmatrix} \tag{3.18}$$

where * denotes convolution.

From the PDF in (3.18), the threshold for detection of change can be formulated. To establish the 1% false alarm rate, the cumulative summation of the PDF area is taken until the 99% point is determined.

3.6 Results

For practical power systems in normal operation the modal parameters are quasi-stationary and these parameters can be estimated from long data records via modal estimate algorithms [11], [28], [12], [13]. These algorithms are applied to data measured at suitable points within a power system, as outlined in [23]. From these estimates PDFs can be generated according to the procedure outlined in Section 3.5. These PDFs can then be used to set thresholds on the various modes so that any rapid deterioration from quasi-stationary operating conditions can be registered. Short data records (e.g. 60 seconds long) can be used for this purpose. Before determining what constitutes a major deterioration in damping it is useful to consider the following Table 3-1 (based on recommendations from NEMMCO [31]) which attempts to quantify damping performance in relation to damping values.

TABLE 3-1 QUALITATIVE REFERENCE TO DAMPING PERFORMANCE (NEMMCO)*

DAMPING Np/s	QUALITATIVE DESCRIPTION
$\sigma > 0$	UNSTABLE
$0 > \sigma > -0.05$	VERY INADEQUATE (VERY POOR)
$-0.05 > \sigma > -0.07$	INADEQUATE (POOR)
$-0.07 > \sigma > -0.139$	MARGINALLY ADEQUATE
$-0.139 > \sigma > -0.2$	ACCEPTABLE (GOOD)
$\sigma < -0.2$	HIGHLY ACCEPTABLE (VERY GOOD)

* National Electricity Marketing Management Company (Australia)

Based on the criteria in Table 3-1 above, a change in damping will be considered unacceptable if damping moves into the marginally adequate region. The following subsections consider the performance of the new method for both simulated and real data.

3.6.1 Simulated Results

The simulation in this section is for a three mode system with the following definition for each individual mode:

$$h_i(n) = A_i e^{-\sigma_i n} \sin(\omega_i n), \quad i = 1, 2, 3. \tag{3.19}$$

Hence the overall impulse response of the measurement site is defined as:

$$h(n) = h_1(n) + h_2(n) + h_3(n). \tag{3.20}$$

The stationary modal parameters and modal weights of (3.20) are based on practically realistic estimates, as listed in Table 3-2.

TABLE 3-2 STATIONARY MODAL PARAMETERS AND WEIGHTS

MODE	PARAMETER	VALUE
1	MAGNITUDE, A_1	7.58
	DAMPING σ_1 *(NP/S)*	-0.28
	FREQUENCY ω_1 *(R/S)*	1.75
2	MAGNITUDE, A_2	1.62
	DAMPING σ_2	-0.58
	FREQUENCY ω_2	2.87
3	MAGNITUDE, A_3	0.10
	DAMPING σ_3	-0.85
	FREQUENCY ω_3	5.473

To test the proposed method, 400 minutes of simulated data were generated with the damping changing from the initial quiescent values as indicated in Table 3-3. The threshold for the output was set to yield a 1% false alarm rate. The simulations were run for 60 second data windows, involving change detection of Mode 1, Mode 2 and Mode 3. The results are shown respectively in Figure 3-3, Figure 3-4, Figure 3-5 and Table 3-4.

TABLE 3-3 DAMPING CHANGES

MODE	DAMPING*			
	0-100MIN	100-200MINS	200-300MINS	300-400MINS
1	-0.28	**-0.1**	-0.28	-0.28
2	-0.58	-0.58	**-0.1**	-0.58
3	-0.85	-0.85	-0.85	**-0.1**

* **BOLD** highlights changes from quiescent state.

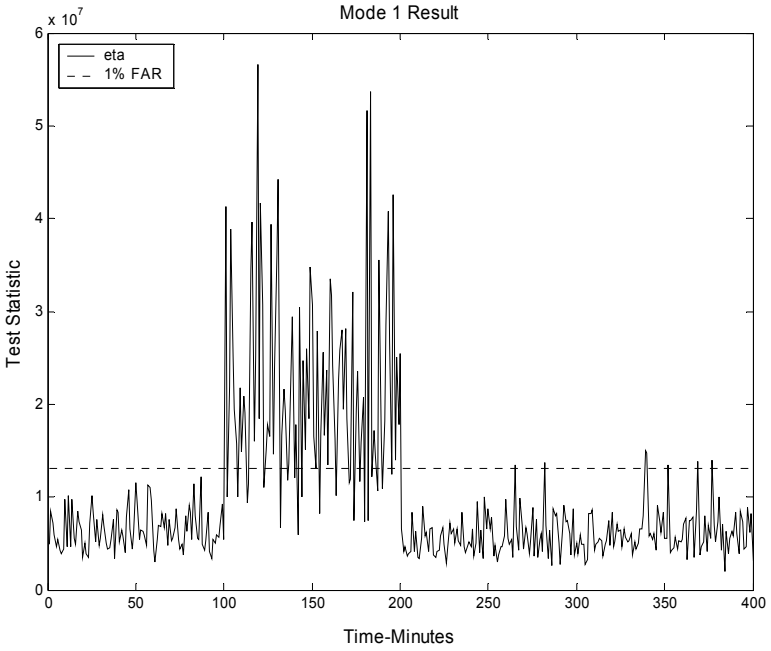

Figure 3-3 Mode 1 test statistic vs alarm threshold.

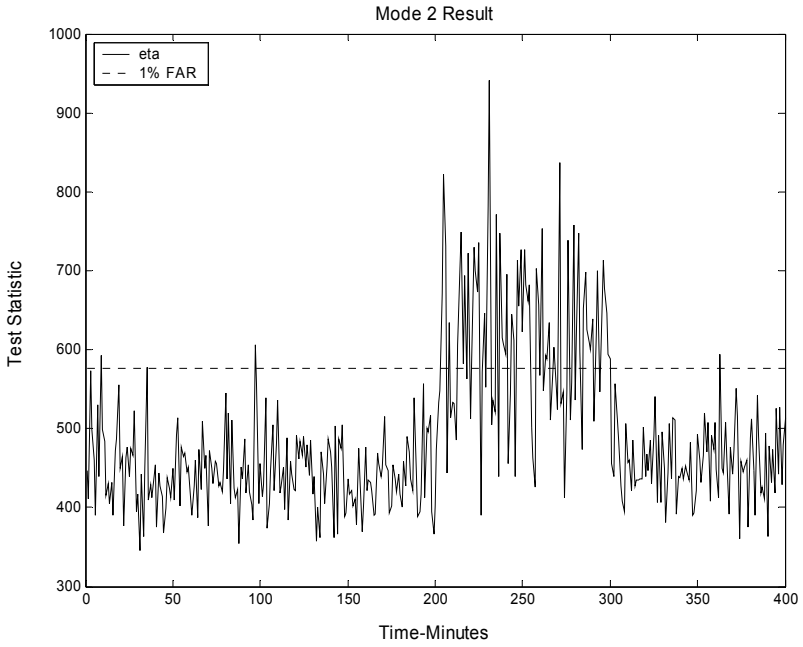

Figure 3-4 Mode 2 test statistic vs alarm threshold.

TABLE 3-4 ALARMS (1% FAR)

MODE	% OF ALARMS DURING TIME PERIOD			
	0-100MIN	100-200MINS	200-300MINS	300-400MINS
1	0	78	2	2
2	3	0	61	1
3	2	1	4	4

It can be seen in Figure 3-3 and Figure 3-4 that the stronger modes, Mode 1 and 2, demonstrate high alarm rates in marginal damping situations. However from Figure 3-5 (and Table 3-4) the Mode 3 processing provided no significant indication that the damping had deteriorated to a marginally adequate condition. This is because the relative strength of the modes affects the performance of the optimal detector. The relative mode strengths in the quiescent state can be observed in Figure 3-5. It can be

seen that Mode 3 is extremely weak in comparison to the other modes. In fact it is hard to even see evidence of it in the diagram. In practice therefore longer windows need to be used for detecting changes in very weak modes.

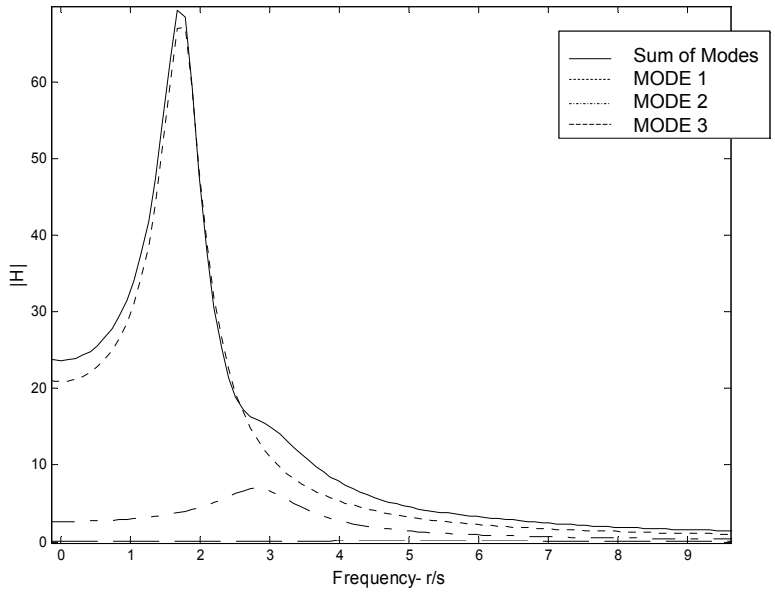

Figure 3-5 Spectral plot of mode contributions within system frequency response.

3.7 Real Data Analysis

To enable modal characterisation, a priori estimates of the quasi-stationary system parameters are required. That is, a long term estimator (LTE) is applied to a relatively long record (typically one hour) of quasi-stationary data. Under normal operating conditions these estimates are updated once every half an hour. The modal deterioration algorithm, on the other hand, is applied continuously. The long term estimator method used in this paper is outlined in [13], and provides estimates of the measurement site transfer functions and modal parameters. From this the individual modal response estimates at each site can be extracted.

It should be noted that in this application the variance of the noise feed is not known and consequently the detector PDFs are initially formulated with the noise variance in (3.18) set to unity. To correctly de-normalise the PDF, a rescaling factor is necessary. The rescaling factor is obtained by simply taking K short-term N length test statistic measurements over the M length long-term analysis window and determining the mean value (where $K = M/N$). The ratio of the mean value of the measurements and the expected value of the theoretical PDF is the scaling factor estimate given by (3.21),

$$\hat{SF} = \frac{E\left\{\sum_{k=1}^{N/2} PSD_{ref}(k)PSD_{obs}(k) + \frac{1}{2}PSD_{ref}(0)PSD_{obs}(0)\right\}}{\int_{-\infty}^{\infty} xf_{\eta}(zw)\,dx}. \tag{3.21}$$

Once the appropriate re-scaling is performed and the threshold is established the detection process begins on all concurrent short term measurements until another threshold update (corresponding to an update set of quasi-stationary conditions) is instigated at a later time. Diagrammatically the complete short-term detection procedure for a single mode at one site is shown in Figure 3-6. For the purposes of this chapter the 30 minute updates only occurred if all modal damping estimates were below $-0.139Nps^{-1}$(i.e. if all modes were in the acceptable to very good range as defined in Table 3-1)**.**

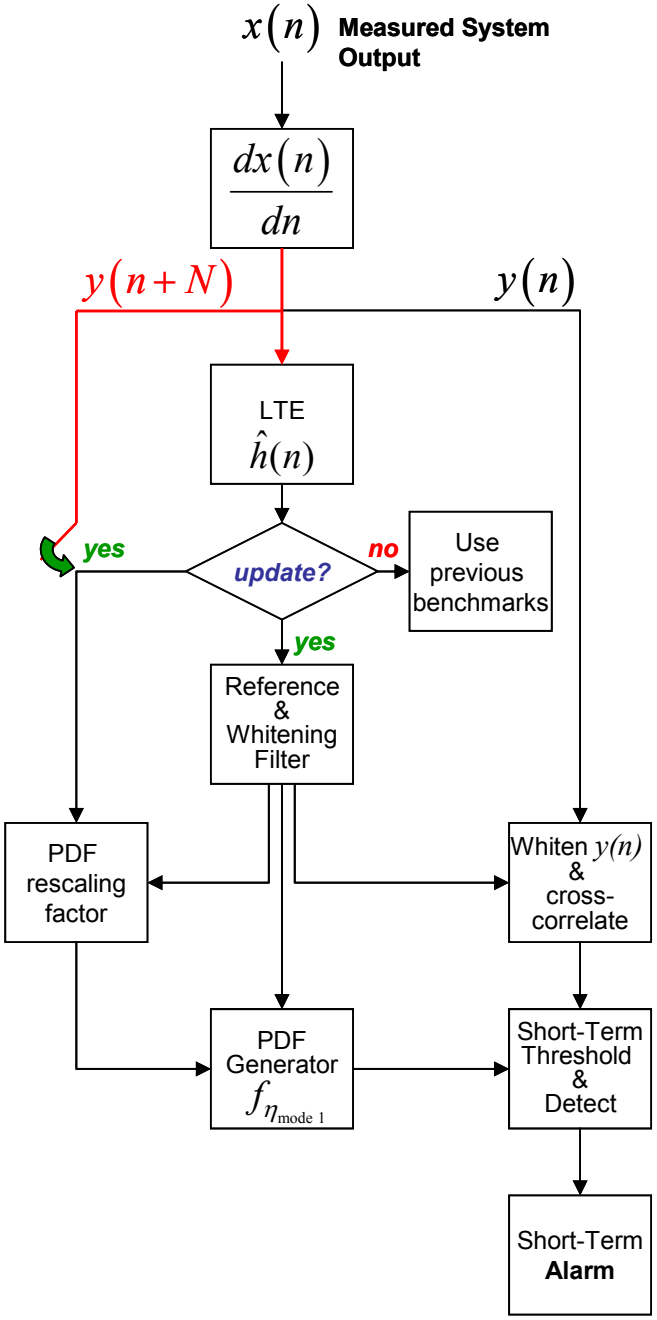

Figure 3-6 Short Term Modal Detection Applied to Real Data.

3.8 Verification of Method

The University of Adelaide MudpackScript data was again used in this verification stage. Case13 was used as the test case and the damping and frequency trajectories for this test case are shown in Figure 3-7 below. Long-term modal estimates from the LTE in [13] were determined for the data corresponding to the first 1.5hrs of the Case13 data. The resulting damping and frequency estimates are shown in Table 3-5.

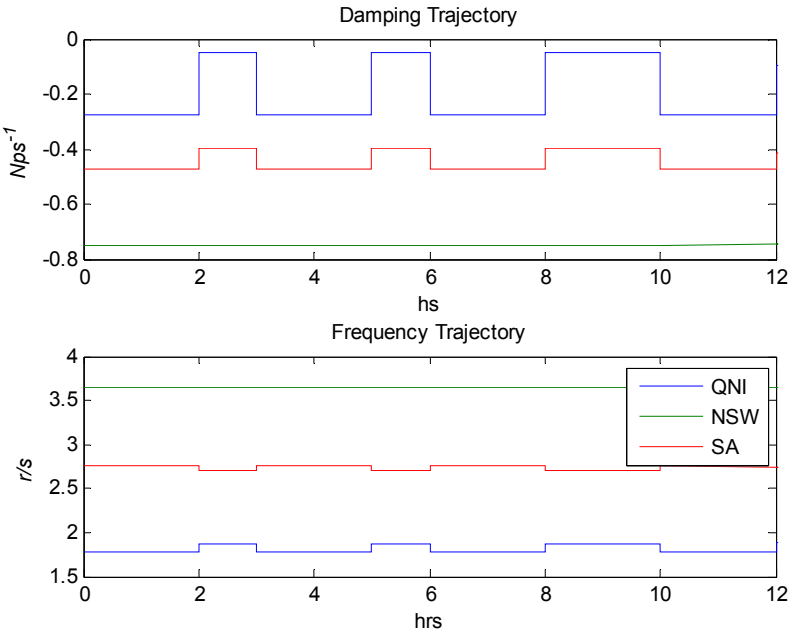

Figure 3-7 Case13 Modal Damping and Frequency Trajectory.

TABLE 3-5 LONG TERM MODAL PARAMETER ESTIMATES

MODE	1.5 HR ANALYSIS	
	DAMPING NPS^{-1}	FREQUENCY R/S
1	-0.278	1.78
2	-0.457	2.76
3	-0.763	3.71

When comparing the known initial damping and frequency in Figure 3-7 with the LTEs in Figure 3-7, it can be clearly seen that the LTE has performed adequately. The individual site frequency responses from the LT estimates are shown in Figure 3-8. It can be seen that the Brisbane response is strongest in Mode 1, with Mode 2 just distinguishable. The Sydney response is strongest in the Mode 2 while the Adelaide site is strongest in Mode 1 with a distinct Mode 3 contribution.

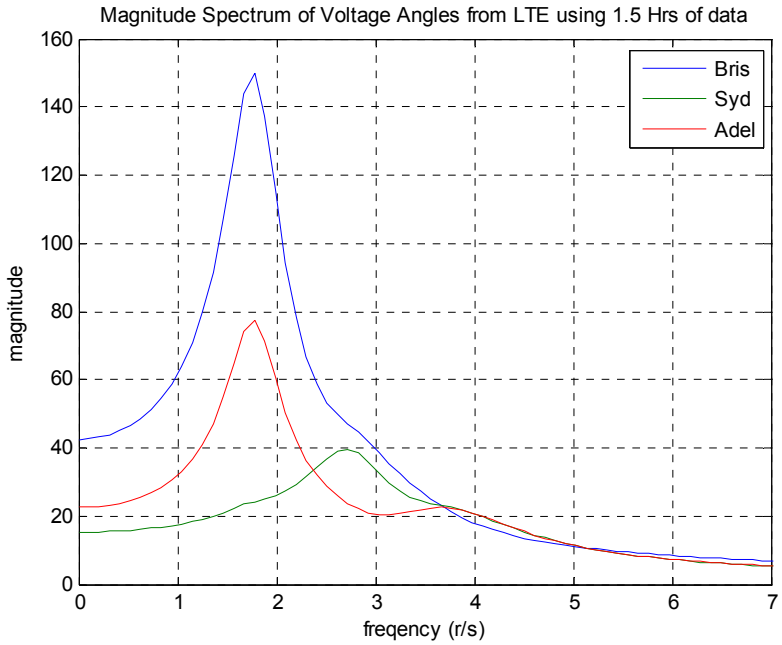

Figure 3-8 Spectral Estimate of Site Magnitude Response.

As discussed previously, the individual modal contributions must be inferred (via partial fraction expansion) from each of the overall site responses. The contributions of the individual modes at each site can be seen in Figure 3-9 to Figure 3-11.

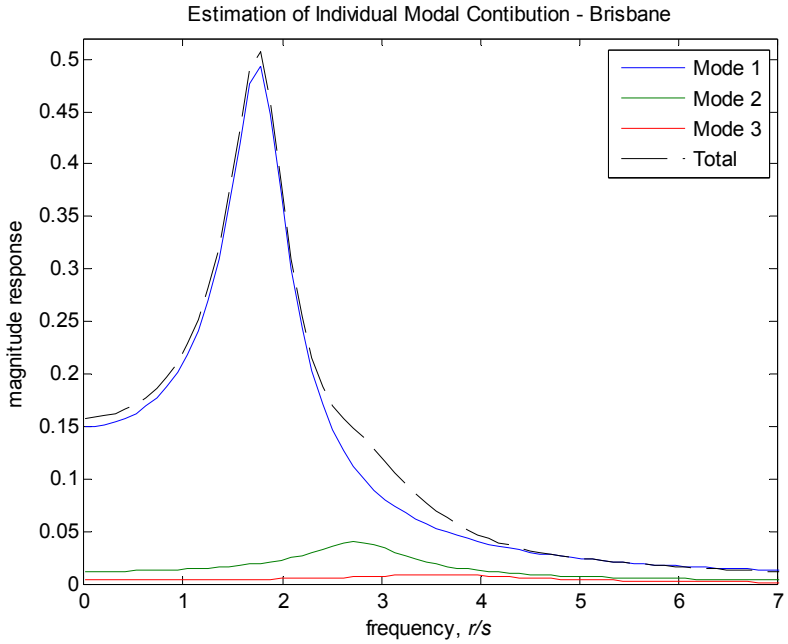

Figure 3-9 Estimates of Individual Modal Spectral Contributions - Brisbane (QNI).

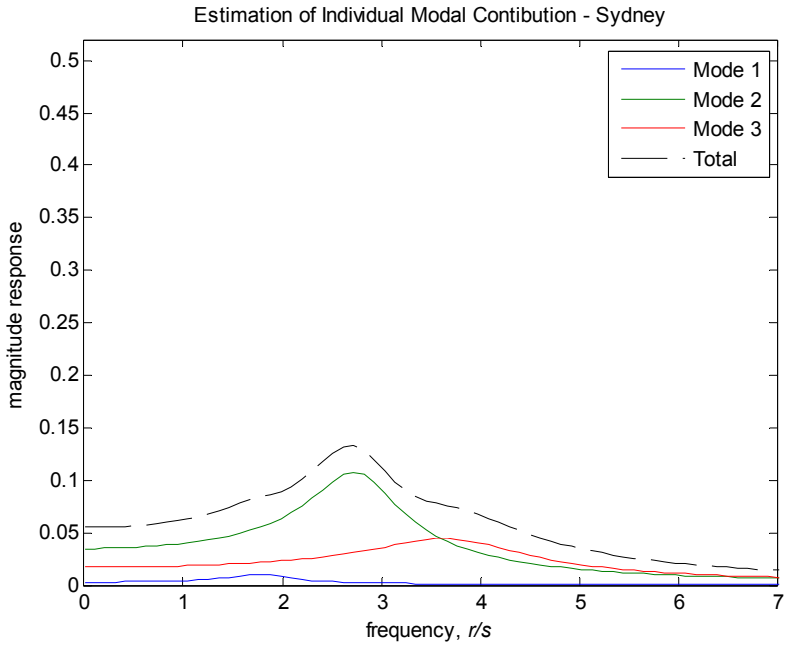

Figure 3-10 Estimates of Individual Modal Spectral Contributions - Sydney (NSW).

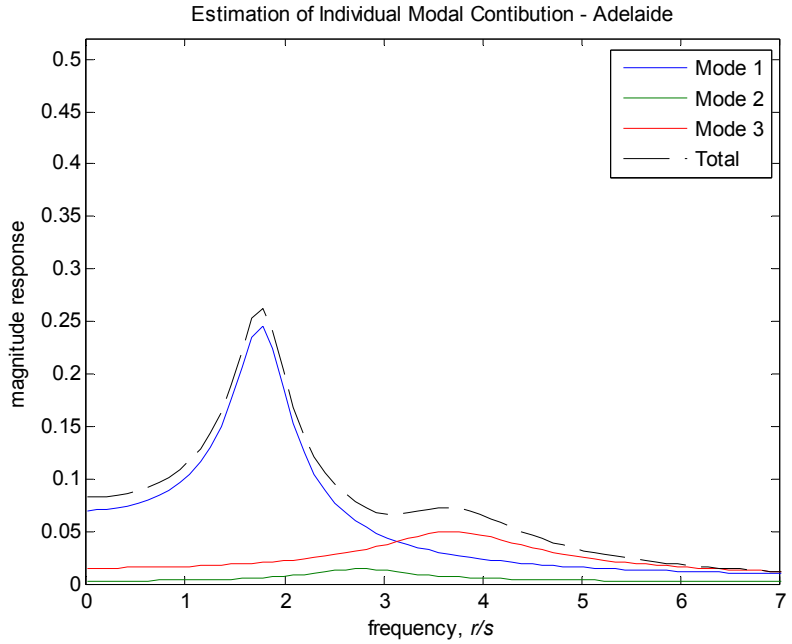

Figure 3-11 Estimates of Individual Modal Spectral Contributions - Adelaide (SA).

The results of the Mode 1 monitoring for each "measurement site" are shown in Figure 3-12 to Figure 3-14 respectively.

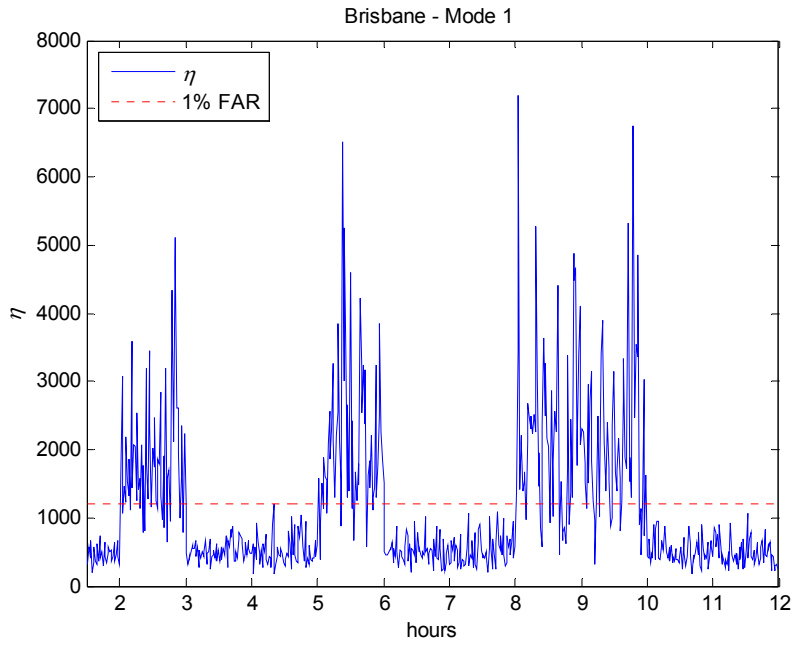

Figure 3-12 Individual Mode Monitoring - Mode 1 Brisbane.

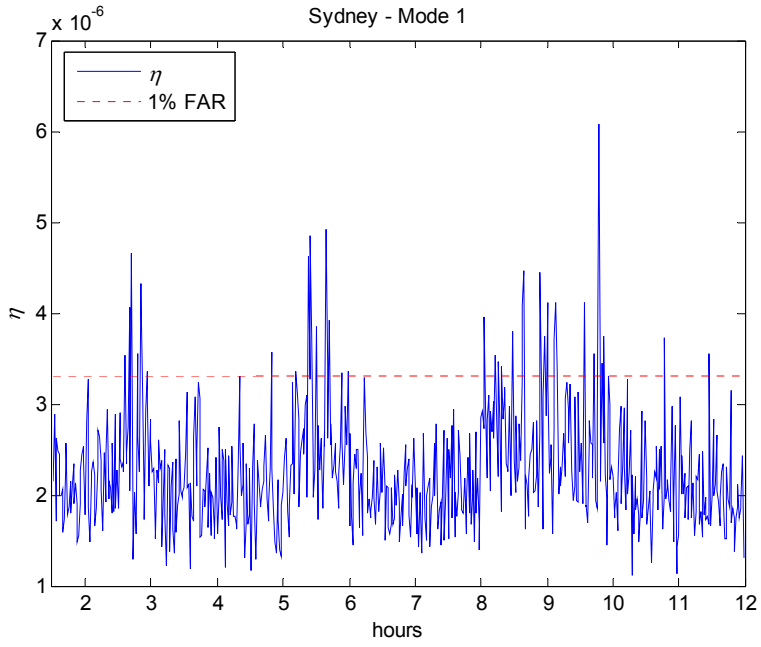

Figure 3-13 Individual Mode Monitoring - Mode 1 Sydney.

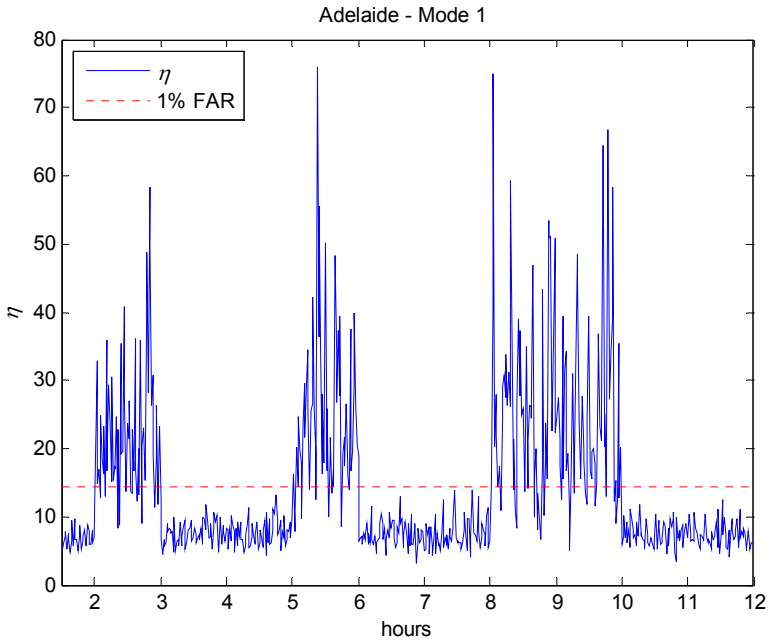

Figure 3-14 Individual Mode Monitoring - Mode 1 Adelaide.

The results of the Mode 1 monitoring at the three sites shown in Figure 3-12 to Figure 3-14 demonstrate the expected alarming of the deteriorating mode. The Brisbane and Adelaide sites test statistic measurement exhibits a very strong response to the poor damping condition; while the Sydney response is less pronounced due to the weaker contribution from Mode 1 within the Sydney frequency response. The Mode 1 contribution to the Sydney site response is seen in Figure 3-14 and can be clearly seen to be quite small in relation to the Mode 2 and 3 contributions. Importantly though, there is still strong ongoing alarming while the poor damping condition exists at Sydney and minimal false alarms when the condition does not exist.

3.9 Real Data Analysis Results

The real data used in this paper was obtained from voltage angle measurements taken at the four sites within the Australian power system (Brisbane, Sydney, Adelaide and Melbourne). The data was collected by Queensland University of Technology (QUT) in conjunction with the National Electricity Market Management Company Limited (NEMMCO). To obtain the quasi-stationary transfer functions, and consequently detection statistic PDFs, the LTE, described in [13], was applied. The results obtained from the LTE tended to indicate that there were no significant damping deteriorations anywhere in the data. The results of the short-term alarming procedure are displayed in Figure 3-15 to Figure 3-18. Observation of the Mode 1 detection statistic measurements at the Brisbane and Sydney sites between 05:30 and 06:00hrs (Figure 3-15 and Figure 3-17) shows that Mode 1 rarely crosses the 99% FAR threshold during the 2 hour period.

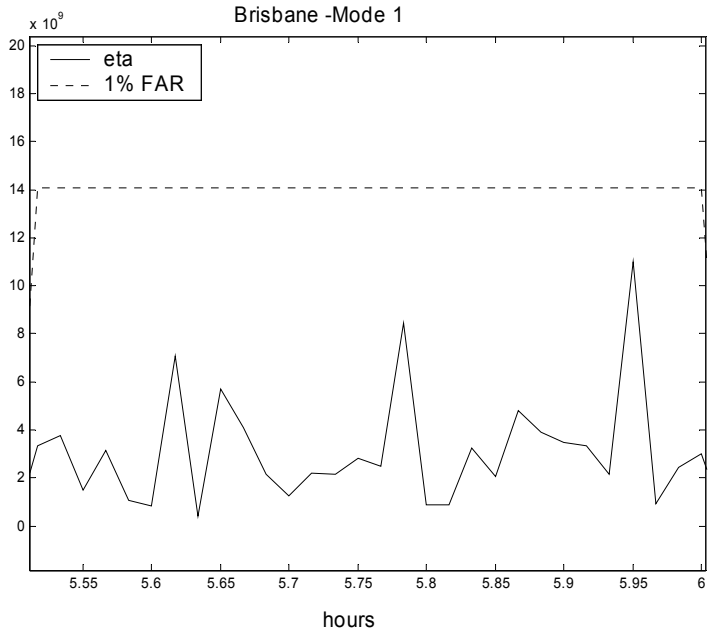

Figure 3-15 Brisbane Mode 1 Test Statistic vs Time (1% FAR).

Only in the Sydney measurements (Figure 3-17) are there any false alarms in this period. The reason for this is highlighted in Figure 3-19, where the spectrum of the magnitude of the voltage angles is shown for each measurement site. It can be seen clearly in Figure 3-19 that in all sites except Sydney, Mode 1 is the dominant mode, whilst in Sydney; Mode 2 is the dominant mode. Table 3-6 shows the percentage of false alarms for each mode at each site over the 24 hours.

TABLE 3-6 FALSE ALARMS (1% FAR)

MODE	% OF FALSE ALARMS OVER 24HRS AT SITE			
	BRISBANE	SYDNEY	MELBOURNE	ADELAIDE
1	0.96*	3.85	1.48*	1.03 *
2	6.00	0.81*	14.74	11.62

* Dominant mode

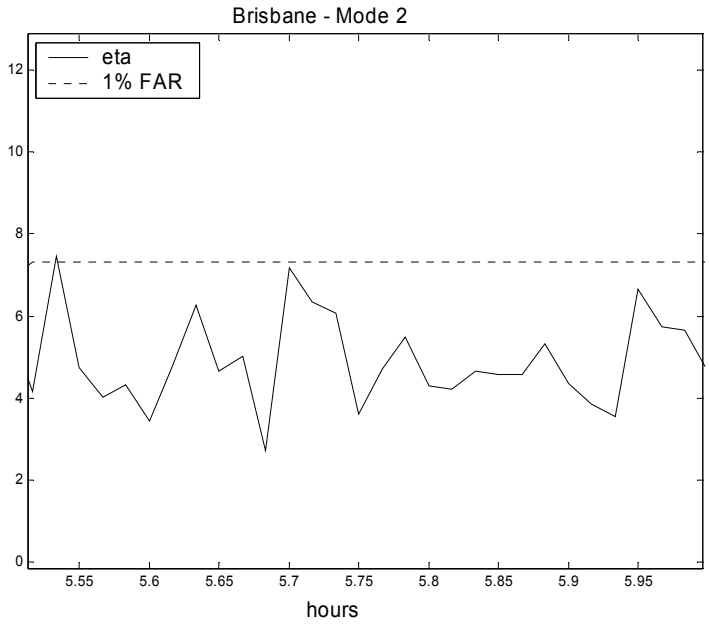

Figure 3-16 Brisbane Mode 2 Test Statistic vs Time (1% FAR).

This table verifies the choice of the 1% FAR with false alarms occurring close to the theoretical level in relation to dominant mode detection. This provides confidence in the reliability of the detector in relation to dominant modes. However Mode 2 has spasmodic results with generally higher than desired FAR with the exception of the Sydney measurements where Mode 2 is the dominant mode.

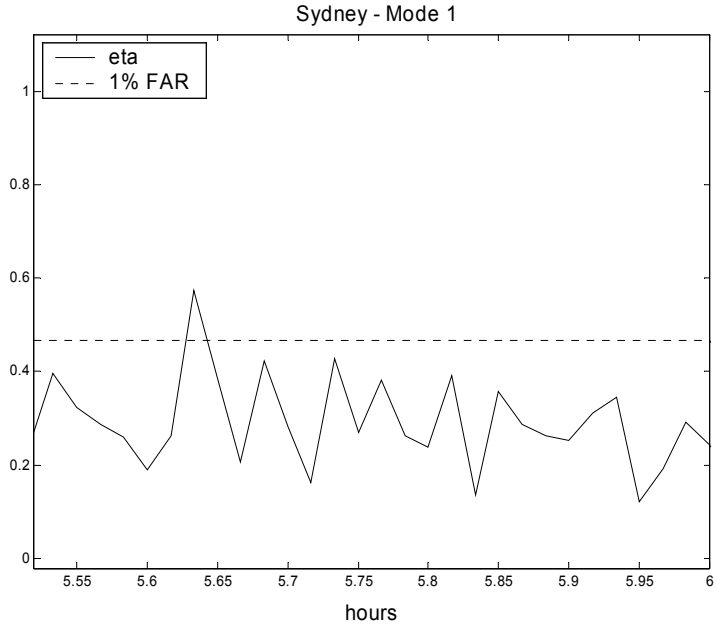

Figure 3-17 Sydney Mode 1 Test Statistic vs Time (1% FAR).

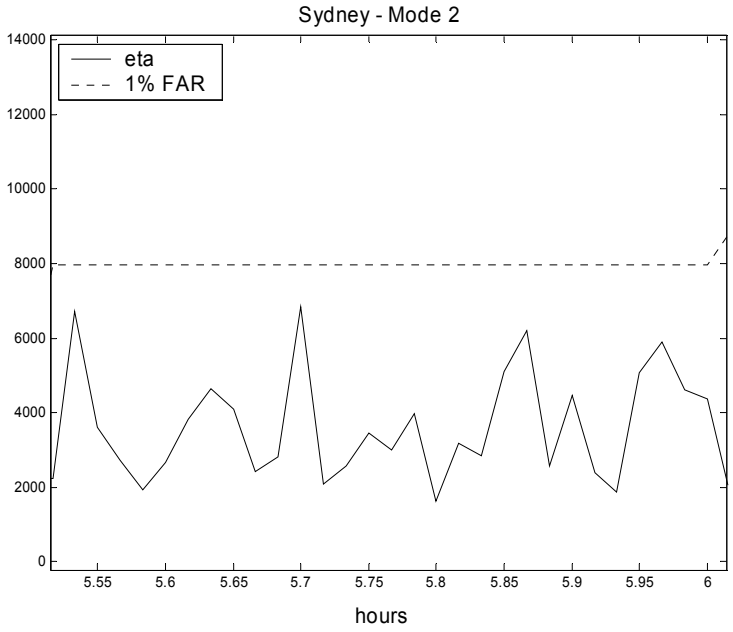

Figure 3-18 Sydney Mode 2 Test Statistic vs Time (1% FAR).

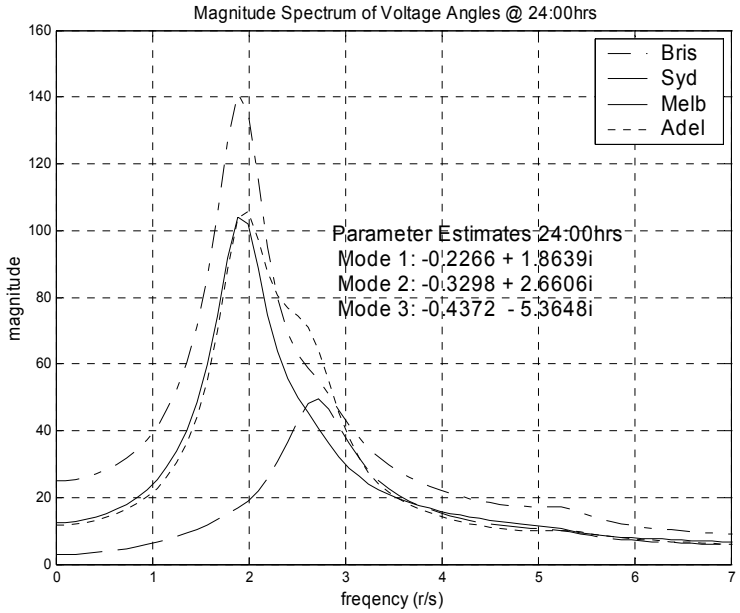

Figure 3-19 Magnitude spectrum of voltage angles at different sites at 24:00hrs.

The higher FAR of the non-dominant mode is due principally to two things. Firstly, the relative mode strength of Mode 2 to Mode 1 will not be stationary, and secondly, the close proximity of the Mode 2 frequency to the Mode 1 frequency. Both of these points will affect the estimating performance of the LTE. Hence the accuracy of the individual modal responses for weaker modes, and the associated reference and whitening filters derived from them, will be compromised.

3.10 Discussion

The simulations in Section 3.6 indicate that the method proposed in this chapter can effectively monitor individual modal changes in power systems. It does so with a predetermined level of confidence that sets the alarm at a desired false alarm rate. The level of confidence is formulated through analytical means by way of providing a PDF function representing a detection statistic for the particular measurement site. The method was then verified in Section 3.8 by exploiting the MudpackScript

data. The method displayed clear and sudden alarming in response to a sudden detrimental damping change to one of the modes. These sections also demonstrated the limitation of the method in individually alarming modes that have weak spectral contributions to the overall frequency response at a given measurement site.

Although not shown in this chapter, longer time windows exhibit a greater degree of confidence in a detected change, and can be used in conjunction with the shorter time windows to confirm or disaffirm a need for remedial action.

In practice the monitoring is done for all modes concurrently. It should be noted that the methods outlined in this chapter only apply to multi-mode systems. In a single mode system the method proposed in Chapter 2 would be more suitable to alarm the rapid detection of sudden deterioration modal damping.

3.11 Conclusion

It can be seen from the results that the proposed method can provide short term alarming of individual modal deterioration in large interconnected power systems. Importantly the alarming can be set to a desired level of confidence whereby false alarms occur within expected theoretical rates when the system is under quasi-stationary conditions. More specifically this method is aimed at alarming large adverse changes in modal damping rather than monitoring small drifts in damping values. The ability of the optimal detector is limited by the relative strength of the modes. However this limitation needs to be put into perspective - the stronger modes are what dominate the system response, and so the inability of the optimal detector to work well with very weak modes is not of paramount concern. To ratify alarms for weaker modes, longer time windows can be used in parallel with shorter time windows and a dynamic alarm response strategy can be formulated. Significantly this chapter provides a simple

method of modal deterioration detection by using the system angles in normal operation. The computational simplicity of the method is particularly appealing and as a consequence accommodates the desire for rapid detection.

Chapter 4

4 A Kalman Filtering Approach to Rapidly Detecting Modal Changes

4.1 Introduction

In the previous two chapters, energy based statistical techniques targeting the detection of detrimental modal damping were presented. In this chapter a unique approach that applies Kalman filtering techniques to the problem of detecting modal changes in large interconnected power systems will be introduced. The short-term alarming procedures are developed based on the statistics of the power spectral density of the Kalman filter innovation. The new technique is tested on simulated data, verified using the MudpackScript data and then used to analyse real data obtained from power systems in normal operation. The particular advantage of the new method is its ability to detect changes very quickly.

As mentioned earlier, conventional damping factor estimation techniques are limited by the requirements of long data records. Even though these estimation methods provide reliable means to monitor power systems under normal operating conditions they do not favourably accommodate the need for rapidly detecting sudden modal damping changes that may be harmful to power system stability and reliability.

This chapter seeks to again address this shortcoming by presenting another method which is able to provide indications of modal parameter change based on short data records.

It is proposed that the change detection be performed using measurements from power systems in normal operation. Section 4.2 of this chapter will reiterate the stochastic model relating random ambient disturbance inputs in the power system, such as customer load changes, to the measured system output. Based on this model a Kalman filter is then set up to estimate the output arising from the disturbances. The *innovation* is then determined as the difference between the measured output and the estimated output. It is well known that the "innovation" from a Kalman filter is spectrally white as long as the assumed model parameters are valid [51] [50]. By monitoring the whiteness of the innovation, therefore, one can detect if there are any changes in the these parameters [50].

The stochastic power system model is presented in Section 4.2. The Kalman filter formalism is provided in Section 4.3. Simulated data results are given in Section 4.4. Verification using the MudpackScript data is undertaken in Section 4.5, while real data examples are considered in Section 4.6. Methods in tuning the Kalman filter are discussed in Section 4.7. Sections 4.8 and 4.9 are devoted to discussion and conclusion respectively.

4.2 Stochastic Power System Model

Once again the experimentally motivated hypothesis from Ledwich and Palmer [11] is used as the initial point of reference for the power system model. In this model the power system itself is modelled as an IIR filter. Therefore the power system response to disturbances can be modelled as the output of an IIR filter driven by integrated white noise.

The formulation of this model was defined earlier in Section 2.2. Equivalent principles still apply whereby the measured power system

output (e.g. power , angle, …) at site *i* is differentiated to provide the signal $y_i(n)$. As illustrated in Figure 4-1, this is the signal that would have been obtained if the white noise, *w(n)*, had excited the power system. Consequently the power system model used in this chapter is the *single* measurement site, *single* excitation model depicted in Figure 4-1.

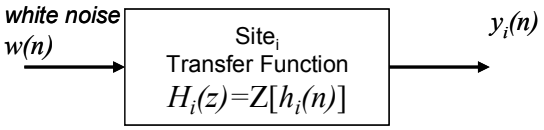

Figure 4-1 Equivalent model for the individual response of a power system to load changes.

We now consider that the IIR power system filter is the "plant". With this in mind we turn to the standard Kalman estimator. The general Kalman estimator for a plant driven by a control signal, *u(n)*, perturbed with white noise, *w(n)*, with (multi-dimensional) output measurements, **y***(n)*, corrupted by measurement noise, **v***(n)*, is depicted in Figure 4-2 [69]. A set of measurements from a set of sites will be driven from the load variations at a wide set of sites.

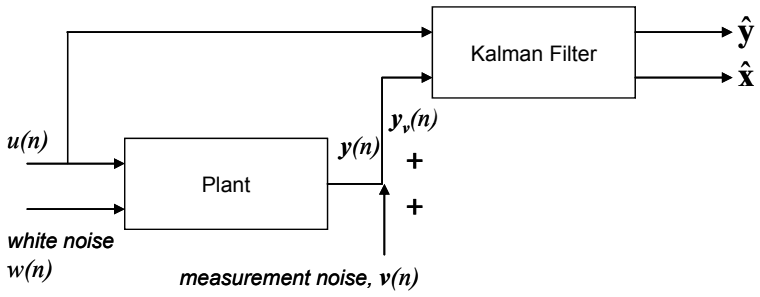

Figure 4-2 General Kalman filter estimator.

For our application the control signal, *u(n)*, is zero and the plant is only excited by the white noise, *w(n)*. Generally the output of the Kalman filter

provides estimates of the plant output, $\hat{\mathbf{y}}(n)$, and of the states, $\hat{\mathbf{x}}(n)$. In this contribution chapter the "plant" represents a large interconnected power system. The current measured plant output, $\mathbf{y}_v(n)$, corresponds to a vector of measurements from multiple recording sites. In practice the measurements are voltage angle measurements rather than power measurements because the potential for modal information extraction is greater for voltage signals than for power signals [11]. The optimal placement of these measurement sites within a large distributed power system is discussed in [23]. The vector $v(n)$ represents noise measurements from each site. In a practical application the plant output measurement vector, $\mathbf{y}_v(n)$, can be recorded at a GPS synchronised wide area monitoring centre [22, 23]. In our application the state estimates themselves are not used, only the innovation. For the model in Figure 4-2 the Kalman estimator of $\hat{\mathbf{y}}(n)$ is optimal [70], as is the estimator of $(\mathbf{y}_v - \hat{\mathbf{y}})$. The latter "innovation" is well known to be white when the signal model presented in Figure 4-2 is valid and stationary [50, 51]. The whiteness of the innovation, then, is a convenient means to monitor any sudden changes which are not accounted for in the model depicted in Figure 4-2.

In a power system operating under stationary conditions, the innovation will be white and will therefore have a flat Power Spectral Density (PSD). On the other hand, if there is a sudden change in the power system response (say a sudden detrimental damping change) the spectrum of the innovation will highlight this change with a peak around the modal frequency in question. Therefore with a suitable threshold set, large undesirable damping changes can be readily detected. A suitable threshold is one which is set to give a False Alarm Rate (FAR). If say the FAR is set to 1% then when an alarm occurs, one knows that it is a genuine alarm with 99% confidence. In choosing the FAR it should be

again highlighted that the aim of this proposed method is to detect sudden large detrimental changes and not to track small drifts in system parameters. As a result, thresholds should be set to minimise false alarms, whilst still providing the required rapid alarming of sudden system deterioration. The innovation can also be used to detect a frequency shift (as opposed to a damping change). In this scenario the innovation's PSD will display a peak around the new modal frequency and a trough around the original modal frequency.

The formula for the Kalman filter estimation and the derivation of the PSD threshold will be examined in the next section.

4.3 The Kalman Application in Power System Analysis

4.3.1 Kalman formulation

In the power system model under consideration the state and output equations are:

$$\mathbf{x}(n+1) = \mathbf{A}\mathbf{x}(n) + \mathbf{G}w(n) \tag{4.1}$$

$$\mathbf{y}_v(n) = \mathbf{C}\mathbf{x}(n) + \mathbf{D}w(n) + \mathbf{v}(n) \tag{4.2}$$

where **A**, **G**, **C** and **D** denote the usual state and output equation matrices [69]. The noise processes, *w(n)* and **v***(n)*, are zero mean Gaussian white noise sequences with covariances given by:

$$E\left\{w(n)\,w(n)^T\right\} = Q \tag{4.3}$$

$$E\left\{\mathbf{v}(n)\,\mathbf{v}(n)^T\right\} = \mathbf{R} \tag{4.4}$$

$$E\left\{w(n)\,\mathbf{v}(n)^T\right\} = \mathbf{N} \tag{4.5}$$

where $E\{\cdots\}$ denotes expected value. It will be assumed hereafter that *w(n)* and **v***(n)* are uncorrelated. It will also be assumed that the plant is excited by a common white noise source, *w(n)*, however the plant response to such excitation is measured at different geographic locations. Hence the measurement noise, **v***(n)*, is a vector that is congruent to the wide-area monitoring of inter-area oscillations introduced in Section 1.2. The load variations become close to Gaussian when there are a large number of independent customer loads [11].

In "normal" stationary operation the optimal Kalman state estimator is given by the following set of discrete equations [55]:

$$\hat{\mathbf{x}}(n+1/n) = \mathbf{A}\hat{\mathbf{x}}(n/n) + \mathbf{G}w(n) \tag{4.6}$$

$$\hat{\mathbf{x}}(n/n) = \hat{\mathbf{x}}(n/n-1) + \mathbf{M}\boldsymbol{\gamma}(k) \tag{4.7}$$

$$\hat{\mathbf{y}}(n) = \mathbf{C}\hat{\mathbf{x}}(n/n-1) \tag{4.8}$$

$$\boldsymbol{\gamma}(n) = \mathbf{y}_v(n) - \hat{\mathbf{y}}(n) \tag{4.9}$$

where $\boldsymbol{\gamma}(n)$ is the white zero-mean Gaussian "innovation" sequence with units rad/sec. The gain matrix, **M**, is calculated from the following equations:

$$\mathbf{P}(n+1/n) = \mathbf{A}\mathbf{P}(n/n)\mathbf{A}' + \mathbf{Q} \tag{4.10}$$

$$\mathbf{V} = \mathbf{C}\mathbf{P}(n/n-1)\mathbf{C}' + \mathbf{R} \tag{4.11}$$

$$\mathbf{M} = \mathbf{P}(n/n-1)\mathbf{C}^T\mathbf{V}^{-1} \tag{4.12}$$

$$\mathbf{P}(n/n) = \mathbf{P}(n/n-1) - \mathbf{M}\mathbf{C}\mathbf{P}(n/n-1) \tag{4.13}$$

where $\mathbf{P}(i/j)$ is the estimation error covariance of the state estimates vector, $\hat{\mathbf{x}}(i/j)$, and **V** is the covariance of the innovation vector, $\boldsymbol{\gamma}(n)$. The gain matrix, **M**, is derived by solving the discrete time Ricatti equations [71].

4.3.2 State space representation of the power system model

To generate the matrices **A**, **G**, **C** and **D** for the power system model in Figure 4-1, the transfer function of *h(n)* is first identified. This enables subsequent formulation of the state space matrices into controllable canonical form. To illustrate the process a power system example comprising a two mode system with single site measurement and disturbance is considered.

The impulse response at the site is assumed to be:

$$h(t) = h_1(t) + h_2(t) \tag{4.14}$$

where

$$h_i(t) = A_i e^{-\sigma_i t} \sin(\omega_i t) \quad i = 1, 2... \tag{4.15}$$

σ_i is the modal damping, ω_i is the modal frequency and A_i is the magnitude respectively of the i^{th} mode.

Taking the Laplace transform of (4.14) yields the continuous time power system transfer function:

$$H(s) = \frac{A_1\omega_1}{(s+\sigma_1)^2 + \omega_1^2} + \frac{A_2\omega_2}{(s+\sigma_2)^2 + \omega_2^2}. \tag{4.16}$$

If the sampling period is *T*, then the discrete time transfer function for the site is:

$$
\begin{aligned}
H(z) &= \frac{A_1\ ze^{-\sigma_1 T}\sin(\omega_1 T)z^{-1}}{1-2e^{-\sigma_1 T}\cos(\omega_1 T)z^{-1}+e^{-2\sigma_1 T}z^{-2}} \\
&\quad + \frac{A_2\ ze^{-\sigma_2 T}\sin(\omega_2 T)z^{-1}}{1-2e^{-\sigma_2 T}\cos(\omega_2 T)z^{-1}+e^{-2\sigma_2 T}z^{-2}} \\
&= \frac{b_1 z^{-1}+b_2 z^{-2}+b_3 z^{-3}}{1+a_1 z^{-1}+a_2 z^{-2}+a_3 z^{-3}+a_4 z^{-4}}
\end{aligned}
\tag{4.17}
$$

where the coefficients, $\{b_1, b_2, b_3, a_1, a_2, a_3, a_4\}$, are given by:

$$b_1 = A_1\ e^{-\sigma_1 T}\sin(\omega_1 T) + A_2\ e^{-\sigma_1 T}\sin(\omega_1 T) \tag{4.18}$$

$$b_2 = -2\ e^{-T(\sigma_1+\sigma_2)}\left(A_1\ \sin(\omega_1 T)\cos(\omega_2 T) + A_2\ \sin(\omega_2 T)\cos(\omega_1 T)\right) \tag{4.19}$$

$$b_3 = \left(A_1\ e^{-T(\sigma_1+2\sigma_2)}\sin(\omega_1 T) + A_2\ e^{-T(2\sigma_1+\sigma_2)}\sin(\omega_2 T)\right) \tag{4.20}$$

$$a_1 = -2\left(e^{-\sigma_1 T}\cos(\omega_1 T) + e^{-\sigma_2 T}\cos(\omega_2 T)\right) \tag{4.21}$$

$$a_2 = e^{-2\sigma_2 T} + 4e^{-T(\sigma_1+\sigma_2)}\cos(\omega_1 T)\cos(\omega_2 T) + e^{-2\sigma_1 T} \tag{4.22}$$

$$a_3 = -2\left(e^{-T(\sigma_1+2\sigma_2)}\cos(\omega_1 T) + e^{-T(2\sigma_1+\sigma_2)}\cos(\omega_2 T)\right) \tag{4.23}$$

$$a_4 = e^{-2T(\sigma_1+\sigma_2)}. \tag{4.24}$$

From the transfer function, the state space matrices in controllable canonical form can be determined [72]:

$$\mathbf{A} = \begin{bmatrix} -a_1 & -a_2 & -a_3 & -a_4 \\ 1 & 0 & 0 & 0 \\ 0 & 1 & 0 & 0 \\ 0 & 0 & 1 & 0 \end{bmatrix} \tag{4.25}$$

$$\mathbf{G} = \begin{bmatrix} 1 \\ 0 \\ 0 \\ 0 \end{bmatrix} \tag{4.26}$$

$$\mathbf{C} = \begin{bmatrix} b_1 & b_2 & b_3 & 0 \end{bmatrix} \tag{4.27}$$

$$\mathbf{D} = \begin{bmatrix} 0 \end{bmatrix}. \tag{4.28}$$

4.3.3 Kalman Solution

With the discrete state space plant defined in (4.25)-(4.28) the Kalman solution depicted in Figure 4-2 can be realised. Accordingly, the Kalman estimator equations, (4.6)-(4.9) are evaluated and then the normalised innovation is defined:

$$\gamma_n(n) = K\gamma(n), \tag{4.29}$$

where K is the normalisation gain that normalises the innovation to unity variance. Therefore the normalisation gain is the square root of the inverse power of the innovation window. If the normalised innovation sequence results from a significantly different system than the one considered, then the concentration of spectral energy around the mode of significant change will still demonstrate a strong threshold crossing. This will be demonstrated Section 4.6.

It must be noted that for the Kalman analysis to operate, the power system model and noise data must satisfy the limitations outlined in [69] whereby the plant and noise data must satisfy the following relationships:

- The plant transfer function state space matrices, (4.30) must be detectable.
- The measurement noise variance, (4.31), must be non-zero.

- The left hand side (LHS) of (4.32), must be non-zero.
- And the matrix defined by the LHS of (4.33) must have no uncontrollable modes on the unit circle [69].

$$\left(\mathbf{C},\mathbf{A}\right), \tag{4.30}$$

$$\bar{\mathbf{R}} > 0, \tag{4.31}$$

$$\bar{Q} - \bar{\mathbf{N}}\bar{\mathbf{R}}^{-1}\bar{\mathbf{N}}^{T} \geq 0, \tag{4.32}$$

$$\left(\mathbf{A} - \bar{\mathbf{N}}\bar{\mathbf{R}}^{-1}\mathbf{C}, \mathbf{Q} - \bar{\mathbf{N}}\bar{\mathbf{R}}^{-1}\mathbf{N}^{T}\right), \tag{4.33}$$

where [69]:

$$\bar{\mathbf{Q}} = \mathbf{G}\mathbf{Q}\mathbf{G}^{T}, \tag{4.34}$$

$$\bar{\mathbf{R}} = \mathbf{R} + \mathbf{D}\mathbf{N} + \mathbf{N}^{T}\mathbf{D}^{T} + \mathbf{D}\mathbf{Q}\mathbf{D}^{T}, \tag{4.35}$$

$$\bar{\mathbf{N}} = \mathbf{G}\left(\mathbf{Q}\mathbf{D}^{T} + \mathbf{N}\right) \tag{4.36}$$

4.3.4 Detection using the Innovation

Under stationary operating conditions the normalised innovation defined in (4.29) is white and Gaussian [51] [50] with zero mean and unity variance. As a result, the innovation's power spectral density (PSD) will be flat. Let us assume that the observation window has *N* samples and that the sampled PSD is created by taking the squared magnitude of the Discrete Fourier Transform (DFT) of $\gamma_n(n)$, i.e.

$$\Lambda(k) = \left|\Im_d\left\{\gamma_n(n)\right\}\right|^2 \qquad k=0,\ 1,\ \ldots N\text{-}1, \tag{4.37}$$

where $\Im_d\{\ \}$ is the discrete Fourier transform (DFT). It is well known that the samples of the DFT of white noise are chi-squared with two

degrees of freedom (also known as the exponential distribution) [14, 15, 73], i.e.

$$f\left\{\Lambda(k)\right\} = Ne^{-\Lambda(k)N}, \tag{4.38}$$

where $f\{x\}$ denotes the probability density function of x [74].

A suitable threshold can be set within the PSD at a theoretically determined confidence level found through the cumulative sum of the area under the Probability Density Function (PDF) (4.38). A 99% Confidence Interval (CI), say, would be determined by solving (4.39) for CI:

$$0.99 = \int_0^{CI} f_\Lambda\{\Lambda\}\, d\Lambda. \tag{4.39}$$

For example, using (4.39), a 60 second analysis window sampled at 10 Hz will yield a 99% Confidence Interval (CI) threshold of 0.0115. This figure is the normalised PSD ensemble threshold in watts/Hz.

As long as the system remains stationary the normalised innovation PSD is expected to remain white and reside within the threshold bounds at a given level of confidence. If the system experiences a large detrimental deviation from the stationary system model defined in (4.1)-(4.2) then a dominant spike is likely to appear above the threshold in the innovation PSD. This can be linked to an alarm in practice.

It should be noted here that the motivation behind the choice of the 60 second analysis window was not to be compliant with settings of protective devices, but to demonstrate the effectiveness of the technique in providing rapid information. In practice, if the damping is deteriorating there would not normally be an automatic protection relay to trip a line. The response would be to ramp back generator settings or to trip an offending item of plant if it could be identified. Hence the choice of using

a 60 second analysis window came about through discussions with the National Electricity Marketing Management Company (NEMMCO), Australia. These discussions focused more on the nature of the alarm to the operator and the requirement to provide rapidly available information as outlined in [65].

The following section will demonstrate the detection process with both simulated and real data.

4.4 Simulated Data Results

Before proceeding any further it is beneficial to qualify what constitutes a major deterioration in damping. Table 4-1 provides an assessment of damping performance as provided by the National Electricity Marketing Management Company (NEMMCO) Australia [31].

Based on the criteria in Table 4-1, a change in damping will be considered unacceptable and detrimental if damping moves into the inadequate region (i.e. damping is worse than $0.07s^{-1}$).

The simulations in this section pertain to a two mode, single measurement system as per equation (4.14). The simulation modal parameters used in this section represent typical modal parameters that may be found within the Australian power system. Hence initial parameters for Modes 1 and 2 (which represent a power system in quasi-stationary operation) were set respectively to:

$$\textbf{Mode 1}:\ A_1 = 1,\ \sigma_1 = 0.25s^{-1} \text{ and } f_1 = 0.25Hz$$

$$\textbf{Mode 2}:\ A_2 = 0.2,\ \sigma_2 = 0.4s^{-1} \text{ and } f_1 = 0.6Hz.$$

All simulations were run on 5 minute records. In all simulations the Mode 2 parameters remained constant over the duration of the 5 minute record, whereas the Mode 1 parameters were changed after an arbitrarily chosen two minutes. Three independent simulations (Type 1, Type 2 and Type 3)

were performed. The reason for undertaking three different simulations will become apparent when reviewing the simulation results. In simulation Type 1 a sudden detrimental change in damping was introduced to Mode 1 after two minutes, while the frequency remained constant.

TABLE 4-1 QUALITATIVE REFERENCE TO DAMPING PERFORMANCE

DAMPING Np/s	QUALITATIVE DESCRIPTION
$\sigma < 0$	UNSTABLE
$0 < \sigma < 0.05$	VERY INADEQUATE (VERY POOR)
$0.05 < \sigma < 0.07$	INADEQUATE (POOR)
$0.07 < \sigma < 0.139$	MARGINALLY ADEQUATE
$0.139 < \sigma < 0.2$	ACCEPTABLE (GOOD)
$\sigma > 0.2$	HIGHLY ACCEPTABLE (VERY GOOD)

In simulation Type 2 a sudden shift in modal frequency was introduced to Mode 1 after two minutes, while the damping was held constant. In simulation Type 3 a sudden shift in both modal frequency and a detrimental change in damping was introduced to Mode 1 after two minutes. These changes are quantified in Table 4-2. The detection process applied a "running" 60 second analysis window to the simulated data.

The PSD of the normalised innovation, as specified in (4.38), was then determined and the PSD was compared directly to the 99% CI threshold. The 99% CI threshold was chosen as an appropriate threshold based on previous work which examined suitable rapid detection of sudden large

changes within a stochastic system [73-76]. In this previous work, detailed in the earlier chapters of this thesis, it was shown that a 99% CI was capable of practically desirable detection [77], whilst minimising false alarms inherent within a stochastically excited system.

The measurement noise covariance matrix (4.4) was set to:

$$E\left\{\mathbf{v}(n)\mathbf{v}(n)^T\right\} = [0.01], \tag{4.40}$$

as the measurement noise in real power systems transducers is comparatively small with respect to the excitation covariance, Q [77]. For the simulations, the excitation covariance, Q, was arbitrarily set to unity for simplicity of analysis. The covariance, **N** in (4.5), is set to zero.

The results are outlined in the following subsections.

TABLE 4-2 DAMPING AND FREQUENCY CHANGES TO MODE 1

SIMULATION	DAMPING*		FREQUENCY*	
TYPE	0-2MIN	2-5MINS	0-2MIN	2-5MINS
1	0.25	**0.07**	0.25HZ	0.25HZ
2	0.25	0.25	0.25HZ	**0.32HZ**
3	0.25	**0.07**	0.25HZ	**0.32HZ**

* **BOLD** highlights changes from quiescent state.

4.4.1 Simulation Type 1- damping change.

One simulation run of the innovation PSD is shown in Figure 4-3 for a) the 60 second interval prior to the damping change, and b) the 60 second interval subsequent to the damping change.

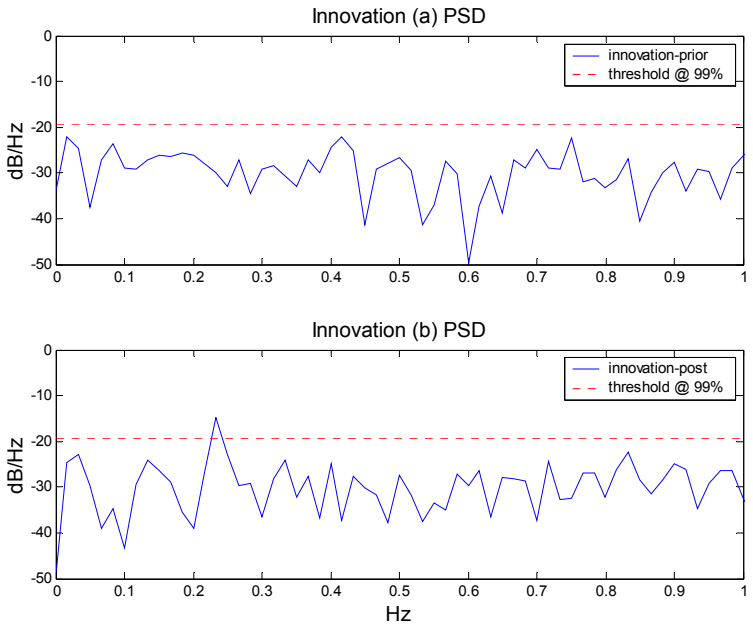

Figure 4-3 Innovation PSD of: a) the 60 second interval prior to the damping change, and b) the 60 second interval subsequent to the damping change.

The high spike around 0.25 Hz indicates a change in the damping of the mode centred at this frequency.

4.4.2 Simulation Type 2- frequency change

One simulation run of the innovation PSD is shown in Figure 4-4 for a) the 60 second interval prior to the frequency shift, and b) the 60 second interval subsequent to the frequency shift.

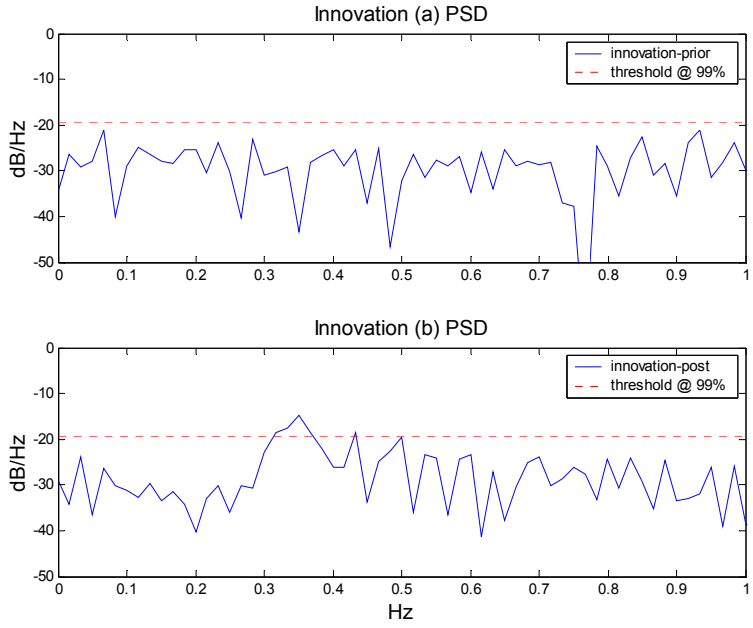

Figure 4-4 Innovation PSD of: a) the 60 second interval prior to the frequency shift, and b) the 60 second interval subsequent to the frequency shift.

In this result, the high spike around 0.32 Hz indicates a change in frequency.

4.4.3 Simulation Type 3- damping and frequency change

One simulation run of the innovation PSD is shown in Figure 4-5 for a) the 60 second interval prior to the damping change, and b) the 60 second interval subsequent to the damping and frequency change.

Note the high spike around 0.32 Hz indicates a change in frequency. It should also be noted that there is no means to distinguish if there is also a damping change; however simulations consistently demonstrated larger peaks when associated with detrimental damping change and frequency shift of a mode. Hence the simulations highlight the ability of this method to detect both a sudden detrimental change in damping as well as a shift in modal frequency.

Similar results were also obtained in the three tests when analysing the detector for changes in the weaker Mode 2, but these results are not shown here.

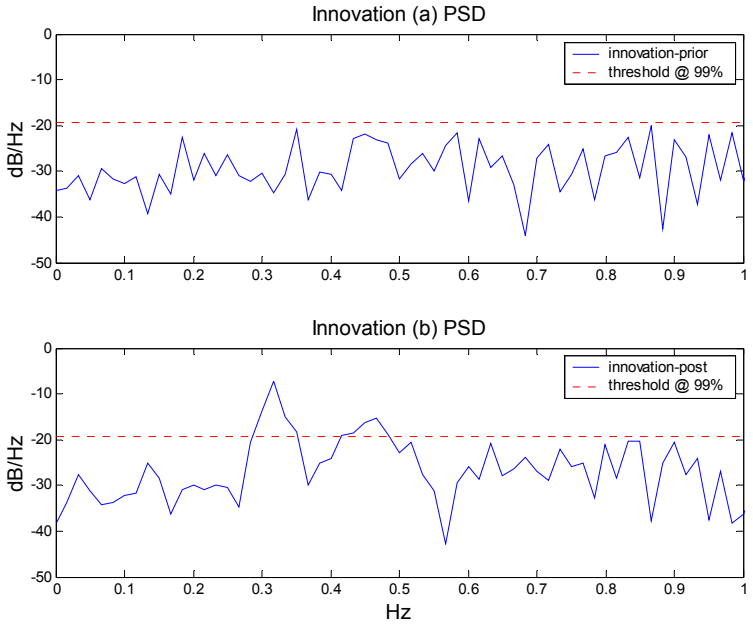

Figure 4-5 Innovation PSD of: a) the 60 second interval prior to the damping change, and b) the 60 second interval subsequent to the damping and frequency change.

Note that this chapter has focused on examining the spectrum of the Kalman innovation so as to detect significant modal changes within a power system. It would also be possible to monitor for changes by examining a waterfall PSD plot of the power system output. The latter has a number of disadvantages, however. Firstly, it is well known that PSD estimation introduces spectral smearing due to finite duration (i.e. windowing) effects. This spectral smearing has very little impact on spectrally white signals (such as Kalman innovations), but can have a large impact on "peaky" spectra (such as power system output PSDs). Secondly, the Kalman innovation is a well studied process and is well characterised statistically. It therefore lends itself well to thresholding and subsequent alarming. The power system output PSD (because it is burdened by finite duration artifacts) is much more difficult to characterise statistically.

4.4.4 Statistics of results

To gauge the reliability of the detector; statistics for 1000 simulation runs were examined. Table 4-3 shows the detection rate in the first 60 second window after the detrimental change has occurred, given a false alarm rate (FAR) of 0.1%.

TABLE 4-3 ALARMS (0.1% FAR)

SIMULATION TYPE	DETECTION RATE
	% OF ALARMS CORRECTLY REGISTERED
1	81.8%
2	82.5%
3	90.6%

4.5 Verification of the Kalman Method

Again the MudpackScript Case13 data is used for verification of the new method. In this analysis 150 minutes of the Case13 QNI data was used. To obtain the long-term system estimates the 1.75 hours of quasi-stationary data was used. After the long-term estimates are established the subsequent data was processed to see if any alarms occur (See Figure 4-6).

In Figure 4-6(a) the innovation at 107 minutes is examined. This section of data is expected to exhibit quasi-stationary characteristics as it is prior to the damping change at 120mins. The innovation spectrum shown in Figure 4-6(b) demonstrates the expected "*white*" spectrum of a system that has not undergone any detrimental changes.

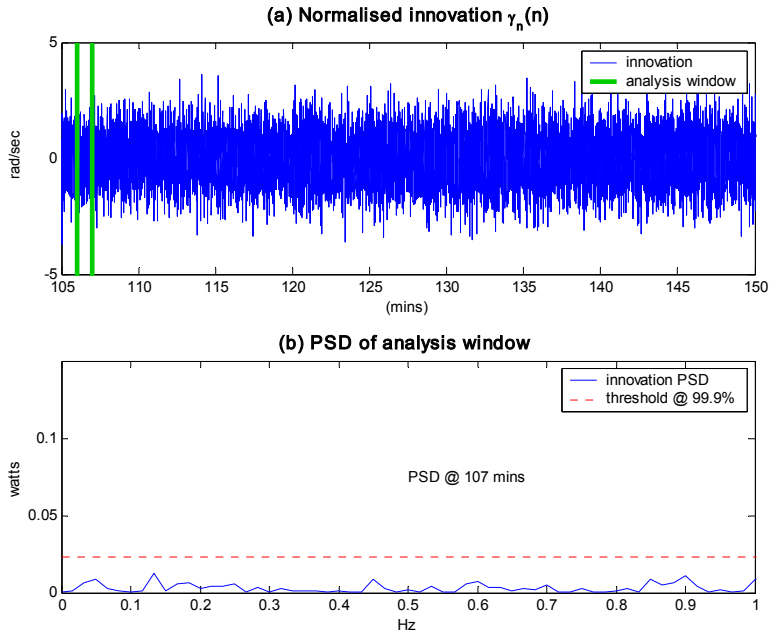

Figure 4-6 Analysis of Normalised Innovation prior to sudden deteriorating damping at 120mins.

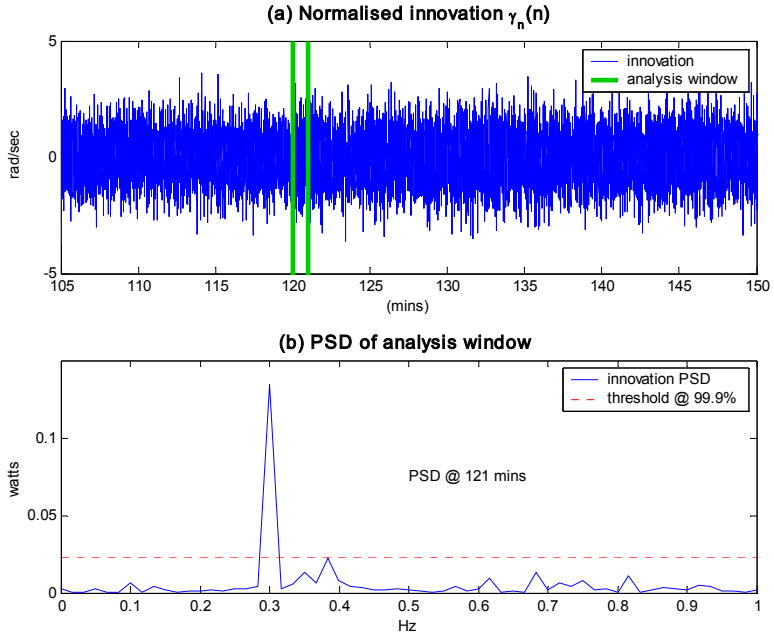

Figure 4-7 Analysis of normalised innovation in the 60 seconds after the deteriorating damping at 121mins.

In Figure 4-7(a) the analysis examines the first 60 seconds of the change at 120 mins. In Figure 4-7(b) the large spectral spike at 0.3Hz can be seen clearly which indicates the detrimental change of the mode centred around 0.3Hz. This corresponds to the expected change of the QNI mode at 2 hrs as shown earlier in Figure 2-5. The new method has thus performed as expected on the MudpackScript simulated data.

The Kalman method of modal analysis will now be applied to real data in the following section.

4.6 Application to Real Data

Data was obtained from the Australian power system, comprising voltage angle measurements at the Adelaide, Melbourne and Sydney measurement sites from 22:00 on 09/04/2004 to 03:05 on 10/04/2004. As mentioned earlier, voltage angle measurements were used rather than power signals because the potential for modal information extraction is

greater than when using power signals [11]. It is generally understood that inter-area modes have frequencies in the range 0.1 to 0.8 Hz and so this will be the region of focus in the PSD [24].

To formulate the state space model and consequently the system Kalman estimator, a knowledge (or at least an accurate estimate) of the power system transfer function must be available. Accordingly, for the work reported in this section, a long term estimator (LTE) was applied to estimate this transfer function [13]. This LTE was determined using a 45 minute window. Short-term (change) detection was then continuously applied to the PSD of the Kalman innovation.

The real data analysis was conducted in two parts. Part I closely examined 305 minutes of the Melbourne measurement data difference from the centre of area of the connected system (called Melbourne-COA) and Part II briefly analysed the data collected at the Sydney and Adelaide sites. Part II also examines the opportunity for combining the multi-site innovation power spectrum data to enhance the detector performance.

4.6.1 Part I: Analysis of the Melbourne Data

The LTE was determined from the data between 120-165 minutes after the start of the measurement record. The LTE quasi-stationary modal estimates were obtained using the technique in [13] and are listed in Table 4-4. The LTE also provides an estimate of the measurement site transfer function in Laplace form. As a result an estimate of the system quasi-stationary frequency response for Melbourne-COA can be observed in Figure 4-8. In Figure 4-8 the Mode 1 peak is quite apparent at 0.33 Hz, while the Mode 2 peak (estimated to be at 0.59Hz) is harder to distinguish due to the relatively heavy modal damping.

TABLE 4-4 DAMPING AND FREQUENCY LONG TERM ESTIMATES OVER 120-165 MINS

MODE	EIGENVALUES	DAMPING	FREQUENCY HZ	DAMPING RATIO %
1	$-0.2913 \pm j2.0735$	0.2913	0.33	13.91
2	$-1.0083 \pm j3.7071$	1.0083	0.59	26.25

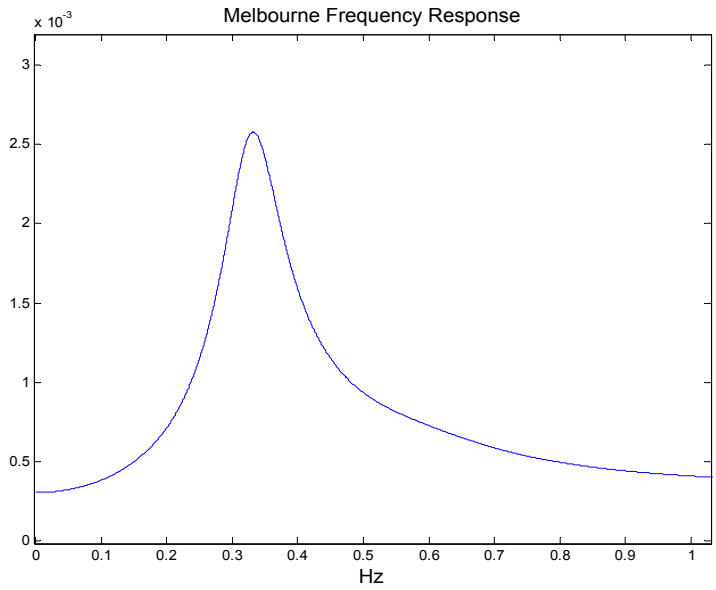

Figure 4-8 Melbourne frequency response estimate from LTE at 165 minutes.

Once the long term estimate of system characteristics was established, the remaining 140 minutes were examined in 1 minute intervals for any sudden detrimental changes to system modes.

To demonstrate the significant information the innovation sequence contains, one only has to compare the differentiated angle measurements with the normalised innovation (4.29) obtained after application of the Kalman estimator, shown in Figure 4-9. The comparison appears to support the result noted by Kailath in [51] – namely that the Kalman filter

innovation sequence contains the same information as the system output sequence, but in a less correlated form.

It is apparent from inspection of Figure 4-9 that the system output and the innovation both demonstrate a deviation from a quasi-stationary operation within the 197-201 minute interval. To lend some numerical support to this visual inspection a 60 second analysis window was applied to the innovation PSD before and during the 197-201 minute interval. The results of the analysis are provided in Figure 4-10 to Figure 4-12. The innovation is shown in Figure 4-10(a) with the 196-197 minute interval marked off by two vertical lines. The spectrum of the 196-197 minute segment of innovation is shown in Figure 4-10(b). To account for the fact that with real data, there is less certainty than there was with simulated data, a different threshold level will be used for the detection. Accordingly, the 99.999% CI threshold is shown as a dashed horizontal line. Even though such a threshold could be regarded as high, the main focus is to detect only large detrimental changes, and minimise false alarms. In the single site analysis, the data does exhibit a wide variance and hence a high threshold is required to minimise the false alarms. However in the following section, this issue is addressed and the ability to have more acceptable threshold CI's is presented along with a measured number of false alarms.

In examining Figure 4-10, no part of the spectrum crosses the threshold. Figure 4-11 depicts the innovation segment and associated spectrum corresponding to the 197-198 minute segment. For this segment the innovation spectrum crosses the threshold. Moreover, the threshold is crossed at the 0.59Hz frequency position, indicating a loss of damping for Mode 2. Figure 4-12 shows the innovation sequence and associated spectrum corresponding to the 198-199 minute segment. For this segment the innovation spectrum crosses the threshold in an even more pronounced way than it did in Figure 4-11(b). Again, the threshold is

crossed at the 0.59Hz frequency position, indicating a damping change for Mode 2.

Further analysis was performed which showed that the loss of damping was temporary. By the 201st minute of the data record, the modes re-set to their original characteristics.

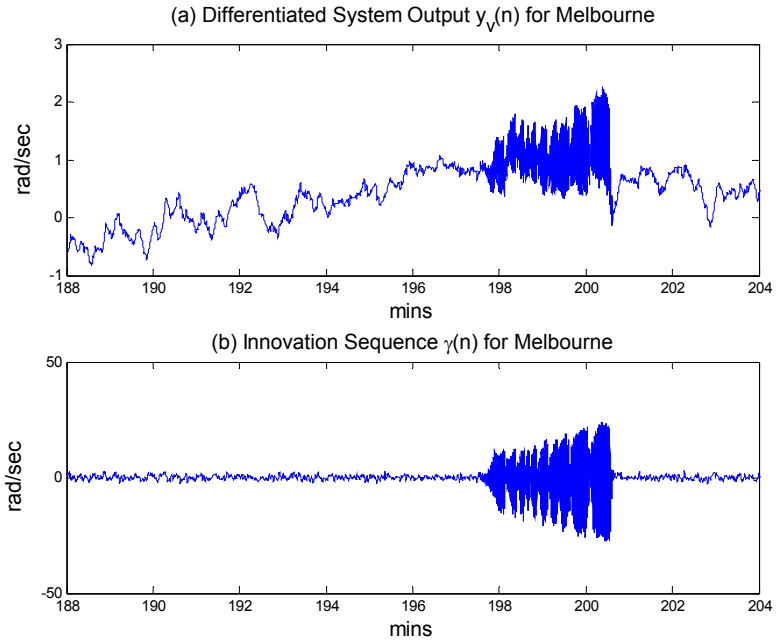

Figure 4-9 Comparison of (a) system output and (b) normalised innovation.

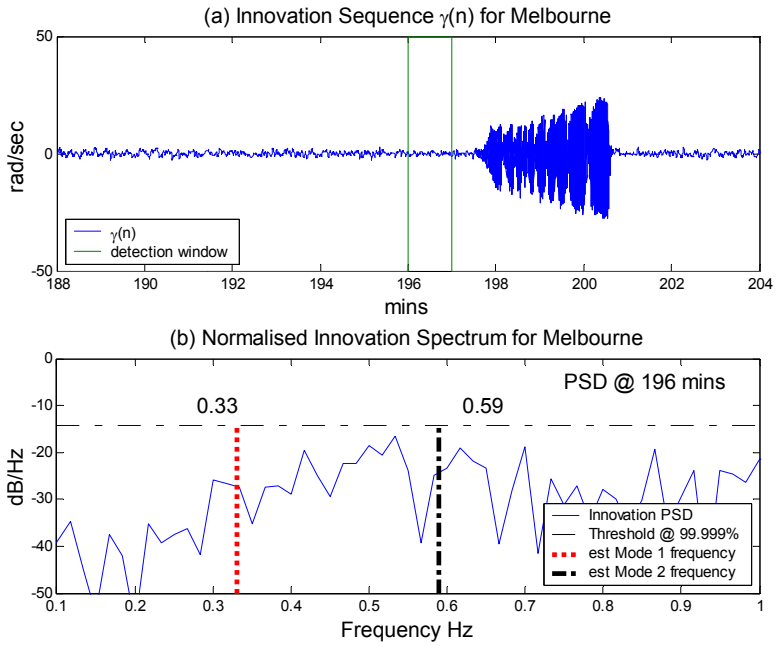

Figure 4-10 (a) Innovation sequence γ(n), (b) Innovation PSD at 196-197 mins.

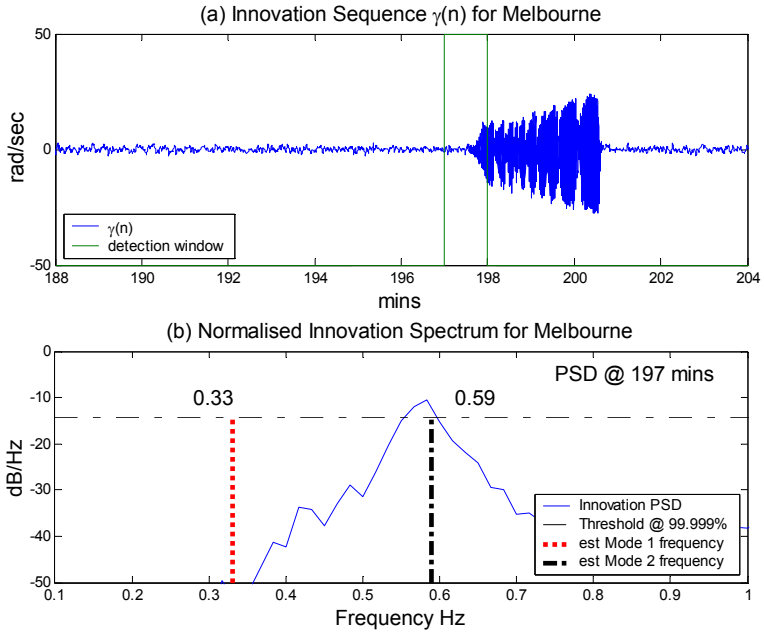

Figure 4-11 (a) Innovation sequence γ(n), (b) Innovation PSD at 197-198 mins.

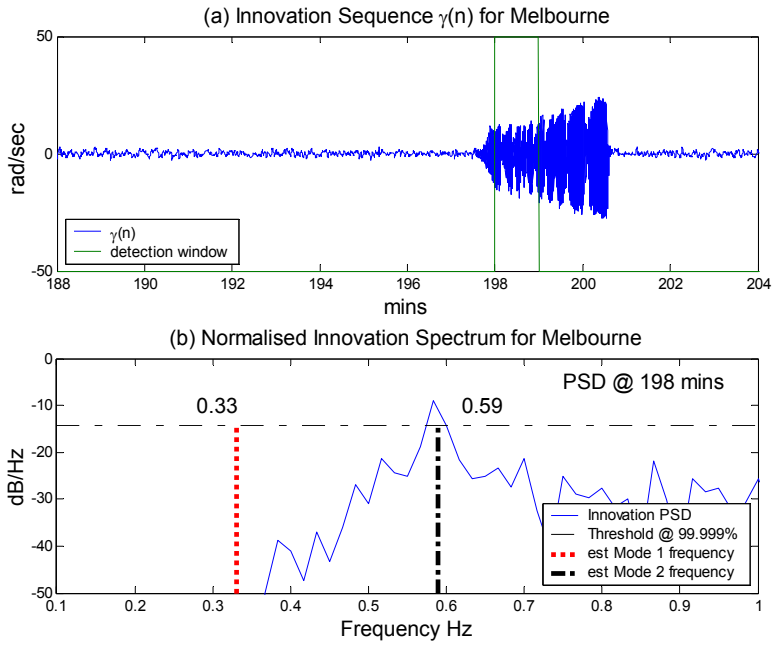

Figure 4-12 (a) Innovation sequence γ(n), (b) Innovation PSD at 198-199 mins.

4.6.2 Part II: Combining multi-site data for enhanced SNR and detection.

Similar data analysis was conducted for the other two measurement sites in Sydney and Adelaide (with COA correction). A comparison of the results for the 196-197 and the 198-199 minute time-frame can be seen in Figure 4-13(a) and Figure 4-14(a) respectively. Figure 4-13(a) demonstrates a spectrum for Sydney and Adelaide which does not cross the threshold prior to the event. Figure 4-14(a) shows a detection of damping deterioration centred at 0.59 Hz at both the Sydney and Adelaide sites. These results confirm the detection registered at the Melbourne site for the same analysis window.

Within these plots all sites exhibit similar responses to detection of damping deterioration. Therefore a combination of the innovation spectrum was examined to assess opportunities for an enhanced detector.

The combined spectrum was obtained by adding the complex innovation spectra from all three sites.

The threshold for the combined innovation spectrum will need to be set differently to that for the individual innovation spectra. Ideally if the individual normalised innovation spectra are all uncorrelated with one another then the samples of the combined innovation spectrum will again have a Chi-squared Probability Density Function (PDF) with 2 degrees of freedom, χ_2^2, but with three times the variance (assuming the individual normalised innovations have unity variance) [68]. In the case of the innovation spectra from the multi-site data as examined in this paper, the innovation spectra will not be strictly independent, as the power system is interconnected. Nonetheless, empirical experiments have indicated that a χ_2^2 distribution, with variance $3\sigma^2$, is a reasonably accurate way to model the PDF.

In the general case where X measurement sites are to be combined, the samples of the combined normalised innovation spectrum would have a Chi-squared PDF with 2 degrees of freedom [15, 76], and variance $X\sigma^2$. Thus using (4.29) the generalised ensemble frequency PDF for a combination of X, N-point innovation spectra would be:

$$f\left\{\Lambda(k)\right\} = \frac{N}{X} e^{-\Lambda(k)\frac{N}{X}}. \tag{4.41}$$

Hence for three measurement sites, $X = 3$, and (4.41) simplifies to:

$$f\left\{\Lambda(k)\right\} = \frac{N}{3} e^{-\Lambda(k)\frac{N}{3}}, \tag{4.42}$$

where (4.42) is the PDF of the three combined spectra assuming the power system is quasi-stationary and the resulting innovation, white.

The resulting combined innovation spectra prior to and during the disturbance are shown in Figure 4-14(b) and Figure 4-14(b) respectively.

It is important to note two significant outcomes attributed to the combining of the normalised innovation spectra. First, the combination of the three sites has led to an improvement in the Signal to Noise Ratio (SNR) for detectable signals. The SNR analysis results are shown in Table 4-5. The improved Signal to Noise Ratios exhibit comparable values to an ideal theoretical improvement of 4.77 dB (4.43), whereby an ideal theoretical improvement is one that would be expected if three identical deterministic signals, with independent, equal variance, Gaussian white noise were spectrally combined. Hence the resulting theoretical expected improvement would be:

$$\begin{aligned} SNR_{improvement} &= 10\log_{10}\left(3_{sites}\right) \\ &= 4.77dB. \end{aligned} \tag{4.43}$$

In practice the responses from the three sites are not perfectly independent and so one would expect less improvement than that predicted by (4.43). This is observed in Table 4-5.

The other significant point to highlight about the combined spectra is the reduced spectral variance. This result has enabled the ensemble spectral threshold to be reduced to a more desirable 99.9% FAR. Analysis of false alarms, from DC-1Hz, over the complete data set displayed an acceptable 0.077% of false alarms (as compared to the predicted 0.1%), providing confidence in the analytically derived ensemble PDF defined in (4.42).

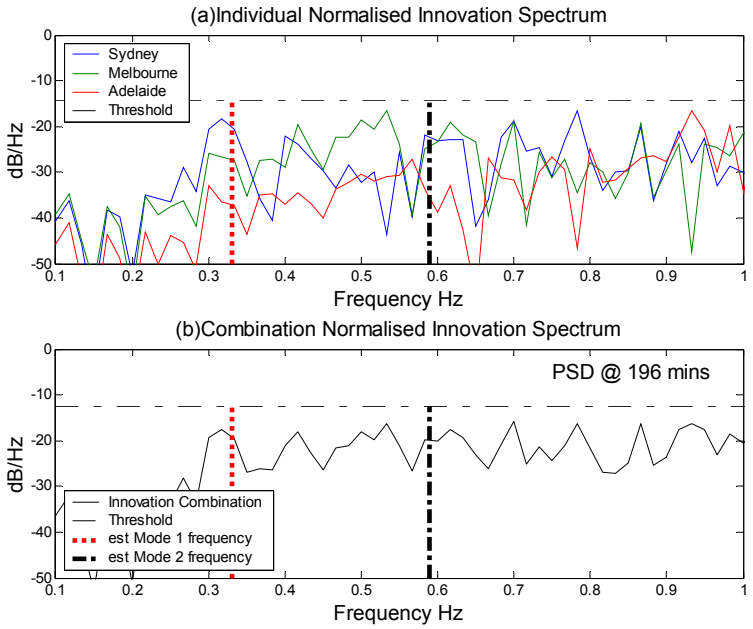

Figure 4-13 Normalised (a) Individual innovation PSDs for Sydney, Melbourne and Adelaide (b) Combination PSD at 196-197 mins. The new threshold corresponding to a 99.9% FAR.

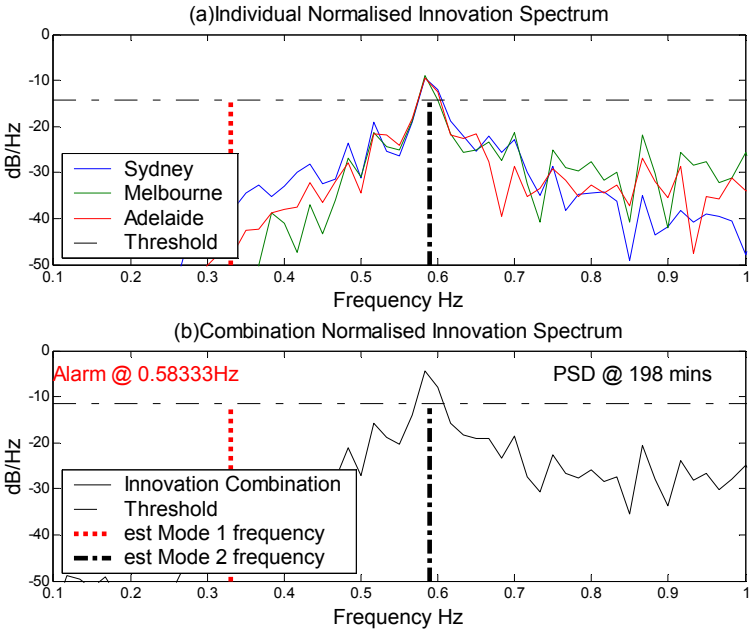

Figure 4-14 Normalised (a) Individual PSD at 198-199 mins (b) Combination PSD at 198-199 mins showing new threshold for CI of 99.9% FAR.

TABLE 4-5 SNR IMPROVEMENT THROUGH COMBINATION OF SITE ANALYSIS

PARAMETER	ANALYSIS WINDOW DURING ALARM SIGNAL (MINUTES)			
	197-198	198-199	199-200	200-201
AVERAGE SINGLE SITE SNR (DB)	9.60	7.60	10.82	11.64
COMBINED SNR (DB)	13.98	12.00	15.27	15.80
SNR IMPROVEMENT (DB)	**4.38**	**4.40**	**4.45**	**4.16**

4.7 Guidance in tuning the Kalman Filter

When dealing with real data applications of the Kalman Filter, the filter requires adequate tuning to achieve the desired optimal estimator. In Section IV, the values for Q and $\mathbf{R}$ are known *a priori* and can therefore be easily set; that is, the Kalman filter can be easily tuned. In real applications, however, such *a priori* knowledge of the error covariance matrices may not be available. Knowledge of the measurement transducer performance (i.e.: the measurement noise), however, could be obtained through testing. Even so, a method of tuning is still required to allow for changes over time. In addressing this issue, [77] notes that the selection of the error covariance Q is particularly important, such that $Q >> \mathbf{R}$. This would ensure the adaptive capability of the Kalman filter. In this thesis, it is also recognised that the measurement error covariance will be small; hence the determination of appropriate values in this analysis was obtained empirically, by first setting Q to unity, and then adjusting $\mathbf{R}$ so that the pseudo-stationary innovation result was close to white. Even

though the original system excitation covariance, Q, is not known, the subsequent normalisation of the innovation in (4.29) negates any effect of the unity assumption. Further techniques for tuning the filter can be derived from the literature (see [78] for example).

4.8 Discussion on real data analysis

From the time record it would appear that the disturbance to quasi-stationary operation occurred at around 197.75 minutes. This disturbance manifested clearly in the innovation spectrum of the 197-198 minute segment, even though only ¼ of this segment corresponded to the "changed" operating conditions. That is, detection of a change was achieved very quickly by the innovation spectrum thresholding, and the change appeared to be detected at the correct frequency (i.e. at the centre frequency of Mode 2). The detection occurred in less than a minute. This is in contrast to conventional estimation of damping, which typically only yields useful results after about half an hour. This provides support for the contention that the PSD of the Kalman innovation is an effective means for rapidly detecting modal changes and for identifying the nature of the modal changes that have occurred. In providing multi-site measurements for the enhanced Kalman detector, the large interconnected power system would require ongoing wide-area observation to ensure secure and reliable operations. To meet these requirements many wide-area monitoring methodologies have been proposed and established [18-20] as outlined earlier. One of the most well accepted approaches is to monitor the power system at various locations within the distribution network and to employ Global Positioning System (GPS) information to synchronise the information acquired [21, 22]. With this approach, the positioning of the measurement locations in the network is an important issue which is discussed in [23].

4.9 Conclusion

The Kalman estimator is an optimal linear estimator and has proved effective for rapidly detecting modal changes in both the simulated and real world power system scenarios considered. The new detection method has demonstrated an ability to not only rapidly detect large changes to power system modes, but has also been able to identify the mode which has changed. Multi-site measurements can be also used to provide greater confidence in the detection alarming. This has significant implications for power utility intervention strategies. Importantly, the method is computationally efficient and can easily be implemented in real-time.

Chapter 5

5 A new class of multi-linear functions for polynomial phase signal analysis

5.1 Introduction

This chapter introduces a new class of multi-linear functions which can be used for estimating/detecting changes to frequency in power systems. The new class of functions is based on modelling the frequency changes as arbitrary polynomial functions of time. The class incorporates a number of existing functions that include the Higher order Ambiguity Functions (HAFs) [79, 80], the Polynomial Wigner-Ville Distributions (PWVDs) [81] and the Higher order Phase (HP) functions [58]. Within this chapter the new class will be presented and the link between existing functions within the class will be explored. Subsequently the class formalism is used to deduce a new function. This new function is particularly suited to the analysis of a 4^{th} order polynomial phase signal. The chapter presents a statistical analysis of this new class member and reveals that it outperforms all existing methods of comparable computational complexity. The new class member is applied to the analysis of both simulated and real power system data.

In the past 15 years there has been a plethora of research contributions related to the analysis of time-varying frequency signals. A common modelling approach within this research field is to regard the time-varying signal as one with polynomial phase (and therefore a frequency trajectory which is a polynomial function of time). Then the problem of

estimating the frequency trajectory reduces to a problem of estimating the polynomial phase parameters. This is the approach adopted within this chapter. Hence it will be assumed that the noise-free signal component, $z_s(n)$, is a discrete-time polynomial phase signal (PPS) defined by:

$$z_s(n) = b_0 e^{j\phi(n)}, \qquad -\frac{N-1}{2} \le n \le \frac{N-1}{2}, \qquad (5.1)$$

where

$$\phi(n) = \sum_{p=0}^{P} a_p n^p. \qquad (5.2)$$

In (5.1) and (5.2), the generalised expressions for the time-varying signal has *P* as the order of the polynomial phase, and $\{b_0, a_0, a_1, a_2, \ldots, a_P\}$ as the unknown parameters, while *N* is an odd integer and the sampling rate is (without loss of generality) unity. Initially the amplitude, b_0, will be assumed to be constant. This assumption, however, can be relaxed later to one of a slowly varying amplitude (with respect to the phase). To avoid estimate ambiguities due to the cyclic nature of the spectra of digitised signals it is also assumed that the polynomial coefficients are bounded by (5.3) [79], [80].

$$|a_p| \le \frac{\pi}{p!\left(\frac{N}{p}\right)^{(p-1)}}, \qquad p = 1, 2, \ldots, P. \qquad (5.3)$$

The observed signal component, $z_r(n)$, is modelled as the noise-free component, $z_s(n)$, added to complex, white, Gaussian noise, $z_w(n)$, of variance, σ^2:

$$z_r(n) = z_s(n) + z_w(n). \tag{5.4}$$

In many cases, Maximum Likelihood (ML) estimation of the $\{b_0, a_0, a_1, a_2, \ldots, a_P\}$ parameter set is computationally prohibitive. Therefore in a quest to obtain computationally efficient parameter estimates with acceptable mean squared errors, researchers have devised alternative methods based on multi-linear functions. Examples of alternative research approaches include the Higher order Ambiguity Function (HAF) method [79], [80], the Polynomial Wigner-Ville distribution (PWVD) method [81] and the Higher order Phase (HP) function method [58]. The HAF, PWVD and HP methods achieve computational efficiency by requiring only one-dimensional maximisations. However, despite achieving computational efficiency, these methods are limited by the SNR threshold at which they can productively operate. The new class of multi-linear functions is partly motivated by this SNR threshold limitation.

This chapter will introduce a new class of multi-linear functions which subsumes a number of previously defined functions (defined in [56, 58, 79-81]). The new class, for example, incorporates the HAFs, the PWVDs and the HP functions; however the new class also develops a framework for the creation of new class members. Within this chapter, one such new member is introduced and applied to the problem of polynomial phase parameter estimation. This new class member is seen to have statistically superior performance to all previously known multi-linear functions.

The formulation of the new class is presented in Section 5.2. Section 5.2 also establishes the link to the previously defined sub-classes. In Section

5.3 the new class member is introduced, and applied to an appropriate parameter estimation problem. Section 5.4 contains a statistical analysis of the new class member introduced in Section 5.3. This is followed by Section 5.5 that presents results from simulations. Real data application and analysis follows in Section 5.6.

5.2 The new class of multi-linear functions

The new class of multi-linear functions introduced in this section is referred to as the Generalised Multi-linear Function Class (GMFC). It is defined in (5.5) below:

$$T_s^p\left(v,\Omega_p\right)=\sum_{over\ v}\ \prod_{i=0}^{I}[z_r^{\$_i}(n+\tau_i+c_i m)]\exp\left(-jd\Omega_p v^x\right). \tag{5.5}$$

The parameters of the generalised multi-linear function class in (5.5) are specified as follows:

s = 0 or 1,

p is the order of the polynomial phase coefficient to be estimated,

$\prod_{i=0}^{I}[z_r^{\$_i}(n+\tau_i+c_i m)]$ is the "kernel",

$\{I,\tau_i,\ c_i,d,x\}$ are an arbitrarily set parameters,

$v=\begin{cases}n & if\ s=0\\ m & if\ s=1\end{cases}$ and

$\$_i=+1$ or -1

where if $\$_i=+1$, then $z^{\$_i}(.)=z(.)$

or if $\$_i=-1$, then $z^{\$_i}(.)=z^*(.)$, the complex conjugate of $z(.)$.

From the generalised multi-linear function in (5.5) one can obtain the HAFs, the PWVDs or the HP functions by making appropriate selections for the various parameters listed above.

For example, if one sets $s=0$, $\tau_i=-iN/p,\ c_i=0\forall i$, $x=1$, $\$_i=\begin{cases}+1 \text{ if } i \text{ is even,}\\ -1 \text{ if } i \text{ is odd.}\end{cases}$ $d=1$, and the kernel is defined as $\prod_{i=0}^{p-1}[z_r^{\$_i}(n-iN/p)]^{\binom{p-1}{i}}$, then the higher ambiguity functions are obtained:

$$HAF^p\left(\Omega_p\right)=\sum_{over\ \mathrm{n}}\ \prod_{i=1}^{p-1}[z_r^{\$_i}(n-iN/p)]^{\binom{p-1}{i}}\exp\left(-j\Omega_p n\right). \qquad (5.6)$$

If the parameters are set such that $s=1$, $x=p$, and the d, $\$_i$ and c_i are resolved according to the principals in [56] and [62], then the HP functions are recovered:

$$HP^p\left(n,\Omega_p\right)=\sum_{over\ \mathrm{m}}\ \prod_{i=0}^{I}[z_r^{\$_i}(n+c_i m)]\exp\left(-jd\Omega_p m^p\right). \qquad (5.7)$$

Finally, to obtain the PWVD functions, one simply sets $p=1$ in (5.7) to get (5.8):

$$PWVD\left(n,\Omega\right)=\sum_{over\ \mathrm{m}}\ \prod_{i=0}^{I}[z_r^{\$_i}(n+c_i m)]\exp\left(-jd\Omega m\right). \qquad (5.8)$$

Therefore from the relationships just presented it can be seen that the GMFC provides a formalism which links various existing multi-linear functions. Additionally, though, the GMFC provides a framework for the creation of new functions. This framework can be exploited by simply varying the parameters in (5.5) to generate new class members. As an illustration of the way new class members can be designed, the next section will do precisely this and in doing so, introduce a new member of

the class which outperforms existing functions in the analysis of 4th order polynomial phase signals.

5.3 Designing new GMFC members

In this section a new member of the GMFC class will be designed to specifically target the analysis of 4th order polynomial phase signals. This is done because existing 4th order multi-linear analysis methods have quite high SNR thresholds.

The approach for designing the new class member will be similar to that used in [56] for generalising the CP function to the HP functions. Initially a set of non-linear equations is set up in the GMFC "coefficients". The target order for the non-linearity of the 4th order polynomial phase signal (PPS) analysis function will be set to 4, so that four multiplicative terms, only, will be in the kernel. This represents an ambitious design as this is a lower order than any other existing multi-linear function for analysing 4th order PPSs. Past experience has demonstrated that more effective multi-linear functions tend to be designed by setting $s=1$ (rather than = 0), therefore this design will pre-set $s=1$. With these initial parameters selected the following function is obtained in (5.9),

$$T_1^p\left(n,\Omega_p\right)=\sum_{over\ m}\left(\prod_{i=0}^{3} z_r^{\$_i}(n+\tau_i+c_i m)\right)\exp\left(-jd\Omega_p m^x\right). \qquad (5.9)$$

The remaining coefficients to be "designed" are the $\{c_i,\tau_i,\$_i\},d,x,$ and p parameters. To ensure that the design of (5.9) is useful in the estimation of the polynomial phase coefficients, $\left(a_0,a_1,\ldots a_{P-1}\right)$, it would be convenient if the function in (5.9) could yield a sharp peak when $\Omega_p=a_p$ and $n=0$, for a given 4th order PPS signal. Such a desirable outcome would occur if the equality in (5.10) can be assured, such that,

$$z_s^{\$_0}(\tau_0 + c_0 m) z_s^{\$_1}(\tau_1 + c_1 m) z_s^{\$_2}(\tau_2 + c_2 m) z_s^{\$_3}(\tau_3 + c_3 m)$$

$$= b_0^{\,I} \exp(jda_p m^x + j\phi), \tag{5.10}$$

where ϕ is an arbitrary constant and where $z_s(n)$ is a 4th order noise-free PPS, as defined in (5.1-2).

Substituting (5.1) and (5.2) into (5.10) and simplifying by taking the $\log_e$ yields:

$$\sum_{k=0}^{4} \sum_{i=0}^{3} (\$_i)(\tau_i + c_i m)^k = da_p m^x + \phi. \tag{5.11}$$

The final stages of the design process involve finding real values for the unknown coefficients, $(\{c_i, \tau_i, \$_i\}, d, x, \text{and } p)$, that will ensure that the non-linear equation in (5.11) is satisfied. Under experimentation certain choices for the coefficients *do* enable (5.11) to be satisfied. These choices are listed in (5.12) as,

$$p = 3,\ x = 2,\ \$_i = (-1)^i,\ \tau_i = (-1)^i \tau \ \text{ for } 0 < \tau < \text{N}/4,\ d = 6\tau \ \text{ and}$$

$$c_i = \begin{cases} 1, & i = 1, 2 \\ -1, & i = 3, 4. \end{cases} \tag{5.12}$$

With the coefficients specified in (5.12) the newly designed function is:

$$T_1^3(n, \Omega_3) = \sum_{over\ m} z_r(n + \tau + m) z_r^*(n - \tau + m) z_r(n + \tau - m) z_r^*(n - \tau - m) e^{-j6\tau\,\Omega_3 m^2} \tag{5.13}$$

If the observation is a noise-free 4th order PPS then it can be shown for a given value of *n*, that the function in (5.13) yields a peak at:

$$\Omega_3 = a_3 + 4a_4 n \quad , \tag{5.14}$$

as desired. The following sub-section will present an algorithm which uses the newly designed multi-linear function in (5.13) to estimate the parameters of a 4th order polynomial phase signal.

5.3.1 Algorithm for estimating the parameters of 4th order PPSs based on $T_1^3(n,\Omega_3)$

Step 1) Estimate two estimates, $\hat{\Omega}_{31}$ and $\hat{\Omega}_{32}$, from $T_1^3(n,\Omega_3)$ using the following estimators:

$$\hat{\Omega}_3(n_1) = \hat{\Omega}_{31} = \arg\max_{\Omega} \left| T_1^3(n_1,\Omega_3) \right| \tag{5.15}$$

$$\hat{\Omega}_3(n_2) = \hat{\Omega}_{32} = \arg\max_{\Omega} \left| T_1^3(n_2,\Omega_3) \right|. \tag{5.16}$$

Step 2) Motivated by (5.14), $\hat{\boldsymbol{\alpha}}$ is determined from the matrix equation:

$$\hat{\boldsymbol{\alpha}} = \mathbf{X}^{-1}\hat{\mathbf{R}}, \tag{5.17}$$

where $\hat{\boldsymbol{\alpha}} = \begin{bmatrix} \hat{a}_3 & \hat{a}_4 \end{bmatrix}^T$, $\hat{\mathbf{R}} = \begin{bmatrix} \hat{\Omega}_{31} & \hat{\Omega}_{32} \end{bmatrix}^T$ and $\mathbf{X} = \begin{bmatrix} 1 & 4n_1 \\ 1 & 4n_2 \end{bmatrix}$.

Step 3) Estimate $\hat{a}_2$ by de-chirping the observation by $\hat{a}_3 n^3 + \hat{a}_4 n^4$ and then using the cubic phase function [62]:

$$z_{rd}(n) = z_r(n) e^{-j(\hat{a}_3 n^3 + \hat{a}_4 n^4)} \tag{5.18}$$

$$\hat{a}_2 = \arg\max_{\Omega_2} \left| \sum_{n=0}^{(N-1)/2} z_{rd}(n+m)\, z_{rd}(n-m) e^{-j\Omega_2 m^2} \right|. \tag{5.19}$$

Step 4) Find $\hat{a}_1$ by de-chirping the observation by $\hat{a}_2 n^2 + \hat{a}_3 n^3 + \hat{a}_4 n^4$ and then using the Fourier transform:

$$D(\Omega_1) = \sum_{n=\frac{-N}{4}}^{\frac{N}{4}} z_r(n) e^{-j\left(\hat{a}_2 n^2 + \hat{a}_3 n^3 + \hat{a}_4 n^4\right)} e^{-j\Omega_1 n}, \tag{5.20}$$

$$\hat{a}_1 = \arg\max_{\Omega_1} \left| D(\Omega_1) \right|. \tag{5.21}$$

Step 5) Refine the initial $\hat{a}_1$, $\hat{a}_2$, $\hat{a}_3$ and $\hat{a}_4$ parameter estimates by using the de-chirping/filtering/phase-unwrapping refinement algorithm described in Section 6 of [62].

This process initially involves de-chirping the observation to obtain a baseband like signal

$$z_{rd}(n) = z_r(n) e^{-j\left(\hat{a}_1 n + \hat{a}_2 n^2 + \hat{a}_3 n^3 + \hat{a}_4 n^4\right)}. \tag{5.22}$$

Because of the effective down-conversion to baseband of the observation signal, the *signal content* of $z_{rd}(n)$ will be spectrally concentrated around *0Hz*. However the noise content will be evenly spread over the entire band, and therefore one can low-pass filter to remove most of the noise without significantly disturbing the signal content. The subsequent low-pass filtered signal can then have its phase unwrapped, and from this linear regression can be used to estimate its polynomial phase parameters. The resulting estimates are essentially the "fine" estimates which are added to the initial coarse estimates obtained in Steps 2-4 above. Importantly, due to the optimality of the phase unwrapping linear regression approach, the final "refined" estimates (respectively denoted as $\hat{a}_{1f}$, $\hat{a}_{2f}$, $\hat{a}_{3f}$ and $\hat{a}_{4f}$) will all have variances which approach the Cramér-Rao (CR) bound asymptotically above threshold.

Step 6) Find $\hat{a}_0$ and $\hat{b}_0$ with the following estimators:

$$\hat{b}_0 = \frac{1}{N} \left| D(\hat{a}_1) \right| \tag{5.23}$$

$$\hat{a}_0 = \text{angle}\left\{ D(\hat{a}_1) \right\}. \tag{5.24}$$

To ensure optimal application of the above algorithm some of the values need to be specified. It is recommended that the following parameters are set such that: $\tau = \frac{N-1}{4}$, $n_1 = 0$ and $n_2 = 0.55N$. It will be mathematically shown in Section 5.4, that these values enable asymptotically optimal final estimates to be obtained. It is important to highlight again that the above algorithm involves only a 4th order non-linearity. In comparison, the equivalent HP function algorithm has a 6th order non-linearity [56], and the corresponding HAF algorithm has an 8th order non-linearity [79]. The new class member therefore has a much more appealing level of non-linearity.

The proposed algorithm implementation is relatively straightforward. To ensure computational efficiency in arguments maximising (5.15), (5.16) and (5.19), sub-band decomposition techniques in the frequency-rate domain can be employed. Employing these techniques will ensure that the computational complexity of the algorithm is $O(N \log N)$.

5.4 Derivation of the Asymptotic Mean Squared Errors

This section derives the asymptotic (i.e. large sample) MSEs for the unknown parameter estimates. The estimates are compared to the values for Cramér-Rao lower bounds defined in [63]. For convenience the approximate formulae for the CRLBs are shown in Table 5-1 [63].

TABLE 5-1 APPROXIMATE FORMULAE FOR CRLBS $(N >> 1)$ [63]

	$p=1$	$p=2$	$p=3$	$p=4$
$CRLB\{a_0\}_p$	$\frac{\sigma_w^2}{2Nb_0^2}$	$\frac{9\sigma_w^2}{8Nb_0^2}$	$\frac{9\sigma_w^2}{8Nb_0^2}$	$\frac{225\sigma_w^2}{128Nb_0^2}$
$CRLB\{a_1\}_p$	$\frac{6\sigma_w^2}{N^3b_0^2}$	$\frac{6\sigma_w^2}{N^3b_0^2}$	$\frac{75\sigma_w^2}{2N^3b_0^2}$	$\frac{75\sigma_w^2}{2N^3b_0^2}$
$CRLB\{a_2\}_p$		$\frac{90\sigma_w^2}{N^5b_0^2}$	$\frac{90\sigma_w^2}{N^5b_0^2}$	$\frac{2205\sigma_w^2}{2N^5b_0^2}$
$CRLB\{a_3\}_p$			$\frac{1400\sigma_w^2}{N^7b_0^2}$	$\frac{1400\sigma_w^2}{N^7b_0^2}$
$CRLB\{a_4\}_p$				$\frac{22050\sigma_w^2}{N^9b_0^2}$

The subsequent asymptotic mean squared error derivations in this section follow the approach used in [16].

First consider the estimates, $\hat{\Omega}_3(n_1)=\hat{\Omega}_{31}$ and $\hat{\Omega}_3(n_2)=\hat{\Omega}_{32}$, determined in (5.15) and (5.16). These estimates are obtained through a maximisation of $T_1^3\left(n,\Omega_3\right)$ at times, n_1 and n_2, respectively. An estimate based on the maximisation of $T_1^3\left(n,\Omega_3\right)$ at some arbitrary time, *n*, is:

$$\hat{\Omega}_3(n)=\arg\max_{\Omega_3}\left|T_1^3(n,\Omega_3)\right|, \tag{5.25}$$

where the new member, $T_1^3\left(n,\Omega_3\right)$, incorporating the optimal choice for τ is given in (5.26) as,

$$T_1^3\left(n,\Omega_3\right)=\sum_{m=0}^{\frac{N}{4}-|n|} z_s^*\left(n+m-\tfrac{N-1}{4}\right)z_s\left(n+m+\tfrac{N-1}{4}\right)\times \\ \ldots z_s^*\left(n-m-\tfrac{N-1}{4}\right)z_s\left(n-m+\tfrac{N-1}{4}\right)e^{-j6\frac{N-1}{2}\Omega_3 m^2}. \tag{5.26}$$

To maintain consistency with the technique in [16, 62], let the signal-to-noise ratio (SNR) be defined as:

$$SNR=\frac{{b_0}^2}{\sigma^2}. \tag{5.27}$$

To determine the MSE of $\hat{\Omega}_3(n)$ the following formulae, (5.28), (5.29), (5.30) and (5.31) are obtained from the appendix of [16]:

$$MSE\left[\Omega_{3t}(n)\right]=\frac{E\left[B^2\right]}{A^2}, \tag{5.28}$$

where $E[.]$ is the expected value.

Terms A and B are respectively defined as:

$$A=2\Re\left\{T_1^3\left(n,\Omega_{3t}\right)\frac{\partial^2 T_1^{3*}\left(n,\Omega_{3t}\right)}{\partial{\Omega_3}^2}+\frac{\partial T_1^3\left(n,\Omega_{3t}\right)}{\partial\Omega_3}\frac{\partial T_1^{3*}\left(n,\Omega_{3t}\right)}{\partial\Omega_3}\right\} \tag{5.29}$$

$$B=2\Re\left\{T_1^3\left(n,\Omega_{3t}\right)\frac{\partial\delta T_1^{3*}\left(n,\Omega_{3t}\right)}{\partial\Omega_3}+\frac{\partial T_1^3\left(n,\Omega_{3t}\right)}{\partial\Omega_3}\delta T_1^{3*}\left(n,\Omega_{3t}\right)\right\}, \tag{5.30}$$

$$z_{ws}(n,m) = z_r^*\left(n+m-\tfrac{N}{4}\right) z_r\left(n+m+\tfrac{N}{4}\right) z_r^*\left(n-m-\tfrac{N}{4}\right) z_r\left(n-m+\tfrac{N}{4}\right)$$

$$= \left[z_s^*\left(n+m-\tfrac{N}{4}\right) + z_w^*\left(n+m-\tfrac{N}{4}\right) \right] \left[z_s\left(n+m+\tfrac{N}{4}\right) + z_w\left(n+m+\tfrac{N}{4}\right) \right] \times$$

$$\cdots\cdots \left[z_s^*\left(n-m-\tfrac{N}{4}\right) + z_w^*\left(n-m-\tfrac{N}{4}\right) \right] \left[z_s\left(n-m+\tfrac{N}{4}\right) + z_w\left(n-m+\tfrac{N}{4}\right) \right]$$

$$\begin{aligned}
&= z_s^*\left(n+m-\tfrac{N}{4}\right) z_s\left(n+m+\tfrac{N}{4}\right) z_s^*\left(n-m-\tfrac{N}{4}\right) z_w\left(n-m+\tfrac{N}{4}\right) \\
&+ z_s^*\left(n+m-\tfrac{N}{4}\right) z_s\left(n+m+\tfrac{N}{4}\right) z_w^*\left(n-m-\tfrac{N}{4}\right) z_s\left(n-m+\tfrac{N}{4}\right) \\
&+ z_s^*\left(n+m-\tfrac{N}{4}\right) z_s\left(n+m+\tfrac{N}{4}\right) z_w^*\left(n-m-\tfrac{N}{4}\right) z_w\left(n-m+\tfrac{N}{4}\right) \\
&+ z_s^*\left(n+m-\tfrac{N}{4}\right) z_w\left(n+m+\tfrac{N}{4}\right) z_s^*\left(n-m-\tfrac{N}{4}\right) z_s\left(n-m+\tfrac{N}{4}\right) \\
&+ z_s^*\left(n+m-\tfrac{N}{4}\right) z_w\left(n+m+\tfrac{N}{4}\right) z_s^*\left(n-m-\tfrac{N}{4}\right) z_w\left(n-m+\tfrac{N}{4}\right) \\
&+ z_s^*\left(n+m-\tfrac{N}{4}\right) z_w\left(n+m+\tfrac{N}{4}\right) z_w^*\left(n-m-\tfrac{N}{4}\right) z_s\left(n-m+\tfrac{N}{4}\right) \\
&+ z_s^*\left(n+m-\tfrac{N}{4}\right) z_w\left(n+m+\tfrac{N}{4}\right) z_w^*\left(n-m-\tfrac{N}{4}\right) z_w\left(n-m+\tfrac{N}{4}\right) \\
&+ z_w^*\left(n+m-\tfrac{N}{4}\right) z_s\left(n+m+\tfrac{N}{4}\right) z_s^*\left(n-m-\tfrac{N}{4}\right) z_s\left(n-m+\tfrac{N}{4}\right) \\
&+ z_w^*\left(n+m-\tfrac{N}{4}\right) z_s\left(n+m+\tfrac{N}{4}\right) z_s^*\left(n-m-\tfrac{N}{4}\right) z_w\left(n-m+\tfrac{N}{4}\right) \\
&+ z_w^*\left(n+m-\tfrac{N}{4}\right) z_s\left(n+m+\tfrac{N}{4}\right) z_w^*\left(n-m-\tfrac{N}{4}\right) z_s\left(n-m+\tfrac{N}{4}\right) \\
&+ z_w^*\left(n+m-\tfrac{N}{4}\right) z_s\left(n+m+\tfrac{N}{4}\right) z_w^*\left(n-m-\tfrac{N}{4}\right) z_w\left(n-m+\tfrac{N}{4}\right) \\
&+ z_w^*\left(n+m-\tfrac{N}{4}\right) z_w\left(n+m+\tfrac{N}{4}\right) z_s^*\left(n-m-\tfrac{N}{4}\right) z_s\left(n-m+\tfrac{N}{4}\right) \\
&+ z_w^*\left(n+m-\tfrac{N}{4}\right) z_w\left(n+m+\tfrac{N}{4}\right) z_s^*\left(n-m-\tfrac{N}{4}\right) z_w\left(n-m+\tfrac{N}{4}\right) \\
&+ z_w^*\left(n+m-\tfrac{N}{4}\right) z_w\left(n+m+\tfrac{N}{4}\right) z_w^*\left(n-m-\tfrac{N}{4}\right) z_s\left(n-m+\tfrac{N}{4}\right) \\
&+ z_w^*\left(n+m-\tfrac{N}{4}\right) z_w\left(n+m+\tfrac{N}{4}\right) z_w^*\left(n-m-\tfrac{N}{4}\right) z_w\left(n-m+\tfrac{N}{4}\right).
\end{aligned}$$

(5.31)

In (5.29) and (5.30) the term, $\Re\{.\}$ signifies the real part of $\{.\}$. It should be noted that B is a random quantity and A is deterministic. The deterministic character of A arises because all the constituent terms are derived from the noise free signal. Equations (5.28)-(5.31) were used to determine the results in (5.32)-(5.34) below:

$$A \approx \frac{-8b_0^8 (3N)^2 \left(\frac{N}{4} - |n|\right)^6}{45} \tag{5.32}$$

$$B \approx -2b_0^4 (3N)\left(\tfrac{N}{4} - |n|\right)\left[\operatorname{Im}\{\Gamma(n)\}\right], \tag{5.33}$$

where $\Gamma(n)$ is defined as:

$$\Gamma(n) \approx e^{j\phi(n)} \sum_{m=0}^{\frac{N}{4}-|n|} \left(m^2 - \frac{\left(\frac{N}{4} - |n|\right)^2}{3} \right) z_{ws}^{*}(n,m) \exp\left(j\Omega_{3t} m^2 \right). \tag{5.34}$$

Then

$$\begin{aligned} MSE\{\Omega(n)\} &\approx E\left\{ \left(\frac{1}{3N} \right)^2 \frac{45\left[\operatorname{Im}\{\Gamma(n)\}\right] 45\left[\operatorname{Im}\{\Gamma(n)\}\right]}{4b_0^4 \left(\frac{N}{4} - |n|\right)^5 4b_0^4 \left(\frac{N}{4} - |n|\right)^5} \right\} \\ &\approx \frac{2025 E\left[\left(\operatorname{Im}\{\Gamma(n)\} \right)^2 \right]}{144 b_0^8 N^{12} \left(\frac{1}{4} - \frac{|n|}{N} \right)^{10}}. \end{aligned} \tag{5.35}$$

Now

$$E\left[\operatorname{Im}\{\Gamma(n)\}^2 \right] \approx \frac{\left(N - 4|n|\right)^5}{11520} \left(\frac{\sigma^8 + 4\sigma^6 b_0^2 + 6\sigma^4 b_0^4 + 4\sigma^2 b_0^6}{2} \right), \tag{5.36}$$

and thus,

$$MSE\left(\hat{\Omega}_3(n)\right) \approx \frac{2025}{144 b_0^8 N^{12} (1/4 - |n|/N)^{10}} \frac{(N-4|n|)^5}{11520} \left(\frac{\sigma^8 + 4\sigma^6 b_0^2 + 6\sigma^4 b_0^4 + 4\sigma^2 b_0^6}{2} \right)$$
$$\approx \frac{640}{N^2 (N-4|n|)^5} \left(\frac{1}{SNR^4} + \frac{4}{SNR^3} + \frac{6}{SNR^2} + \frac{4}{SNR} \right). \tag{5.37}$$

Substituting $n = 0$ and $n = 0.55N$ in (5.37) gives:

$$MSE(\hat{\Omega}_3(0)) = MSE\left(\hat{\Omega}_{31}\right)$$
$$\approx \frac{640}{N^7} \left(\frac{1}{SNR^4} + \frac{4}{SNR^3} + \frac{6}{SNR^2} + \frac{4}{SNR} \right), \tag{5.38}$$

$$MSE(\hat{\Omega}_3(0.55N)) = MSE\left(\hat{\Omega}_{32}\right)$$
$$\approx \frac{2216.7}{N^7} \left(\frac{1}{SNR^4} + \frac{4}{SNR^3} + \frac{6}{SNR^2} + \frac{4}{SNR} \right). \tag{5.39}$$

Using (5.17), it follows that:

$$MSE(\hat{a}_3) = MSE\left(\hat{\Omega}_{31}\right) \tag{5.40}$$

and hence

$$MSE\{\hat{a}_3\} \approx \frac{640}{N^7 SNR} \left(\tfrac{1}{SNR^3} + \tfrac{4}{SNR^2} + \tfrac{6}{SNR} + 4 \right)$$
$$\approx \frac{2560}{N^7 SNR} \left(\tfrac{1}{4SNR^3} + \tfrac{1}{SNR^2} + \tfrac{3}{2SNR} + 1 \right). \tag{5.41}$$

The ratio of the MSE of $\hat{a}_3$ to the CRB (see Table 5-1) at high SNR is:

$$\frac{MSE_{\hat{a}_3}}{CRB_{\hat{a}_3}} \approx 10\log_{10}\left(\frac{2560}{1400}\right) = 2.62\text{dB}. \tag{5.42}$$

From (5.17) $\hat{a}_4$ is given by:

$$\hat{a}_4 = \frac{\hat{\Omega}_{32} - \hat{\Omega}_{31}}{4(n_2 - n_1)}. \tag{5.43}$$

If $n_1 = 0$ and $n_2 = 0.055N$, then, the MSE of $\hat{a}_4$ is:

$$\begin{aligned} MSE\{\hat{a}_4\} &= \frac{MSE\{\Omega_{32}\} + MSE\{\Omega_{31}\} - 2E\{\Omega_{32}\Omega_{31}\}}{16(0.055)^2} \\ &\approx \frac{\left(\frac{2560}{N^7} + \frac{8866.8}{N^7}\right)\left(\frac{1}{4SNR^4} + \frac{1}{SNR^3} + \frac{3}{2SNR^2} + \frac{1}{SNR}\right) - 2E\{\Omega_{32}\Omega_{31}\}}{16(0.055)^2} \\ &\approx \frac{2.36077e5\left(\frac{1}{4SNR^4} + \frac{1}{SNR^3} + \frac{3}{2SNR^2} + \frac{1}{SNR}\right) - 41.33E\{\Omega_{32}\Omega_{31}\}}{N^9} \\ &\approx \frac{1.305e5 + 2.36077e5\left(\frac{1}{4SNR^3} + \frac{1}{SNR^2} + \frac{3}{2SNR}\right)}{N^9 SNR}. \end{aligned} \tag{5.44}$$

The ratio of the MSE of $\hat{a}_4$ to the CRB at high SNR is:

$$\frac{MSE_{\hat{a}_4}}{CRB_{\hat{a}_4}} \approx 10\log_{10}\left(\frac{1.3505e5}{2.2050e4}\right) \approx 7.8\text{dB} \tag{5.45}$$

$\hat{a}_2$ and $\hat{a}_1$ are determined according to (5.19) and (5.21). If one uses a similar analysis to that which was used in [82] and [62], the MSEs for $\hat{a}_2$ and $\hat{a}_1$ are found to be:

$$MSE\{\hat{a}_2\} \approx \frac{6075.9 + 10836\left(\frac{1}{4SNR^3} + \frac{1}{SNR^2} + \frac{3}{2SNR}\right)}{N^5 SNR} \tag{5.46}$$

$$MSE\{\hat{a}_1\} \approx \frac{63.6 + 57.6\left(\frac{1}{4SNR^3} + \frac{1}{SNR^2} + \frac{3}{2SNR}\right)}{N^3 SNR}. \tag{5.47}$$

The ratio of the MSEs of $\hat{a}_2$ and $\hat{a}_1$ to their respective CR bounds are:

$$\frac{MSE_{\hat{a}_2}}{CRB_{\hat{a}_2}} \approx 10\log_{10}\left(\frac{6075.9}{1102.5}\right) \approx 7.4\text{dB} \tag{5.48}$$

$$\frac{MSE_{\hat{a}_1}}{CRB_{\hat{a}_1}} \approx 10\log_{10}\left(\frac{63.6}{37.5}\right) \approx 2.3\text{dB}. \tag{5.49}$$

As previously mentioned, the final parameter estimates, $\hat{a}_{1f}$, $\hat{a}_{2f}$, $\hat{a}_{3f}$ and $\hat{a}_{4f}$, are obtained from the initial intermediate estimates, $\hat{a}_1$, $\hat{a}_2$, $\hat{a}_3$ and $\hat{a}_4$. The refining process applies the de-chirping/filtering/phase unwrapping algorithm described in Section 6 of [62]. It should be noted that the final estimates are all asymptotically optimal. This is due to the asymptotically optimal results the phase unwrapping/least squares estimation approach provides. This optimality relies upon the initial intermediate estimates being close enough such that the down-converted signal content is truly concentrated around 0Hz. Therefore with the signal content at baseband it will not be unduly disturbed by low-pass filtering. The analysis conducted within this section demonstrated that all the intermediate estimates are very close, giving estimate variances of the same order as the CRB. Therefore this implies that the de-chirped signal's spectral content will be near 0Hz and will not extend further than $O\left(N - 1/2\right)$ Hz from 0Hz.

5.5 Simulations

The estimation algorithm in Section 5.3 was applied to a fourth order polynomial phase signal submerged in additive noise for a range of different noise levels. The noise model applied was complex, white, zero

mean Gaussian noise. The additive noise levels used corresponded to the SNR range of 0 to 9dB. Monte-Carlo simulations were conducted over one hundred runs with a 1031 sample length observation.

The signal parameters defined in (5.1) and (5.2) were set as per Table 5-2.

TABLE 5-2 PARAMETER VALUES OF 4TH ORDER POLYPHASE SIGNAL USED IN SIMULATIONS

SIGNAL PARAMETER $_{(P=4)}$	VALUE
a_0	1.0
a_1	0.3927
a_2	$6e-4$
a_3	$1.0e-6$
a_4	$1.0e-9$
b_0	1.0

It should be noted that the choice of coefficients, a_{1-4}, in Table 5-2 adhere to the required unambiguous bounds defined in (5.3).

The following figures; Figure 5-1 to Figure 5-6 show the results of the simulations whereby:

i) the simulated Mean Square Errors (MSEs) for the final parameter estimates, $\hat{a}_{1f}$, $\hat{a}_{2f}$, $\hat{a}_{3f}$ and $\hat{a}_{4f}$ are denoted with plus signs,

ii) the CR bounds are shown as solid lines,

iii) the simulated MSEs of the intermediate parameter estimates, $\hat{a}_1$, $\hat{a}_2$, $\hat{a}_3$ and $\hat{a}_4$ are circled and

iv) the theoretically derived MSEs for the intermediate estimates are denoted with dashed lines.

As seen in Figure 5-1 to Figure 5-6, the final estimates are very close to the Cramér-Rao bounds, supporting the claim in this chapter that the final estimates are asymptotically optimal above the threshold.

Also observed for the new algorithm, is the SNR threshold of 1dB. This is an extremely favourable improvement when compared with the threshold of approximately 10dB given in [83] for the HAFs. Another pleasing aspect is the close alignment of the simulated MSEs of the intermediate estimates with the theoretically derived MSEs.

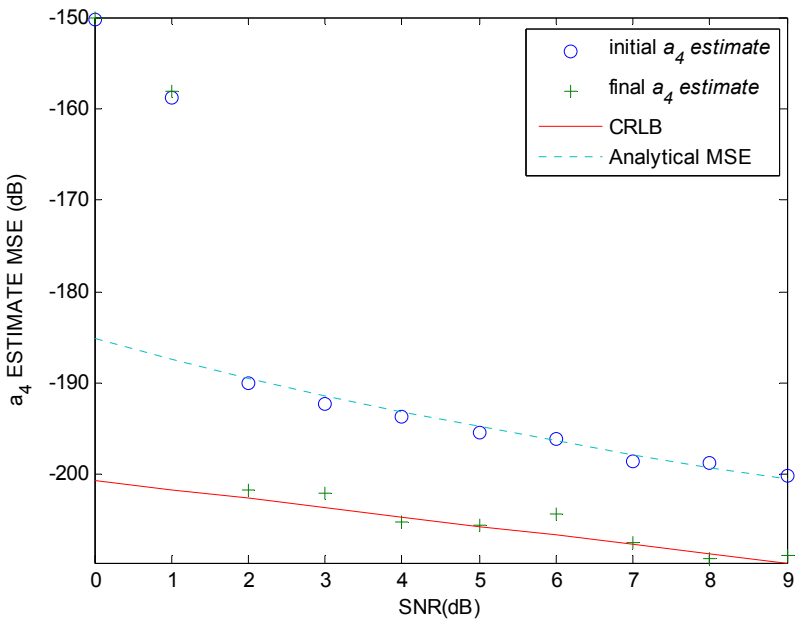

Figure 5-1 a_4 estimate MSE vs. SNR for the final and intermediate parameter estimates.

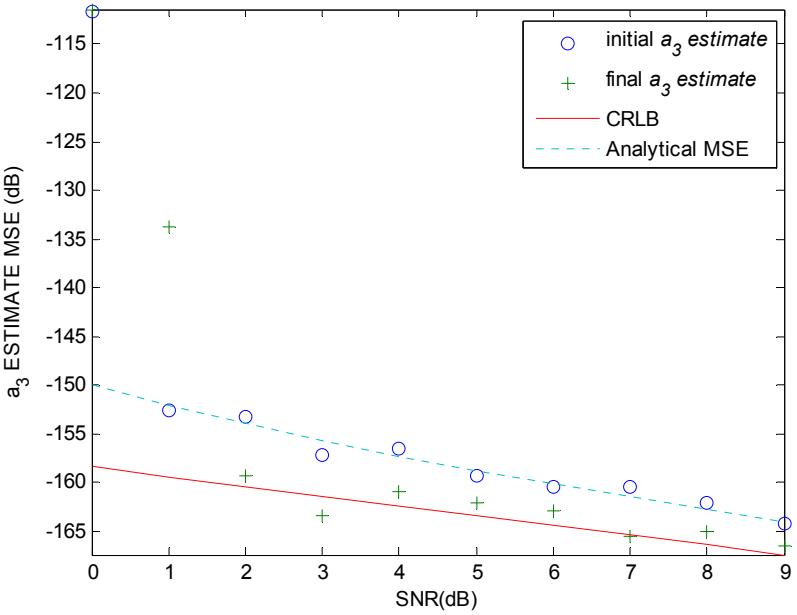

Figure 5-2 a_3 estimate MSE vs. SNR for the final and intermediate parameter estimates.

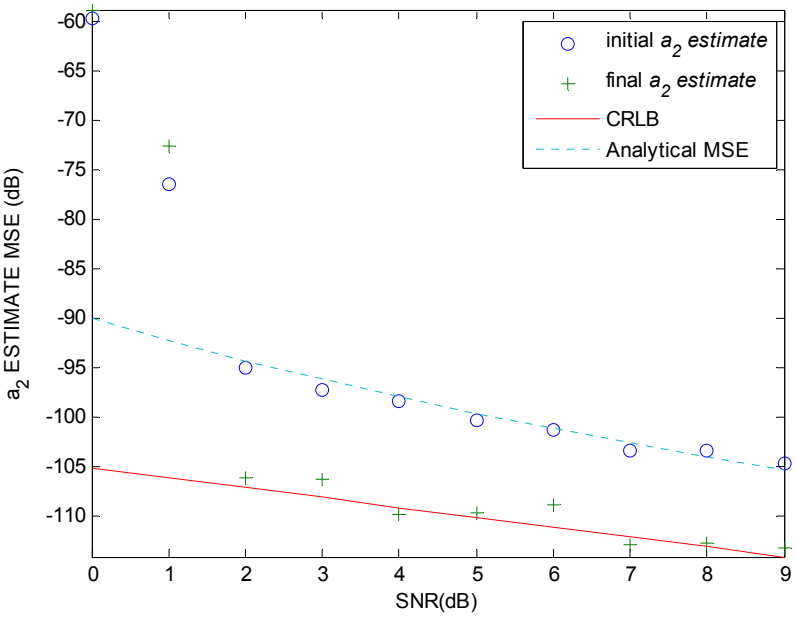

Figure 5-3 a_2 estimate MSE vs. SNR for the final and intermediate parameter estimates.

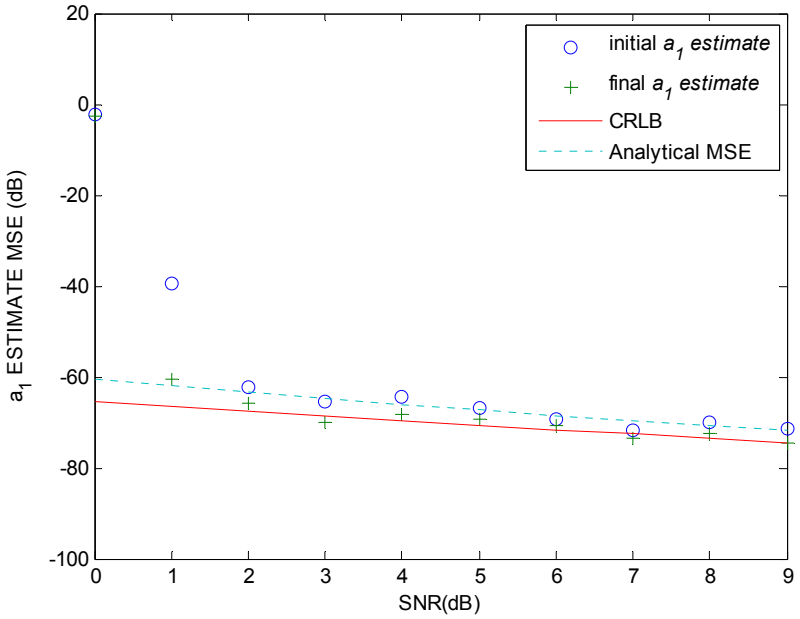

Figure 5-4 a_1 estimate MSE vs. SNR for the final and intermediate parameter estimates.

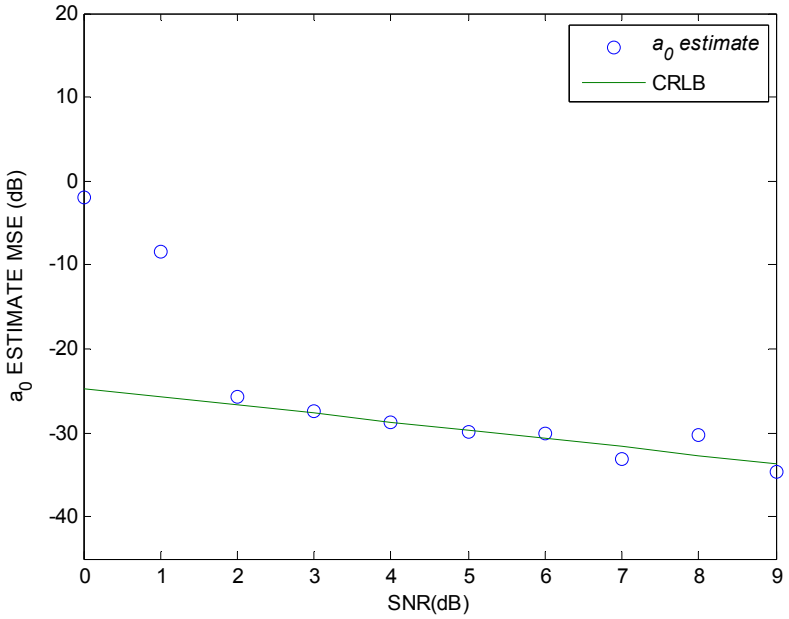

Figure 5-5 a_0 estimate MSE vs. SNR for the final parameter estimates.

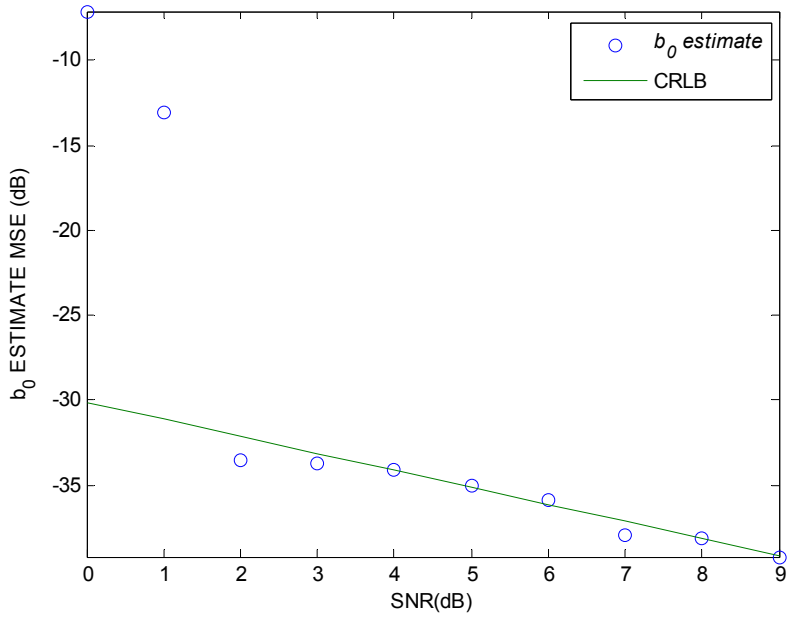

Figure 5-6 b_0 estimate MSE vs. SNR for the final parameter estimates.

5.6 Application in Power System Monitoring

A new class of multi-linear functions has been introduced and shown to out-perform previously available techniques. Analytical studies in the previous section have demonstrated the method's effectiveness in the analysis of a fourth order PPS. The previous sections also established the low computational overhead of the method. Together these attributes are an attractive option in situations that require accurate parameter estimates of frequency varying signals in short-time frames, combined with the requirement of low computational overhead. As a consequence this section will demonstrate the value of the method by analysing real power system data.

Monitoring the frequency variations of the power system is necessary because power system load variations and system dynamics are time-varying. As a consequence, power flows, system modal parameters and frequencies are also time-varying. It has been established in earlier

chapters that the power system may be regarded as quasi-stationary over short time periods when operating under normal conditions. With the short-term quasi-stationary system in mind, methods to enable the rapid detection of sudden detrimental change were also formulated in the earlier chapters. These rapid detection methods employed system parameter estimates of modal frequency and damping which were established using long-term parameter estimators. The multi-linear functions however can present better monitoring of the frequency trends in the power system than the LT estimator employed in previous chapters. This is because the multi-linear function provides both ongoing frequency estimates and the rates of frequency change (chirp) in relatively short time frames. The higher order chirp estimates $(\hat{a}_2, \hat{a}_3$ and $\hat{a}_4)$ provide a clearer picture of the frequency dynamics and will indicate visibly rapid changes if they occur. Rapid changes are indicated because under quasi-stationary conditions the higher order chirp estimates would ideally be around zero. A scenario where frequency rate information is useful is when the *separation* of a generation node occurs. Prior to *separation* the large interconnected power system will have associated modal parameters established through LTE. In a separation scenario, these parameters may no-longer be valid, as one power generation node (South Australia for example) is no longer connected to rest of the system (composed of Victoria, N.S.W and Queensland for example). Hence the system dynamics will change and the formulation of new modal characteristics will be established post-separation.

In separation scenarios it is generally understood the remaining modal frequencies will shift spectrally as the swing between remaining generation COA's establishes a *new* equilibrium within the *new* system dynamic. This also applies to the separated generation node. The sudden shift in frequency will be highlighted by a non-zero trajectory of estimates in the higher order chirp estimates. As a consequence of the

separation, the previously established rapid detection benchmarks at each COA measurement site will be invalid. This is of major concern as the post-separation system dynamics can be extremely vulnerable to further unstable behaviour and may result in the consequential loss of supply**.**

Under these circumstances the establishment of a "*worst case benchmark*" to immediately monitor the system in the critical time just after separation may be formulated. Pre-set damping conditions combined with estimates of the modal frequencies can establish short-term approximate benchmarks until enough time has passed for more accurate methods (which require longer data sets) to provide the system modal parameters estimates.

This is just one possible scenario for the application of this PPS estimation method within the power system environment. Another is to supply the Kalman methods outlined in the Chapter 4 with more accurate frequency estimates. The Kalman innovation is very much dependant on the original LT estimates. Section 4.5.2 demonstrated the effect upon the innovation spectrum when the system had experienced a modal frequency shift even though there was no damping change. More accurate estimates of modal frequency would assist the Kalman innovation method of Chapter 4 to be more of a modal damping detector and identifier rather than modal frequency and damping detector. Without an up-to-date and reasonably accurate frequency estimate in the Kalman formulation, any spectral detections, which occur, may contribute to an ambiguous situation in answering the hypothesis; *Has the damping changed or has the frequency changed or is it both?*

With the above in mind the following section will now apply the multi-linear function method to real power system data. This section will estimate the chirp co-efficients, $\hat{b}_0, \hat{a}_0, \hat{a}_1, \hat{a}_2, \hat{a}_3, \hat{a}_4$ of the observed signal and examine the results.

5.6.1 Real Data Analysis and Results

Data was obtained from the Australian power system, comprising voltage magnitude, $|V(t)|$, and phase measurements, $\phi(t) = \angle V(t)$, from the Adelaide measurement site starting at 01:15 on 10/04/2004 to 01:25 on 10/04/2004. A plot of this data is shown in Figure 5-7.

The voltage magnitude and phase measurements represent a positive sequence signal originally sampled at 50 Hz. Therefore a positive sequence analytic signal was reconstructed from the magnitude and phase measurements as below:

$$z_r(t) = |V(t)| e^{j\phi(t)}. \tag{5.47}$$

The reconstructed Adelaide signal in (5.47) can be viewed in Figure 5-8. The data was then re-sampled, taking every eighth sample, providing a 6.25Hz sampling rate.

The choice of down-sampling by 8 samples $(f_s = 6.25Hz)$ was devised through experimentation. It was observed that when the analysis was undertaken with a 1Hz sampled signal (down-sampling by every 50^{th} sample) then the estimates displayed erratic tendencies and parameter trajectories were more difficult to see clearly. Higher sampling $(eg: f_s = 10Hz)$ however did not provide adequate signal information with an analytical length of 511 samples. However taking every 8^{th} sample tended to demonstrate smoother transitions between estimate points and enhance the ability to establish reliable trends in the data.

The following plots of parameter estimates were from 511 samples taken in a sliding window that incremented one sample at a time through the full data set. Each analytic window of 511 samples is equivalent to 81.72sec of data when sampled at 6.25Hz. Examples of the 511 point window with respect to the data are shown in Figure 5-9 and Figure 5-10

respectively. The choice of the areas shown in Figure 5-9 and Figure 5-10 were made to highlight parts of the signal where suddenly large frequency changes can be observed.

The results for parameter estimates of $\hat{b}_0, \hat{a}_0, \hat{a}_1, \hat{a}_2, \hat{a}_3, \hat{a}_4$ are shown in Figure 5-11 to Figure 5-16 respectively.

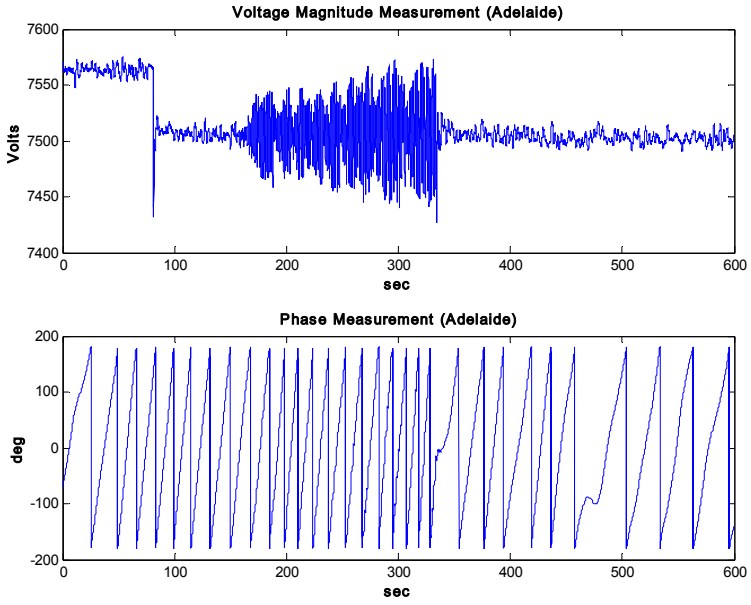

Figure 5-7 Measured Data, (a) Voltage Magnitude and (b) Phase.

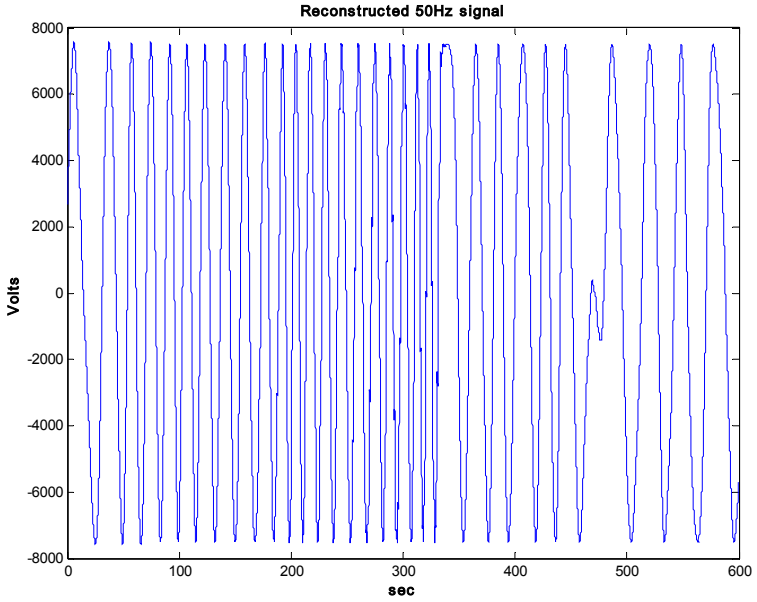

Figure 5-8 Reconstructed Signal $z_r(t)$.

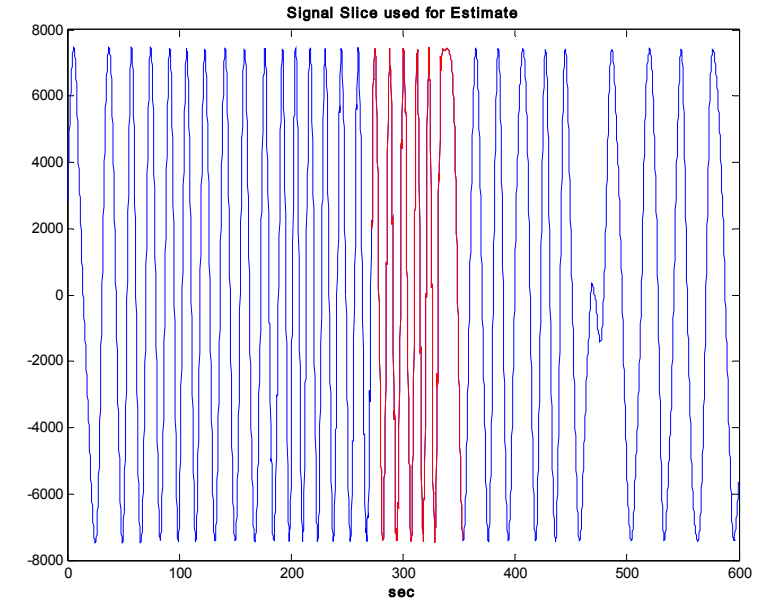

Figure 5-9 Example of signal slice used for parameter estimation, down-sampled to 6.25Hz. Coloured signal shown is around the first phase disturbance.

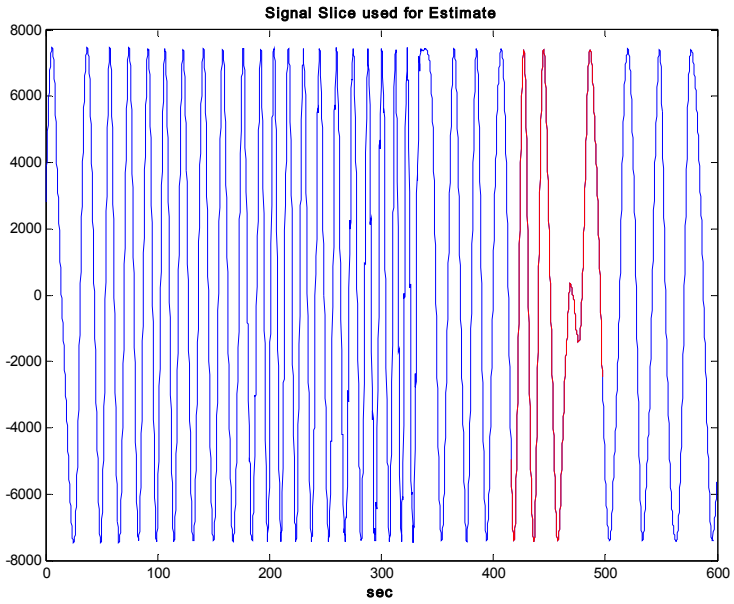

Figure 5-10 Second example of signal slice used for parameter estimation, down-sampled to 6.25Hz. Coloured signal shown is around the second phase disturbance.

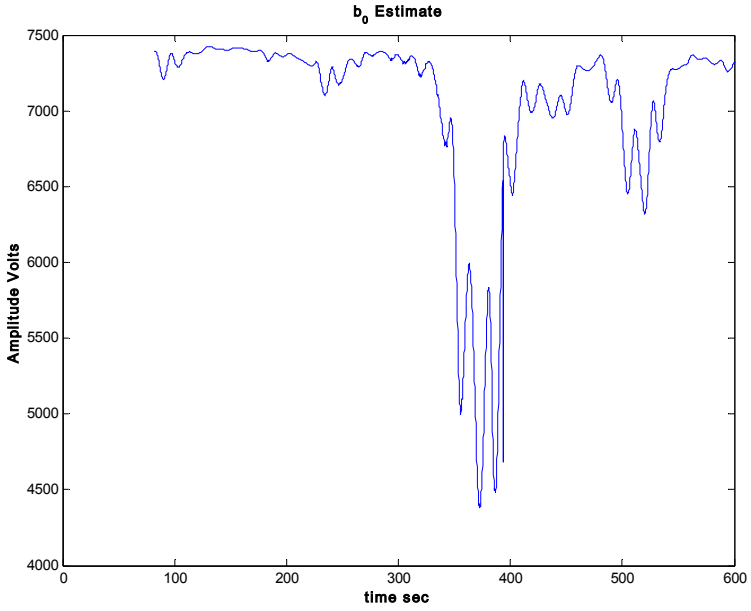

Figure 5-11 b_0 estimate.

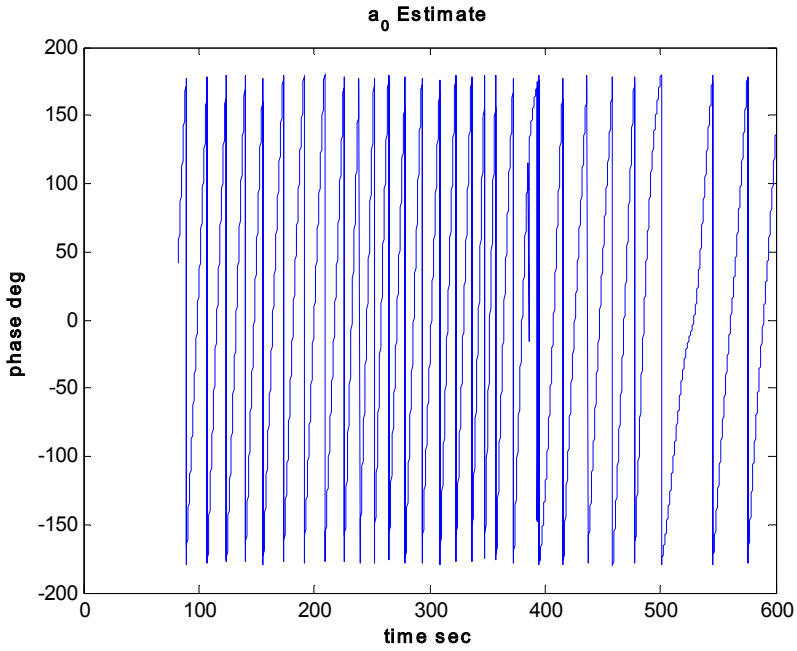

Figure 5-12 a_0 estimate (phase deg).

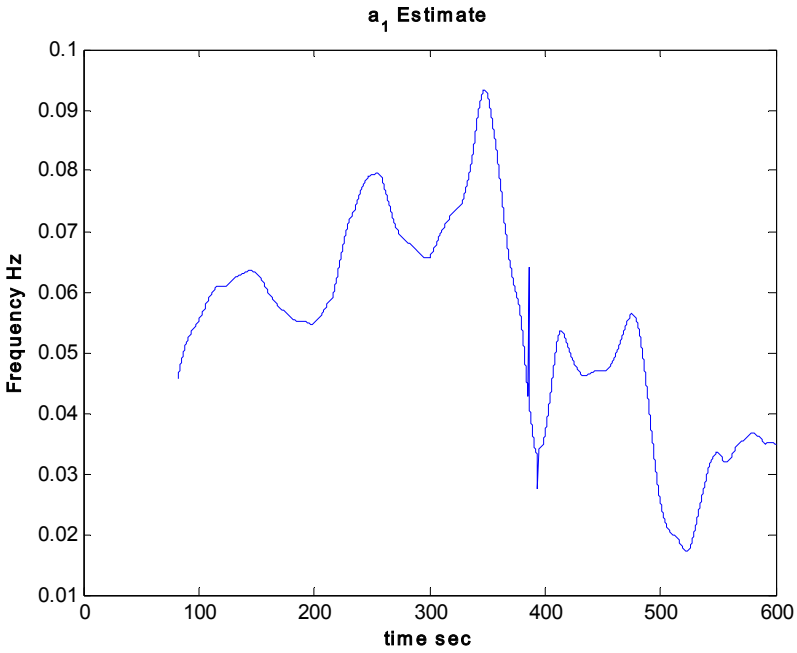

Figure 5-13 a_1 estimate, $f = \frac{\omega}{2\pi}$.

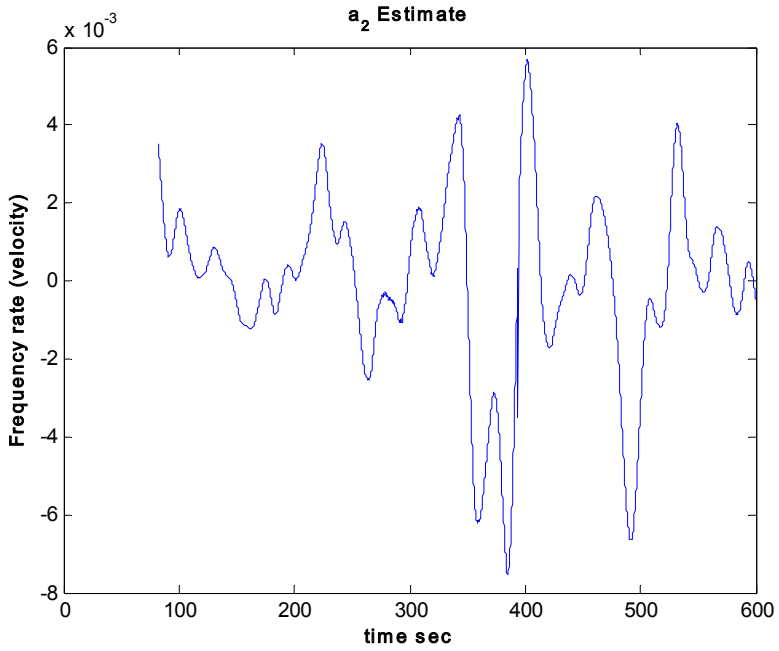

Figure 5-14 a_2 estimate (frequency rate), $\dot{\omega}$.

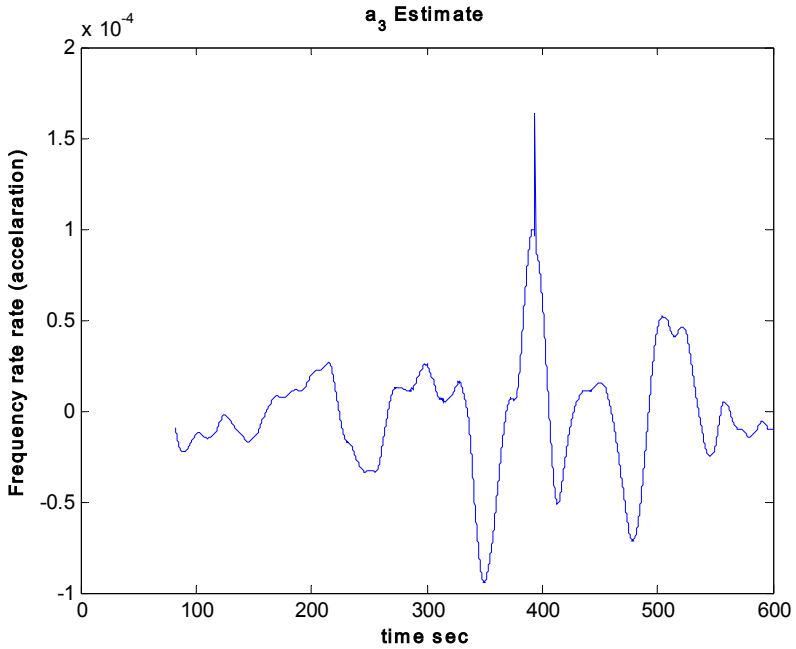

Figure 5-15 a_3 estimate, $\ddot{\omega}$.

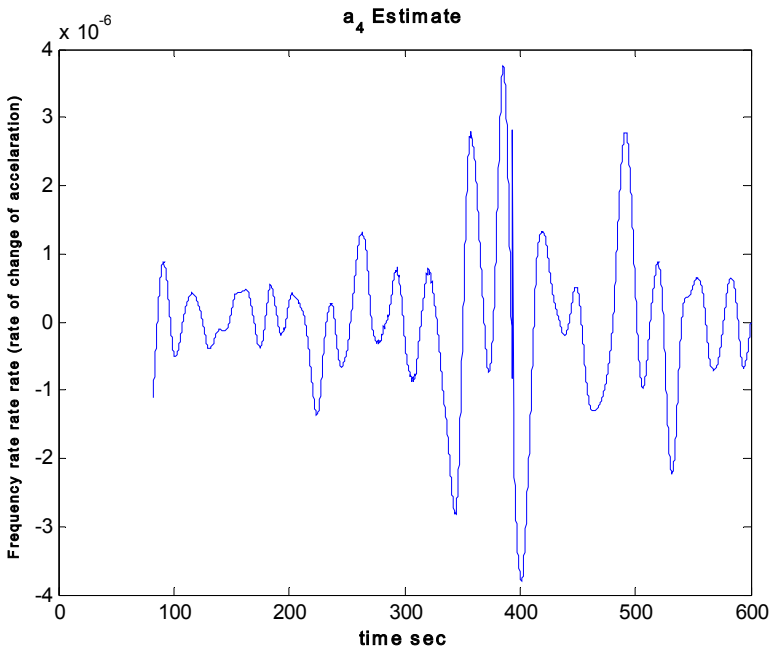

Figure 5-16 a_4 estimate, $\dddot{\omega}$.

5.6.2 Discussion on Real Data Analysis

In examining the real analysis results, the first points of notable interest are the sudden phase shifts in the original data record (at approximately 350 and 490 seconds, Figure 5-9 and Figure 5-10 respectively). These large and sudden shifts are clearly highlighted by large non-zero trajectories in the subsequent a_2, a_3 and a_4 estimates.

In Figure 5-13, the a_1 estimate shows a definite increase in frequency between approximately 100-320 seconds. This increase in frequency is reflected in the original data shown in Figure 5-8. Over this time frame the higher order parameters, a_3 and a_4, do not display large non-zero trajectories indicating that the frequency acceleration and rate of change of acceleration is low. However the a_2 estimate in Figure 5-14 does display larger non-zero trajectories confirming increase in frequency, indicating a slow rate of change in the signal chirp.

5.7 Conclusion

A new class of multi-linear functions has been introduced which has subsumed a number of existing sub-classes. The formalism of the new class has allowed the creation of a new multi-linear function which has been very effective in analysing a 4^{th} order PPS as it has outperformed previously available techniques of comparable complexity. Analytical studies and simulation results have been presented with the two supporting one another. Applications of the method to power system analysis have been presented. An example of the effectiveness in estimating real data and showing trends and frequency trajectories within this data has also been demonstrated.

Chapter 6

6 Discussion

With increasing economic pressures, power systems have become larger, more interconnected, and more dynamically able to provide appropriate levels of generation to efficiently meet the continual variation of consumer demand. The rationale of the interconnected power systems is to provide both flexibility of generation and competitive pricing of energy through the marketing and sale of electrical energy. Competition in pricing provides industry with affordable energy supply that in-turn underpins economic stability and growth. However for such economies to operate as envisaged, the power supply and distribution network must be both secure and reliable. To ensure secure and reliable generation and distribution, the power system, like any dynamic system, requires ongoing monitoring, feedback and control. The rationalisation to large interconnected power systems, though, has given rise to the phenomenon of inter-area modes. These particular modes have proven to be a challenge to monitor and estimate, especially in comparison to localised generation modes. As a result there has been much research into the estimation of inter-area modal parameters. However the estimation methods developed have typically required large data sets in the order of hours (at least when monitoring under normal power system operation is performed). Under quasi-stationary conditions this may be tolerable, but in cases of sudden detrimental changes, the power system integrity could be severely compromised. Such scenarios may lead to huge stresses in the

transmission, distribution and generation infrastructure, resulting in the possible loss of supply. This is clearly unacceptable. Therefore it was the aim of this research to develop alternative means to monitor inter-area modal responses to disturbances, specifically targeting the rapid alarming of sudden detrimental changes.

In Chapter 2 a new and simple concept of alarming detrimental change was introduced. It was recognised early in Chapter 2 that for reliable alarming to prevail, an understanding of the possible system output required characterisation. The system characterisation developed in Chapter 2 encompassed the formulation of a probability density function of the expected energy of a measured signal. The formulation of the PDF was done theoretically, based on long term estimates of the system parameters during quasi-stationary conditions. Although the construction of the PDF requires the convolution of many ensemble weighted components of the system's frequency response, this was not a computational issue as FFT and inverse FFT methods could easily be employed to maintain low computational overhead. Once the system characterisation was formulated, a user defined false alarm rate could then be used to set the threshold. In practice the implementation of the method to monitor rapid changes was both successful and computationally efficient, as only the energy of the observed signal required comparing to the set threshold, a reasonably simple task. The energy alarming method is particularly suited to smaller systems that only contain one major mode. This is because the method does not attribute any alarm state to any particular mode, it simply indicates that there is an undesirable level of damping currently within the system. To distinguish the particular mode undergoing sudden detrimental damping the method in Chapter 3 was developed.

Chapter 3 extended the work in Chapter 2 and examined optimal detection strategies for signals embedded in noise and interference (i.e.

other modes). The new method attempted to separate and enhance the individual modal contribution with the application of optimal "whitening-like" filters. The resulting output from the filtering and cross-correlation process generated a "test statistic". Again the method in Chapter 3 was focused on the rapid alarming of detrimental change, but with the added feature of mode identification. Therefore in a similar vein to Chapter 2, the method in Chapter 3 required a characteristic PDF of the test statistic. Once again analytical methods were used to formulate this PDF. Although the process was slightly more complex than in Chapter 2, computational efficiency in generating the PDF was again assured through the use of FFTs. Within the simulation, validation and real data analysis stages, the effectiveness of the method to rapidly alarm detrimental change and still maintain an acceptable level of false alarms during quasi-stationary phases was demonstrated.

In Chapter 4 the innovation characteristic associated with the Kalman filter was examined. The innovation is defined as the difference between the observed signal and that of the Kalman filter output (i.e. the estimate of the observed signal). It is generally acknowledged that this innovation will remain white as long as the system under consideration remains stationary. This was the motivation behind using the Kalman innovation, because if the power system underwent sudden detrimental changes in damping then obviously the power system would no longer be stationary and the Kalman innovation would reflect the changes. Therefore the normalised spectra of the Kalman innovation was used to monitor and alarm detrimental changes in damping conditions. It was shown in simulation, verification and real data analysis that the effect of sudden detrimental changes was a "disturbance" in the normally white innovation spectra. In all cases the alarming of the change was almost instantaneous, strong, and even more importantly, identified the mode of interest. As demonstrated, the threshold for the alarm was simplistic to generate as the

ideal normalised innovation spectrum may be modelled by white noise. Hence the PDF is a simple exponential, Chi-Squared function, χ_2^2. Combining the innovation spectra from multi-site data provided more coherent alarming over the threshold with respect to the disturbance. In regards to computational efficiency the Kalman filter is already regarded as an optimal linear estimator, so with only a difference, normalisation and FFT stage required to provide the innovation spectrum, it can be seen that this method is not computationally demanding. However the method does have a possible ambiguity associated with it. This was clearly demonstrated in the simulations where both the frequency and the damping of the mode were changed. Therefore a means to efficiently determine shifts in frequency of the modes was required. The requirement to monitor shifts in frequency through the estimation of polynomial phase signals was therefore addressed in Chapter 5.

Within this contribution of work, Chapter 5 returned to the requirement of estimating parameters rather than detection of change. However it must be noted again that the primary focus of this research was to provide information of modal damping and frequency status as rapidly as possible. Hence computational efficiency would also be a requirement of any polynomial phase signal estimator employed. Another point to note was a requirement of the estimator to operate adequately with potentially noisy signals. With this in mind a thorough investigation into current PPS estimators was undertaken. Through the understanding of current PPS estimators a new generalised class emerged that effectively linked many current methods together under a single Generalised Multi-Linear function Class, GMLC. In doing so, this also provided the opportunity to generate a new member to the class through careful and informed design. The new estimator specifically targeted the 4^{th} order polynomial phase signal, as first, second and third order signals already had very acceptable estimation methodologies available through current literature. The result

is a new 4th order polynomial phase signal estimator that has the following desirable characteristics: It has a practically useful SNR threshold of ~1dB, it produces asymptotically optimal estimates just above (or on) the Cramér-Rao bounds, and importantly, was shown to be computationally efficient. The performance characteristics of the new member were shown to be very competitive in relation to the current 4th order PPS methods available. These characteristics are also favourable to the requirements of ongoing, rapid monitoring of power system signals. Simulation and analysis of the new method validated the performance in relation to MSE and CRLB. Analysis of real data demonstrated clear trends in frequency changes, specifically highlighting rapid changes through large estimates of the higher order phase co-efficients. Admittedly, such an optimal 4th order PPS estimator is attractive to a wider variety of signal analysis, than just power system frequency trends. Therefore it is hoped that this section of work is recognised and implemented accordingly in other appropriate areas.

In this final part of the discussion it is important to note the requirement of a suitable long-term estimator in relation to the methods used in Chapters 2, 3 and 4. In all cases the methods created appropriate PDFs (in Chapter 2 and 3) and plant model (in Chapter 4) based on the output of a long term estimator. In this body of work the same LTE [13] was used throughout for reasons of both consistency and ease of access. In all cases the LTE provided adequate system estimates over from the long-term quasi-stationary data analysed. Therefore it should be noted that the methods presented in Chapters 2-4 need to be implemented in conjunction with a suitable LTE as presented within each Chapter.

In the final part of this discussion, a comparison of the proposed detectors from Chapters 2, 3 and 4 will be presented in the following subsection.

6.1 Comparison of Proposed Detectors

To finish off the discussion, a comparison of the three detector methods will be presented in this section.

In this section, the data used for the Kalman innovation detector in Section 4.5 of Chapter 4 is again used for a comparison of the proposed methods presented in Chapters 2 to 4. The comparison will present the relative detection results and provide insight into the relative advantages, disadvantages, superiority and real-world viability of the different methods.

For the comparison 45min of data was used by the LTE (as it was in Chapter 4) to estimate the system parameters and set up the relevant system PDFs required by the different methods. Again the data of interest is between 188 and 206 mins, where a clear disturbance in mode 2 occurs during 197-200 mins. This disturbance was clearly identified in Chapter 4 using the Kalman Innovation Detector (KID).

Firstly the Energy Based Detector (EBD), from Chapter 2, was implemented and the resulting energy measurements from the three sites are shown in Figure 6-1. A clear crossing of the respective thresholds between 196-202 minutes can be seen at all three sites. This supports the results in Chapter 4, namely that there is a large disturbance within this time frame. However the EBD does not indicate which mode has changed.

Next, the data was analysed using the Optimal Individual Mode Detector (OIMD) proposed in Chapter 3. As can be seen in Figure 6-2 the disturbance in mode 2 is only strongly detected at the NSW site, with weak “detections” at 201 mins for the Victorian and South Australian sites. Mode 1, on the other hand, is clearly detected at all three sites between 199-202 minutes, Figure 6-3. This really is a failure of the OIMD method in this case. The reason for the failure may be put down to

the fact that mode 2 is relatively weak with respect to mode 1. The estimate of the spectral contribution of mode 2, at all three sites, can be seen in Figure 6-4. Because of the weak mode 2 spectral influence, the whitening of the data containing a strong disturbance may not spectrally decouple the modes adequately for detection purposes. It is this facet that limits the OIMD effectiveness when working with systems that exhibit a spectrally dominate mode. However, as shown in Table 6-1 the strongest peak was the NSW Mode 2 detection, which provides an encouraging scenario that with a correctly formulated hypothesis test then the correct mode could still be adequately detected and selected.

The final comparison is the Kalman Innovation Detector (KID) and this simply draws on the previous results in Chapter 4.

All of the results from the comparison are in Table 6-1. The results compare detection statistics with respect to relative thresholds at the 200 minute measurement point of the data. It should be noted here that all of the methods employed a 60 second analysis window.

As can be seen in the results, the EBD is both simple and reliable. Correlation between sites is strong and the detection statistic is also strong relative to the respective thresholds. In the case of the OIMD, the mode information has not been spectrally decoupled successfully; however an alarm situation does coincide with the other methods in four of the 6 tests (two modes per site). The strongest detection (NSW-Mode 2 at 15.64 dB above threshold) indicates that mode 2 is undergoing an undesirable disturbance. The KID, as discussed in Chapter 4, overcomes the shortcomings of the previous two methods by providing a clear indication of the disturbance and mode identification.

In application to real systems, the EBD is simplistic and reliable and easily tuned to the power system. It will provide a rapid indication of sudden detrimental change but not precisely which mode the change is associated with. Therefore it provides detection, but not identification.

The EBD method would be well suited to single mode power systems, but is still attractive to multi-modal systems to provide short-term monitoring. The OMID method may only be useful under certain conditions or hypotheses. Although one site did provide the largest detection statistic of all the methods (over the relative threshold) the comparison demonstrated the OMID's limitations. More work may need to be done to ascertain whether these limitations can be relaxed and the OMID method exploited for application in dominant mode, multi-modal systems. The OMID method can provide detection, but may be ambiguous in identification under undesirable conditions. The KID method has shown to be able to provide both detection and mode identification but one must keep in mind the difficulty in tuning the Kalman filter adequately. In practice this may not be an easy task. Hence the more informative detector is also the most complicated to implement.

On a final point it is important to reflect that all of these methods do rely on adequate long-term estimates of the power system in *normal operation*. In the case of the comparison shown, only 45mins of data was used to provide a system estimate. This was mainly for the benefit of the Kalman detector as it tends to be more sensitive than the other methods and needs to be kept up to date on the system characteristics.

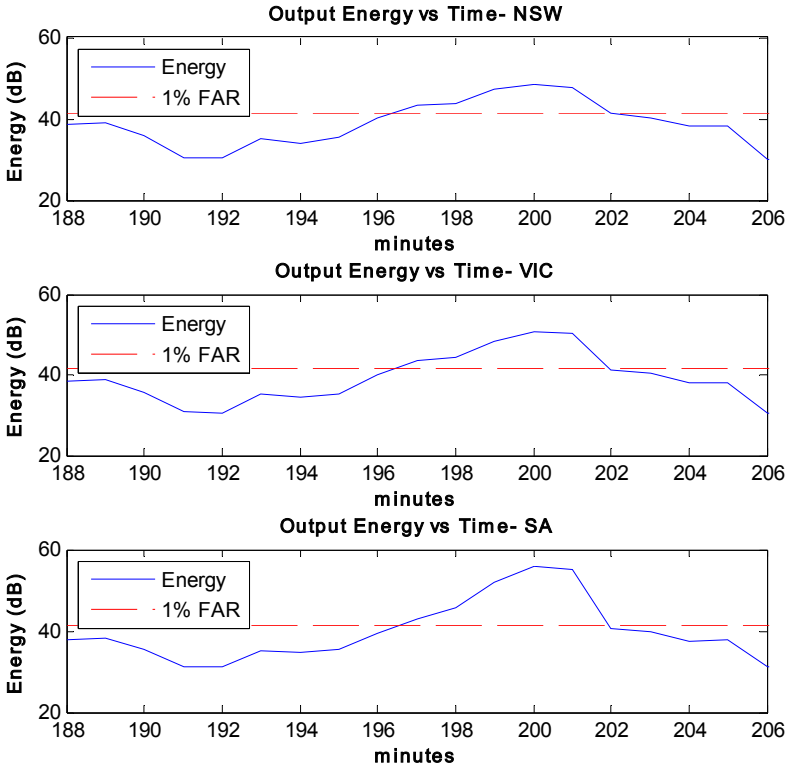

Figure 6-1 EBD outputs from three sites, NSW, VIC and SA.

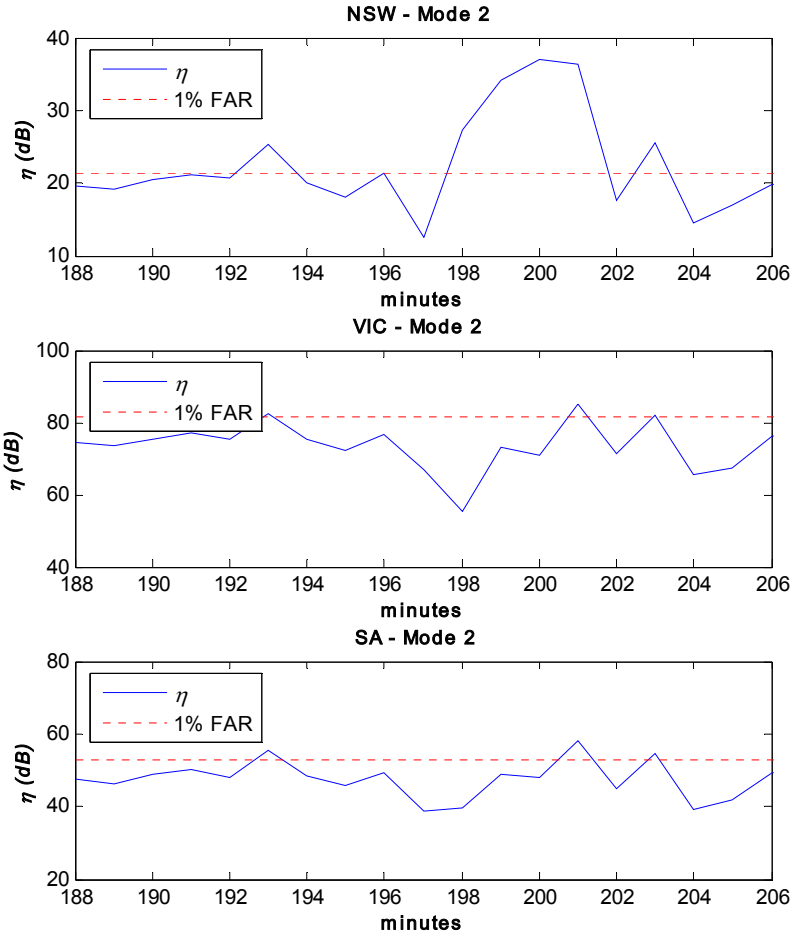

Figure 6-2 OMID Mode 2 outputs from three sites, NSW, VIC and SA.

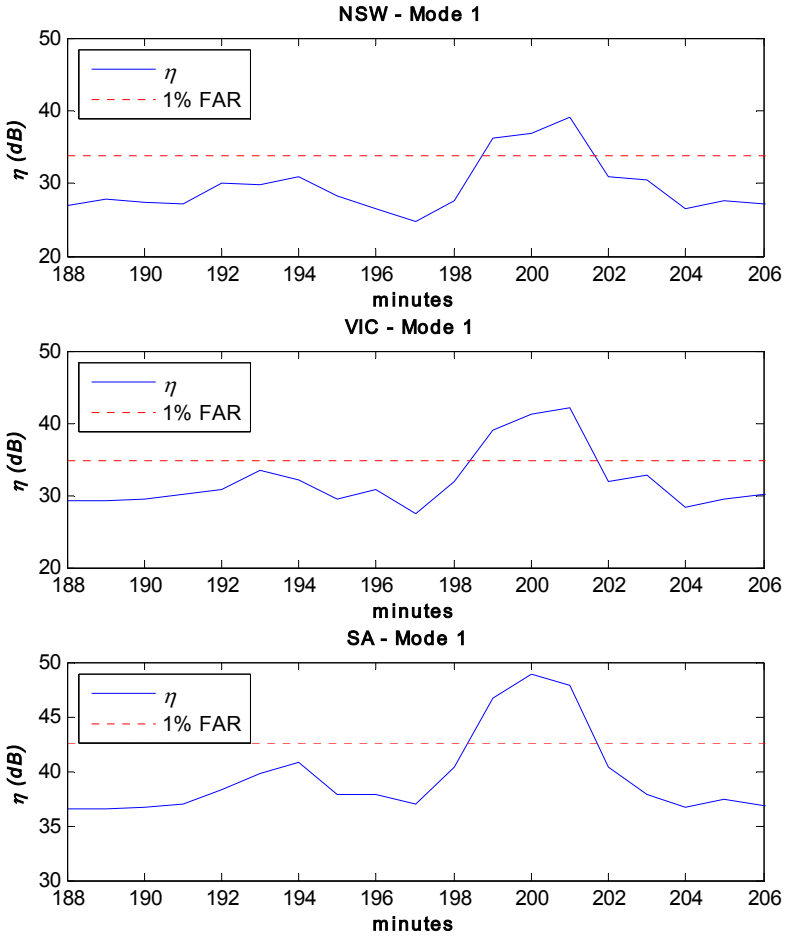

Figure 6-3 OMID Mode 1 outputs from three sites, NSW, VIC and SA.

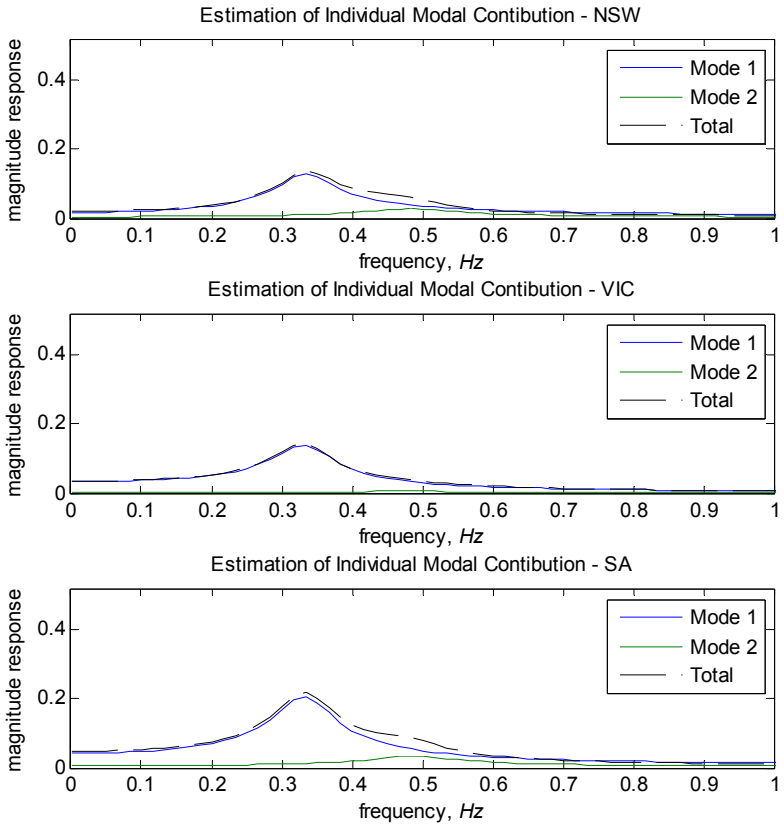

Figure 6-4 Estimation of Spectral Mode Contributions from three sites, NSW, VIC and SA.

TABLE 6-1 COMPARISON OF DETECTION METHOD TEST STATISTICS.

METHOD	CHAPTER	SITE	THRESHOLD (DB)	TEST STATISTIC @ 200 MINS (DB)	STRENGTH OF DETECTION (DB ABOVE THRESHOLD)
EBD	2	NSW	41.20	48.44	7.24
EBD	2	VIC	41.43	50.80	9.37
EBD	2	SA	40.51	55.64	15.13
OIMD	3	NSW-MODE 1	33.77	36.95	3.18
OIMD	3	VIC-MODE 1	37.50	41.18	3.68
OIMD	3	SA-MODE 1	42.64	48.85	6.21
OIMD	3	NSW-MODE 2	21.38	37.02	15.64
OIMD	3	VIC-MODE 2	81.65	70.85	NOT DETECTED
OIMD	3	SA-MODE 2	52.80	48.11	NOT DETECTED
KID	4	COMBINED	-11.61	-3.28	8.33

Chapter 7

7 Conclusions and Future Directions

7.1 Conclusion

The body of research work within this thesis is comprised of techniques designed to assist power utilities to rapidly ascertain the modal condition within a large interconnected power system. Within this work three new methods of rapidly detecting deteriorating modal damping have been presented; the energy based method, the optimal detection in Gaussian noise method and the Kalman innovation method. The first of these methods is excellent for monitoring the system output as a whole and would be particularly suitable for single mode systems. The latter two of these techniques are designed to provide both alarming of sudden detrimental damping and the identification of the offending mode. The effectiveness of the methods in simulations, verification and real data analysis was demonstrated in both alarming poor damping conditions as well as providing close to expected false alarms when the power system was under adequately damped quasi-stationary conditions. All three methods use analytical means to characterise the expected system measurement and determine the desired threshold. All three methods provide computationally efficient means to provide ongoing monitoring and rapid alarming.

The final work presented in this research returned to the problem of time-varying frequency estimation. Within this work a generalised form of multi-linear functions was initially defined that linked existing methods

under one encapsulated form. From this a new member of the multi-linear function class was devised that specifically focused upon the estimation of coefficients in a noisy 4^{th} order polynomial phase signal. The ambitious aim of the design was to obtain SNR thresholds that were practical, produced estimates that were as close as possible to the Cramér-Rao lower bounds and, finally, not lose sight of the need to perform the estimation as computationally efficiently as possible. Through careful design, all of these aims were met and demonstrated with the appropriate statistical analysis and simulation. The real power system data analysis demonstrated clear trends in the change and subsequent rates of change using short analysis windows. The ability to monitor such changes quickly, as opposed to estimates from long term estimators, would help considerably in the detector methods outlined within the earlier thesis chapters.

7.2 Future Directions

Some suggested future directions for research are presented below.

The issue of alarming is a significant issue. The question begs to be asked, *"...when a single alarm is "triggered", do you act on that one alarm (with the knowledge of a realistic FARs) or do you wait for more subsequent alarms?"* With a simple single type of detector this may be the only possible hypothesis upon which to base a decision. Combining alarms from different length windows has been proposed, and may provide a beneficially "rounded" alarm without the false alarm *jitter* of just one analysis window. Therefore one future direction of research could be to statistically formulate optimal methods of combining the alarms from multiple data lengths. Such a study could provide a decision technique based on alarm level (i.e. the *severity* of the alarm), rather than a simple binary hypothesis that exists with a simple detector. Such an alarm system can also make use of the analytically formulated PDF.

Systems with different damping conditions will provide different locations of the respective PDFs. In the case of the simple energy detector, measured energy levels can be related to certain values of damping with given levels of confidence. Therefore the severity of alarm could provide approximate estimates of damping. Although not presented in this thesis, such an investigation was initiated early-on and showed potential to provide such short-term approximate estimates.

It would be useful to implement the techniques in this thesis into a real time wide-area monitoring system. Such a system would call-on long term estimates, updates of frequency trajectories and combine this information to provide analytically generated thresholds that provide a level of alarm, identification of the disruptive mode/s and approximate short-term damping estimates. A system of such nature would require computationally efficient coding (C or C++) and would possibly need to operate on a platform with parallel, real-time processing ability.

Publications

Conference Publications

i. R. A. Wiltshire, P. O'Shea, and G. Ledwich, "Rapid Detection of Deteriorating Modal Damping in Power Systems," Proceedings of Australasian Universities Power Engineering Conference 2004, ISBN 1-864-99775-3, Paper number 73, Brisbane, Queensland, Australia, Sep 26-29, 2004.

ii. R. A. Wiltshire, P. O'Shea, and G. Ledwich, "Monitoring of Individual Modal Damping Changes in Multi-Modal Power Systems," Proceedings of Australasian Universities Power Engineering Conference 2004, ISBN 1-864-99775-3, Paper number 74, Brisbane, Queensland, Australia, Sep 26-29, 2004. (Also invited for inclusion in the Australian Journal of Electrical and Electronic Engineering).

iii. R. A. Wiltshire, P. O'Shea, G. Ledwich and M. Farquharson, "Application of Statistical Characterisation to the Rapid Detection of Deteriorating Modal Damping in Power Systems," presented at The Seventh IASTED International Conference on Signal and Image Processing, pp. 511-516, Honolulu, Hawaii, USA, Aug 15-17, 2005.

iv. R. A. Wiltshire, P. O'Shea, and G. Ledwich, “Rapid Detection of Changes to Individual Modes in Multimodal Power Systems” presented at IEEE TENCON 05 International Conference, Melbourne, Victoria, Australia, Nov 22-24, 2005

Journal Publications

v. R. A. Wiltshire, P. O'Shea, and G. Ledwich, "Monitoring of Individual Modal Damping Changes in Multi-Modal Power

Systems," Australian Journal of Electrical and Electronics Engineering, Vol 2, No 3, pp 217-222. Institution of Engineers, Australia, 2005.

vi. R. A. Wiltshire, P. O'Shea, and G. Ledwich, "A Kalman Filtering Approach to Rapidly Detecting Modal Changes in Power Systems," IEEE Transactions on Power Engineering Systems, 2007.

Journal Publications under Revision

vii. P. O'Shea and R. A. Wiltshire, "A new class of multi-linear functions for polynomial phase signal analysis". Under revision after submission to IEEE Transaction on Information Theory, 2007.

Bibliography

[1] R. Kumaresan, "On a frequency domain analog of Prony's method," *IEEE Transactions on Acoustics, Speech, and Signal Processing*, vol. 38, pp. 168-170, 1990.

[2] R. Kumaresan and Y. Feng, "FIR prefiltering improves Prony's method," *IEEE Transactions on Signal Processing*, vol. 39, pp. 736-741, 1991.

[3] R. Kumaresan and D. W. Tufts, "Singular Value Decomposition and Improved Frequency Estimation Using Linear Prediction," *IEEE Transactions on Acoustics, Speech and Signal Processing*, vol. ASSP-30, pp. 671-675, 1982.

[4] R. Kumaresan and D. W. Tufts, "Estimating the Parameters of Exponentially Damped Sinusoids and Pole-Zero Modelling in Noise," *IEEE Transactions on Acoustics, Speech and Signal Processing*, vol. ASSP-30, pp. 833-840, 1982.

[5] R. Kumaresan, D. W. Tufts, and L. L. Scharf, "Prony Method for Noisy Data: Choosing the Signal Components and Selecting the Order in Exponential Signal Models," *Proceedings of the IEEE*, vol. 72, pp. 230-233, 1984.

[6] R. Gomez Martin and M. C. Carrion Perez, "Extended Prony Method Applied to Noisy Data," *Electronics Letters*, vol. 22, pp. 613-614, 1986.

[7] R. T. Byerly, R. J. Bennon, and D. E. Sherman, "Eigenvalue Analysis of Synchronising Power from oscillations in Large Power Systems," *IEEE Transactions, PAS-101*, pp. 235-243, 1982.

[8] P. O'Shea, E. Palmer, and G. Frazer, "Power system disturbance monitoring using spectral analysis techniques," presented at Acoustics, Speech, and Signal Processing, ICASSP-95., 1995 International Conference on, Detroit, Michigan, USA, vol. 4, pp. 2731-2734, 9-12 May, 1995.

[9] P. O'Shea, "The use of sliding spectral windows for parameter estimation in power system disturbance monitoring," *Power Systems, IEEE Transactions on*, vol. 15, pp. 1261-1267, 2000.

[10] P. O'Shea, "A high-resolution spectral analysis algorithm for power-system disturbance monitoring," *Power Systems, IEEE Transactions on*, vol. 17, pp. 676-680, 2002.

[11] G. Ledwich and E. Palmer, "Modal estimates from normal operation of power systems," *Power Engineering Society Winter Meeting, IEEE*, vol. 2, pp. 1527-1531, 2000.

[12] M. Banejad and G. Ledwich, "Correlation based mode shape determination of a power system," presented at Acoustics, Speech, and Signal Processing, 2002 IEEE International Conference on, Orlando, Florida, vol. 4, pp. 3832-3835, 13-17 May, 2002.

[13] C. L. Zhang and G. F. Ledwich, "A new approach to identify modes of the power system based on T-matrix," presented at Advances in Power System Control, Operation and Management, 2003. ASDCOM 2003. Sixth International Conference on (Conf. Publ. No. 497), Hong Kong, vol. 2, pp. 496-501, 11-14 Nov, 2003.

[14] J. Huillery, F. Millioz, and N. Martin, "On the Probability Distributions of Spectrogram Coefficients for Correlated Gaussian Process," presented at Acoustics, Speech and Signal Processing, 2006. ICASSP 2006 Proceedings. 2006 IEEE International Conference on, Toulouse, France, vol. 3, pp. III-436-III-439, May 15-19, 2006.

[15] H. Urkowitz, "Energy detection of unknown deterministic signals," *Proceedings of the IEEE*, vol. 55, pp. 523-531, 1967.

[16] P. O'Shea, "A new technique for instantaneous frequency rate estimation," *Signal Processing Letters, IEEE*, vol. 9, pp. 251-252, 2002.

[17] V. Vittal, "Consequence and impact of electric utility industry restructuring on transient stability and small-signal stability analysis," *Proceedings of the IEEE*, vol. 88, pp. 196-207, 2000.

[18] M. Begovic, D. Novosel, D. Karlsson, C. Henville, and G. Michel, "Wide-area protection and emergency control," *Proceedings of the IEEE*, vol. 93, pp. 876-891, 2005.

[19] M. Zima, M. Larsson, P. Korba, C. Rehtanz, and G. Andersson, "Design aspects for wide-area monitoring and control systems," *Proceedings of the IEEE*, vol. 93, pp. 980-996, 2005.

[20] J. Bertsch, C. Carnal, D. Karlson, J. McDaniel, and K. Vu, "Wide-area protection and power system utilization," *Proceedings of the IEEE*, vol. 93, pp. 997-1003, 2005.

[21] K. E. Holbert, G. I. Heydt, and H. Ni, "Use of satellite technologies for power system measurements, command, and control," *Proceedings of the IEEE*, vol. 93, pp. 947-955, 2005.

[22] C. L. Zhang and G. F. Ledwich, "Analysis of Major Australian Events Using an Angle Measurement System," presented at AUPEC 2005, Hobart, Tasmania Australia, vol. 1, pp. 159-164, 25-28 Sep, 2005.

[23] E. W. Palmer and G. Ledwich, "Optimal placement of angle transducers in power systems," *Power Systems, IEEE Transactions on*, vol. 11, pp. 788-793, 1996.

[24] M. Klein, G. J. Rogers, and P. Kundur, "A fundamental study of inter-area oscillations in power systems," *Power Systems, IEEE Transactions on*, vol. 6, pp. 914-921, 1991.

[25] N. Uchida and T. Nagao, "A new eigen-analysis method of steady-state stability studies for large power systems: S matrix method," *Power Systems, IEEE Transactions on*, vol. 3, pp. 706-714, 1988.

[26] D. M. Lam, H. Yee, and B. Campbell, "An efficient improvement of the AESOPS algorithm for power system eigenvalue calculation," *Power Systems, IEEE Transactions on*, vol. 9, pp. 1880-1885, 1994.

[27] P. W. Sauer, C. Rajagopalan, and M. A. Pai, "An explanation and generalization of the AESOPS and PEALS algorithms [power system models]," *Power Systems, IEEE Transactions on*, vol. 6, pp. 293-299, 1991.

[28] G. R. B. Prony, "Essai experimental et analytique, etc.," *Paris, J. de L'Ecole Polytechnique*, vol. 1, pp. 24-76, 1795.

[29] J. F. Hauer, "Application of Prony analysis to the determination of modal content and equivalent models for measured power system response," *Power Systems, IEEE Transactions on*, vol. 6, pp. 1062-1068, 1991.

[30] D. J. Trudnowski, J. M. Johnson, and J. F. Hauer, "Making Prony analysis more accurate using multiple signals," *Power Systems, IEEE Transactions on*, vol. 14, pp. 226-231, 1999.

[31] D. Vowles (UA), M. Gibbard (UA), and D. Bones (NEMMCO), "Testing Continuous-Monitoring Modal-Estimation Methods: Assessment of the QUT Energy-Based Method (QUT Version)," The University of Adelaide, Adelaide, South Australia, Confidential Report AIR C00120, 10 August 2004.

[32] P. Kundur and P. L. Dandeno, "Practical Applications of Eigenvalue Techniques in the Analysis of Power Systems Dynamic Stability Problems," presented at 5th Power System Computation Conference, Cambridge, England, September, 1975.

[33] C. E. Grund, J. J. Paserba, J. F. Hauer, and S. L. Nilsson, "Comparison of Prony and eigenanalysis for power system control design," *Power Systems, IEEE Transactions on*, vol. 8, pp. 964-971, 1993.

[34] J. F. Hauer, C. J. Demeure, and L. L. Scharf, "Initial results in Prony analysis of power system response signals," *Power Systems, IEEE Transactions on*, vol. 5, pp. 80-89, 1990.

[35] M. K. Donnelly, D. J. Trudnowski, and J. F. Hauer, "Advances in the Identification of Transfer Functions Models using Prony Analysis," presented at Proceedings of the 1993 American Control Conference, San Francisco, CA, vol. 2, pp. 1561-1562, 21-23 Jun, 1993.

[36] A. H. Nuttall, "Spectral Analysis of a Univariate Process with bad data points via Maximum Entropy and Linear Predictive Techniques," *NUSC Scientific and Engineering Studies, Spectral Estimation, NUSC, New London, CT*, 1976.

[37] N. Kannan and D. Kundu, "Estimating parameters in the damped exponential model," *Signal Processing*, vol. 81, pp. 2343-2351, 2001.

[38] A. A. Beex and P. Shan, "Time-varying Prony method for instantaneous frequency estimation at low SNR," *Proceedings - IEEE International Symposium on Circuits and Systems*, vol. 3, pp. III-5 - III-8, 1999.

[39] K. K.-P. Poon and K.-C. Lee, "Analysis of transient stability swings in large interconnected power systems by Fourier

transformation," *Power Systems, IEEE Transactions on*, vol. 3, pp. 1573-1581, 1988.

[40] P. O'Shea, "The use of sliding spectral windows for parameter estimation of decaying sinusoidal signals," presented at TENCON '97. IEEE Region 10 Annual Conference. Speech and Image Technologies for Computing and Telecommunications'., Proceedings of IEEE, Brisbane, Australia, vol. 2, pp. 827-830, 2-4 Dec, 1997.

[41] K. C. Lee and K. P. Poon, "Analysis of power system dynamic oscillations with beat phenomenon by Fourier transformation," *Power Systems, IEEE Transactions on*, vol. 5, pp. 148-153, 1990.

[42] P. O'Shea, "A high resolution spectral analysis algorithm for power system disturbance monitoring," *Transactions on Power Systems*, vol. 17, 2001.

[43] A. V. Oppenheim, R. W. Schafer, and J. R. Buck, *Discrete-time signal processing*, 2nd ed. Upper Saddler River, N.J.: Prentice Hall, 1999.

[44] P. Swerling, "Parameter Estimation for Waveforms in Additive Gaussian Noise," *Journal of the Society for Industrial and Applied Mathematics*, vol. 7, pp. 152-166, 1959.

[45] R. E. Kalman, "A New Approach to Linear Filtering and Prediction Problems," *Transactions of the ASME - Journal of Basic Engineering*, vol. 82, pp. 35-45, 1960.

[46] N. Funk, "A Study of the Kalman Filter Applied to Visual Tracking," University of Alberta 7th December 2003.

[47] R. E. Kalman and R. S. Bucy, "New Results in Linear Filtering and Prediction Theory," *Transactions of the ASME - Journal of Basic Engineering*, vol. 83, pp. 95-107, 1961.

[48] A. Stubberud and H. Wabgaonkar, "Approximation and Estimation Techniques for Neural Networks," presented at 28th Conference on Decision and Control, Honolulu, Hawaii, pp. 2736-2740, 5-7 Dec, 1990.

[49] S. J. Julier and J. K. Uhlmann, "A New Extension of the Kalman Filter to Nonlinear Systems," presented at The proceedings of AeroSense; The 11th International Symposium on Aerospace/Defense Sensing, Simulation and Controls, SPIE,

Orlando, FL, USA, vol. Tracking and Resource Management II, April 21–24, 1997.

[50] R. K. Mehra and J. Peschon, "An innovations approach to fault detection and diagnosis in dynamic systems," *Automatica*, vol. 7, pp. 637-640, 1971.

[51] T. Kailath, "An innovations approach to least-squares estimation--Part I: Linear filtering in additive white noise," *Automatic Control, IEEE Transactions on*, vol. 13, pp. 646-655, 1968.

[52] F. Caliskan and C. M. Hajivyev, "Innovation sequence application to aircraft sensor fault detection: comparison of checking covariance matrix algorithms," presented at Decision and Control, Proceedings of the 38th IEEE Conference on, Phoenix, USA, vol. 4, pp. 3956-3961, 7-10 Dec, 1999.

[53] C. M. Hajiyev and F. Caliskan, "Fault detection in flight control systems based on the generalized variance of the Kalman filter innovation sequence," presented at American Control Conference, Proceedings of the, San Diego, CA, USA, vol. 1, pp. 109-113, 2-4 June, 1999.

[54] W. Martin and A. Stubberud, "An additional requirement for innovations testing in system identification," *Automatic Control, IEEE Transactions on*, vol. 19, pp. 583-584, 1974.

[55] A. S. Willsky, "A survey of design methods for failure detection in dynamic systems," *Automatica*, vol. 12, pp. 601-611, 1976.

[56] M. Farquharson, P. O'Shea, and G. Ledwich, "A computationally efficient technique for estimating the parameters of polynomial-phase signals from noisy observations," *Signal Processing, IEEE Transactions on [see also Acoustics, Speech, and Signal Processing, IEEE Transactions on]*, vol. 53, pp. 3337-3342, 2005.

[57] S. Peleg and B. Friedlander, "The discrete polynomial-phase transform," *IEEE Transactions on Signal Processing*, vol. 43, pp. 1901-1914, 1995.

[58] S. Barbarossa, A. Scaglione, and G. B. Giannakis, "Product high-order ambiguity function for multicomponent polynomial-phase signal modeling," *Signal Processing, IEEE Transactions on [see also Acoustics, Speech, and Signal Processing, IEEE Transactions on]*, vol. 46, pp. 691-708, 1998.

[59] B. Boashash and P. O'Shea, "Polynomial Wigner-Ville distributions and their relationship to time-varying higher order spectra," *Signal Processing, IEEE Transactions on [see also Acoustics, Speech, and Signal Processing, IEEE Transactions on]*, vol. 42, pp. 216-220, 1994.

[60] M. Benidir and A. Ouldali, "Polynomial phase signal analysis based on the polynomial derivatives decompositions," *Signal Processing, IEEE Transactions on [see also Acoustics, Speech, and Signal Processing, IEEE Transactions on]*, vol. 47, pp. 1954-1965, 1999.

[61] B. Barkat and B. Boashash, "Design of higher order polynomial Wigner-Ville distributions," *Signal Processing, IEEE Transactions on [see also Acoustics, Speech, and Signal Processing, IEEE Transactions on]*, vol. 47, pp. 2608-2611, 1999.

[62] P. O'Shea, "A fast algorithm for estimating the parameters of a quadratic FM signal," *Signal Processing, IEEE Transactions on [see also Acoustics, Speech, and Signal Processing, IEEE Transactions on]*, vol. 52, pp. 385-393, 2004.

[63] B. Ristic and B. Boashash, "Comments on The Cramer-Rao lower bounds for signals with constant amplitude and polynomial phase," *Signal Processing, IEEE Transactions on [see also Acoustics, Speech, and Signal Processing, IEEE Transactions on]*, vol. 46, pp. 1708-1709, 1998.

[64] Matlab, "Statistics Toolbox: skewness," vol. Release 6.1, 2001.

[65] T. George, J. Crisp, and G. Ledwich, "Advanced tools to manage power system stability in the National Electricity Market," presented at AUPEC, Brisbane, Australia, 26-29 Sep, 2004.

[66] H. VanTrees, *Detection, Estimation and Modulation Theory, Part 1*. New York: John Wiley, 1968.

[67] S. Kay, *Modern Spectrum Analysis*: Prentice-Hall, 1988.

[68] P. Z. Peebles, *Probability, random variables, and random signal principles*, 4th ed. New York, NY: McGraw Hill, 2001.

[69] Matlab, "Control Systems Toolbox: Kalman," 2001.

[70] G. F. Franklin, J. D. Powell, and M. L. Workman, *Digital control of dynamic systems*, 3rd ed. Menlo Park, Calif: Addison-Wesley, 1998.

[71] D. G. Lainiotis, K. N. Plataniotis, M. Papanikolaou, and P. Papaparaskeva, "Discrete Riccati Equation Solutions: Distributed Algorithms," *Mathematical Problems in Engineering*, vol. 2, pp. 319-332, 1995.

[72] K. Ogata, *Discrete-time control systems*, 2nd ed. Englewood Cliffs, N.J: Prentice Hall, 1995.

[73] R. A. Wiltshire, P. O'Shea, and G. Ledwich, "Rapid Detection of Changes to Individual Modes in Multimodal Power Systems," presented at TENCON 2005 IEEE Region 10, Melbourne, Australia, pp. 1-6, 22-24 Nov, 2005.

[74] R. A. Wiltshire, P. O'Shea, G. Ledwich, and M. Farquharson, "Application of Statistical Characterisation to the Rapid Detection of Deteriorating Modal Damping in Power Systems," presented at The Seventh IASTED International Conference on Signal and Image Processing, Honolulu, Hawaii, USA, 15-17 Aug, 2005.

[75] R. A. Wiltshire, P. O'Shea, and G. Ledwich, "Rapid Detection of Deteriorating Modal Damping in Power Systems," presented at AUPEC 2004, Brisbane, Australia, pp. Paper 73, 26-29 Sep, 2004.

[76] R. A. Wiltshire, P. O'Shea, and G. Ledwich, "Monitoring of Individual Modal Damping Changes in Multi-Modal Power Systems," *Journal of Electrical & Electronics Engineering Australia, JEEEA*, vol. 2, pp. 217-222, 2005.

[77] J. A. R. Macias and A. G. Exposito, "Kalman filter tuning for digital protection applications," presented at Power Tech Conference Proceedings, 2003 IEEE Bologna, Italy, vol. 4, pp. 5, 23-26 June, 2003.

[78] B. R. J. Haverkamp, M. Verhaegen, C. T. Chou, and R. Johansson, "Tuning of the continuous-time Kalman filter from sampled data," presented at American Control Conference, Proceedings of the, San Diego, CA, USA, vol. 6, pp. 3895-3899, 2-4 June, 1999.

[79] S. Peleg and B. Porat, "Estimation and classification of polynomial-phase signals," *Information Theory, IEEE Transactions on*, vol. 37, pp. 422-430, 1991.

[80] S. Peleg and B. Friedlander, "The discrete polynomial-phase transform," *Signal Processing, IEEE Transactions on [see also Acoustics, Speech, and Signal Processing, IEEE Transactions on]*, vol. 43, pp. 1901-1914, 1995.

[81] B. Boashash and P. O'Shea, "Polynomial Wigner-Ville distributions and their relationship to time-varying higher order spectra," *IEEE Transactions on Signal Processing*, vol. 42, pp. 216-220, 1994.

[82] S. Peleg and B. Porat, "Linear FM signal parameter estimation from discrete-time observations," *Aerospace and Electronic Systems, IEEE Transactions on*, vol. 27, pp. 607-616, 1991.

[83] B. Porat and B. Friedlander, "Asymptotic statistical analysis of the high-order ambiguity function for parameter estimation of polynomial-phase signals," *Information Theory, IEEE Transactions on*, vol. 42, pp. 995-1001, 1996.